The effects of methadone and morphine on neuronal development

In vivo and in vitro studies done in chicken embryos and PC12 cells

Carolyn Sofie Coelho

Master's Thesis for the degree of
Master in Pharmacy
45 credits

Department of Pharmaceutical Biosciences
Faculty of Mathematics and Natural Sciences

UNIVERSITY OF OSLO

May 2023

The effects of methadone and morphine on neuronal development

In vivo and in vitro studies done in chicken embryos and PC12 cells

Carolyn Sofie Coelho

Master's Thesis for the degree of
Master in Pharmacy
45 credits

Department of Pharmaceutical Biosciences
Faculty of Mathematics and Natural Sciences

UNIVERSITY OF OSLO

May 2023

Supervisors:

Professor Ragnhild Elisabeth Paulsen

Post Doc Öyküm Kaplan Arabaci

PhD student Kristine Dolva

May 2023

The effects of methadone and morphine on neuronal development

In vivo and in vitro studies done in chicken embryos and PC12 cells

Carolyn Sofie Coelho

http://www.duo.uio.no/

Print: Reprosentralen, Universitetet of Oslo

Abstract

Every year, approximately 30 children are born from mothers who receive treatment for opioid dependence. Opioid exposure of the foetus during pregnancy has been linked to several effects on the central nervous system, such as developing autism and ADHD, but the exact mechanisms of neuronal development need more research. Pregnant women are rarely included in clinical studies, as they are considered a vulnerable group. Therefore, it is important to use good animal models for safety-pharmacological research.

In vitro studies were conducted to study the effects of methadone and morphine on the neuronal development of chicken cerebellar granule neurons and PC12 cells. Viability was studied using an MTT assay, and the effects of the opioids were studied in the presence and absence of ANA-12 and TAT-Pep5, which are inhibitors of important signalling pathways promoting neuronal survival and apoptosis. Neurite outgrowth and synaptogenesis were studied using live-cell imaging and high-content imaging. The expressions of the genes MOR, DOR, KOR, PENK, PDYN, BDNF, CREB1, GluN2B and CYP3A4 were studied using real-time qPCR. MOR, DOR, KOR and GluN2B encode receptors and receptor subunits involved in opioid signalling and are linked to processes in neurodevelopment. PENK and PDYN encode precursors of endogenous opioid peptides. BDNF and CREB1 are involved in signalling through the TrkB receptor, which is linked to important processes in neurodevelopment. CYP3A4 encode the main metabolising enzyme of methadone. *In ovo* injections were conducted to study *in vivo* distribution of methadone and its main metabolite EDDP in the brain, lungs, and yolk of the chicken embryo. This was done to advance our understanding of the distribution in the chicken model, with the goal of enhancing its utility in safety-pharmacological studies.

Neurite outgrowth was unaffected by methadone and morphine at therapeutic concentrations, but 100 µM methadone was toxic for both the PC12 cells and the chicken granule neurons. In the presence of ANA-12, the toxic effect of methadone was exacerbated. Therapeutic concentrations of the opioids did not affect the expression of the genes studied. However, 100 µM methadone increased the expression of MOR, PDYN, and CYP3A4, and decreased the expression of PENK and GluN2B. These findings should be validated by conducting western blots and additional real-time qPCR in future research, as these changes can cause neurodevelopment consequences. *In vivo*, the uptake of methadone into the brain, lungs and

yolk happened rapidly, and the main metabolite, EDDP, reached the lungs at higher concentrations than the brain initially. Additionally, there seemed to be an accumulation of methadone and EDDP in the yolk.

Sammendrag

Hvert år blir det født omtrent 30 barn av mødre som mottar behandling for opioidavhengighet. Opioideksponering av fosteret under graviditeten er knyttet til flere effekter på sentralnervesystemet, slik som utvikling av autisme og ADHD. Det trengs flere studier på mekanismene bak nevronal utvikling. Gravide kvinner blir sjelden inkludert i kliniske studier, da de regnes som en sårbar gruppe. Derfor er det viktig å bruke gode dyremodeller i sikkerhetsfarmakologi.

In vitro-studier ble utført for å studere effektene av metadon og morfin på nevronal utvikling i kyllingkornceller og PC12-celler. Viabilitet ble studert ved hjelp av MTT assay, og effektene av opioidene ble studert både med og uten ANA-12 og TAT-Pep5, som er hemmere av viktige signalveier knyttet til overlevelse og apoptose i nevroner. Neurittutvekst og synaptogenese ble studert ved hjelp av live-cell og high-content imaging. Genekspresjonen til MOR, DOR, KOR, PENK, PDYN, BDNF, CREB1, GluN2B og CYP3A4 ble studert ved hjelp av RT-qPCR. Genene MOR, DOR, KOR og GluN2B koder for reseptorer og reseptorsubenheter involvert i signalveiene til opioider og er knyttet til prosesser i nevronal utvikling. PENK og PDYN koder for forløpere for endogene opioidpeptider. BDNF og CREB1 er involvert i signalveiene mediert av TrkB-reseptoren, som er knyttet til viktige prosesser i nevronal utvikling. CYP3A4 koder for hovedenzymet for metaboliseringen av metadon. *In ovo*-injeksjoner ble utført for å studere *in vivo*-distribusjonen av metadon og den viktigste metabolitten EDDP i hjernen, lungene og eggeplommen til kyllingembyoet. Dette ble gjort for å få bedre forståelse av distribusjonen i kyllingmodellen.

Neurittutveksten ble ikke påvirket av metadon og morfin ved terapeutiske konsentrasjoner, men 100 µM metadon var toksisk for både PC12-cellene og kyllingkorncellene. Sammen med ANA-12 ble den toksiske effekten av metadon forverret. Terapeutiske konsentrasjoner av opioidene påvirket ikke genekspresjonen av de studerte genene. Imidlertid økte 100 µM metadon ekspresjonen av MOR, PDYN og CYP3A4, og reduserte ekspresjonen av PENK og GluN2B. Disse funnene bør valideres ved å utføre western blots sammen med flere RT-qPCR studier, siden endringer i disse genene kan ha konsekvenser for nevronal utvikling. *In vivo* skjedde opptaket av metadon til hjernen, lungene og eggeplommen raskt. Hovedmetabolitten EDDP ble fordelt til lungene i større grad enn i hjernen de første timene. I tillegg ble det observert en akkumulering av metadon og EDDP i eggeplommen.

Acknowledgements

This thesis was carried out at the Department of Pharmaceutical Biosciences, School of Pharmacy at the University of Oslo from August 2022 to May 2023. The thesis is part of ongoing projects in the PharmaTox Strategic Research Initiative. Their aim is to generate knowledge on the effects of pharmaceuticals on neurodevelopment and neurotoxicity.

I would especially like to thank my supervisors Ragnhild Elisabeth Paulsen, Öyküm Kaplan Arabaci, and Kristine Dolva. Ragnhild, your passion and knowledge in this field is inspiring. You guided me when things seemed impossible, and for that I am truly grateful. Öyküm, thank you for all the help in the lab. After you arrived, the lab work was so much more fun. Kristine, thank you for all the advice and encouragement.

I would also like to thank both former and current staff at ZEB for all the training and help I received. I would especially like to thank Beata Urbanczyk Mohebi for helping with qPCR and all our interesting conversations. As for my lab partner, Alexander Håvardstun, we have helped each other throughout the whole journey, and I'm so grateful I had someone to share my frustrations and findings with.

Additionally, I would like to thank Elisabeth Nerem and Jannike Mørch Andersen at the Department of Forensic Science at Oslo University Hospital, Agata Impellizzeri, Jarle Ballangby and Oddvar Myhre at the Norwegian Institute of Public Health, and Fred Haugen at the National Institute of Occupational Health for helping me with analysis and equipment.

Finally, I would like to thank my family and friends for their support. Mum and Dad, you have been my biggest supporters throughout this whole period as a pharmacy student. I would also like to thank my brother for making sure that I was all right. Thank you all for cheering me up when things seemed impossible. Lastly, I would like to thank Anne Marte Baarset for putting up with me through these five years. Throughout this journey, we have experienced frustration and happiness through long days and late nights at VB. I don't think I could have finished Pharmacy School without you.

Oslo, May 2023,

Carolyn Sofie Coelho

Abbreviations

ACN	Acetonitrile
ADHD	Attention deficit hyperactivity disorder
ANOVA	Analysis of Variance
AUC	Area under the curve
BBB	Blood-brain barrier
BDNF	Brain-derived neurotrophic factor
BME	Basal Medium Eagle
BSA	Bovine serum albumin
CAM	Chorioallantoic membrane
cAMP	Cyclic adenosine monophosphate
cDNA	copy deoxyribonucleic acid
CGN	Chicken granule neurons
C_{max}	Maximum concentration
CNS	Central nervous system
CREB	cAMP responsive element binding protein 1
CYP	Cytochrome P450
DAPI	4′,6-diamidino-2-phenylindole
DMEM	Dulbecco's Modified Eagle Medium
DMSO	Dimethyl sulfoxide
DNA	Deoxyribonucleic acid
DNase	Deoxyribonuclease
DOR	Delta (δ) opioid receptor
E10-E18	Embryonic day 10-18
EDDP	2-Ethylidene-1,5-dimethyl-3,3-diphenyl pyrrolidine
EGL	External germinal layer
ESI	Electrospray ionisation
FBS	Foetal bovine serum
GAPDH	Glyceraldehyde 3-phosphate dehydrogenase
GluN1/GluN2(B)/GluN3	N-methyl-D-aspartate receptor subtypes 1, 2 (2B) and 3
HS	Horse serum
IGL	Internal granular layer
KOR	Kappa (κ) opioid receptor

LC	Liquid chromatography
LC-MS-MS	Liquid chromatography with tandem mass spectrometry
m/z	Mass-to-charge ratio
MAP2	Microtubule-associated protein 2
MeOH	Methanol
ML	Molecular layer
MOR	Mu (μ) opioid receptor
MQ	Milli-Q
MS-MS	Tandem mass spectrometry
MTT	3-(4,5-Dimethylthiazol-2-yl)-2,5-Diphenyltetrazolium Bromide
NC-IUPHAR	Nomenclature and Standards Committee of the International Union of Basic and Clinical Pharmacology
NGF	Nerve growth factor
NIPH	Norwegian Institute of Public Health
NMDA	N-methyl-D-aspartate
OMT	Opioid maintenance treatment
P5 and P9	Passage number 5 and 9
$p75^{NTR}$	Neurotrophin receptor p75
PBS	Phosphate-buffered saline
PBS+	Phosphate-buffered saline with calcium and magnesium
PCL	Purkinje cell layer
PDYN	Prodynorphin
PENK	Proenkephalin
PLL	Poly-L-Lysine
POMC	Proopiomelanocortin
PSD95	Postsynaptic density protein 95
RNA	Ribonucleic acid
RT-qPCR	Real-time quantitative polymerase chain reaction
SOP	Standard operating procedure
SYP	Synaptophysin
T_3	Triiodo-L-thyronine sodium salt
T_{max}	Time of maximum concentration
TrkB	Tyrosine receptor kinase B

Table of contents

ABSTRACT V

SAMMENDRAG VII

ACKNOWLEDGEMENTS VIII

ABBREVIATIONS IX

TABLE OF CONTENTS XI

1 INTRODUCTION 1

1.1 OPIOIDS 1
1.1.1 The opioid receptors and their endogenous ligands 2
1.1.2 Morphine 4
1.1.3 Methadone 5
1.2 OPIOIDS DURING PREGNANCY 6
1.3 DEVELOPMENT OF THE NERVOUS SYSTEM 6
1.3.1 The cerebellum 7
1.3.2 Receptors and molecules important for neuronal development 8
1.3.3 The blood-brain barrier 10
1.4 MODEL SYSTEMS 11
1.4.1 The chicken model 11
1.4.2 PC12 cells 12
1.5 THE AIM OF THE STUDY 13

2 MATERIALS AND METHODS 14

2.1 PRODUCTS AND MATERIALS. 14
2.2 PC12 CELLS 18
2.3 THE CHICKEN EMBRYO 18
2.3.1 Preparation of chicken granule neurons for in vitro exposure 19
2.3.2 Injection in ovo for the distribution study 20
2.4 MTT IN PC12 CELLS AND CHICKEN GRANULE NEURONS 20
2.5 INCUCYTE 21
2.6 RT-QPCR IN CHICKEN GRANULE NEURONS 21
2.7 HIGH-CONTENT IMAGING IN CHICKEN GRANULE NEURONS 22
2.8 PREPARATION OF WHOLE BRAINS, LUNGS, AND YOLK FROM CHICKENS FOR KINETICS 23
2.8.1 Homogenisation of the tissue 23
2.8.2 Sample preparation 23
2.8.3 LC-MS-MS 24
2.9 STATISTICS 25

3 RESULTS 26

3.1 VIABILITY 26
3.1.1 Viability of chicken granule neurons determined with MTT assay 26
3.1.2 Viability of methadone-exposed PC12 cells determined with MTT assay 28
3.2 LIVE-CELL IMAGING OF CHICKEN GRANULE NEURONS 30
3.2.1 Neurite length was reduced in chicken granule neurons exposed to 100 µM methadone 30
3.2.2 Neurite length was not significantly reduced in chicken granule neurons exposed to 100 µM morphine 35
3.3 GENE EXPRESSION IN CHICKEN GRANULE NEURONS EXPOSED TO METHADONE AND MORPHINE 40
3.3.1 The opioid receptors 40
3.3.2 Opioid polypeptide precursors 40
3.3.3 BDNF and CREB1 40
3.3.4 GluN2B 41
3.3.5 CYP3A4 41

3.4 High-content imaging of chicken granule neurons 47
3.5 Pharmacokinetics and distribution of methadone and its metabolite EDDP to the brain, lungs, and yolk 49
3.5.1 Methadone concentration in the brain, lungs, and yolk 49
3.5.2 Pharmacokinetics of methadone in the brain and lungs 49
3.5.3 Distribution of the main metabolite of methadone, EDDP, in the brain, lungs, and yolk 53
4 DISCUSSION 55
4.1 The model systems 55
4.1.1 The in vivo model 55
4.1.2 The in vitro models 57
4.2 Choice of exposures 58
4.3 *In vitro* methods 60
4.3.1 MTT assay 60
4.3.2 RT-qPCR 60
4.4 Biological findings 61
4.4.1 Viability and neurite outgrowth 61
4.4.2 Gene expression in the chicken granule neurons 63
4.4.3 Distribution of methadone and its metabolite in the chicken model 65
4.5 Future perspectives 68
5 CONCLUSION 69
6 REFERENCES 70
7 APPENDIX A – RECIPES 80
8 APPENDIX B – PROTOCOLS 88
8.1 Splitting of PC12 cells to a new passage 88
8.2 Splitting of PC12 cells to 96-well plates 88
8.3 Preparation of chicken granule cell suspension 89
8.4 Coating with PLL 91
8.5 *In ovo* injection 91
8.6 Determination of viability with MTT 91
8.7 Lysis of cells for RT-qPCR 92
8.8 RNA isolation 92
8.9 Conversion of RNA to cDNA and RT-qPCR 93
8.10 Immunocytochemistry 94
8.10.1 Fixation 94
8.10.2 Immunostaining 94
8.11 Homogenisation of lungs, brains, and yolk 95
8.12 Determination of drug distribution in lungs, brains, and yolk 95
9 APPENDIX C – SUPPLEMENTARY FIGURES 97

1 Introduction

The Norwegian Institute of Public Health reported in 2018 that every year there are approximately 30 children born from women who receive treatment for opioid dependence (1). The most common opioids used as opioid maintenance treatment (OMT) are methadone and buprenorphine (2), where 33% of approximately 8200 patients receiving OMT used methadone in 2021 (3). In the event that a patient becomes pregnant while undergoing methadone treatment, it is recommended that they continue with the methadone treatment rather than switching to buprenorphine, despite buprenorphine being considered a safer option for the developing foetus (4). In a cohort study from 2022, the use of methadone during pregnancy was associated with a higher risk of adverse neonatal outcomes when compared with buprenorphine (5). However, the neuronal development of foetuses has not been extensively studied. Pregnant women are rarely included in clinical studies due to being classified as a vulnerable group (6), which is problematic in the light of assessing the safety of the use of drugs during pregnancy. Therefore, there is a need for good *in vitro* and *in vivo* models that can simulate the effects of drugs used during pregnancy.

1.1 Opioids

Opioids are classified as drugs that mimic the opium alkaloids found in the opium poppy plant *Papaver somniferum*. These compounds can be naturally occurring in the plant, or they can be semi-synthetic or completely synthetic (7). Morphine, papaverine and codeine are some of the naturally occurring alkaloids in the poppy extract (8). In 1902, the structure of morphine was determined, which laid the foundation for discovering semi-synthetic and synthetic opioids (9). Examples of semi-synthetic opioids are oxycodone and buprenorphine, and synthetic ones are substances like fentanyl and methadone (8, 10).

The use of opium dates back to ancient times, with the earliest known reference originating from Sumeria around 3,400 BC, where the opium poppy plant was referred to as "the joy plant" (7, 11). Today, opioids are used as prescription medications or illegal drugs. Commonly prescribed opioids include oxycodone, morphine, codeine, methadone, and fentanyl, whereas heroin is an example of an illegal opioid. Although opioids are primarily utilised in the medical field for pain management, their ability to induce euphoria makes them a popular recreational drug as well. Recreational use of heroin is associated with numerous

problems, including high societal costs, increased crime, and a significant risk of overdose (12, 13). However, opioid maintenance treatment (OMT), known as "legemiddelassistert rehabilitering" in Norway, offers a potential solution. Patients undergoing OMT receive a substitute for heroin in a specific dosage to treat abstinence symptoms which lowers the risk of overdose (14).

1.1.1 The opioid receptors and their endogenous ligands

Opioids work by binding to specific receptors, the most important ones being the three opioid receptors mu (MOR), delta (DOR), and kappa (KOR) (8). Opioids used as analgesics are full agonists or partial agonists of the mu-opioid receptor. The opioid receptors are G-protein coupled, and when opioids bind to them, they lower neurotransmitter release involved in nociception and reduce neuronal excitability, which can affect neurodevelopment (15, 16). All three opioid receptors promote analgesia when binding ligands. Additionally, the binding of ligands to MOR controls many other different physiological functions, such as memory, respiration, mood (euphoria), dependence and motivation (17, 18). Of the three opioid receptors, MOR is the most abundant in the CNS, and MOR agonists are therefore often regarded among the most powerful analgesics (19, 20). The binding of ligands to KOR promotes dysphoria, whereas DOR plays a role in gastric motility (21). The NC-IUPHAR nomenclature for the opioid receptors are MOP, DOP, and KOP (derived from *o*pioid *p*eptide) (22), but in this thesis, they will be called MOR, DOR, and KOR (derived from *o*pioid *r*eceptor).

The main function of the opioid receptors is to bind endogenous opioid peptides, such as endorphins, dynorphins and enkephalins, to relieve pain. The enkephalin peptides, such as met-enkephalin and leu-enkephalin, are derived from the precursor proenkephalin (PENK) (23), whereas the dynorphins are derived from the precursor prodynorphin (PDYN) (21). The enkephalins and dynorphins bind to the three opioid receptors with different affinities (23). The endogenous dynorphins have a high affinity to KOR (24), whereas enkephalins have a high affinity to DOR, and MOR to some degree. The endorphins, derived from Proopiomelanocortin (POMC), have a high affinity to MOR (21) but are not studied in this thesis. The opioid peptides and the opioid receptors are illustrated in Figure 1.1. The figure also presents the effects of the binding to each type of receptor. Dynorphins are believed to have a regulatory role in many different pathways in the central nervous system, including

binding of NMDA receptors (24). Met-enkephalin has been shown to play a role in cell proliferation (25).

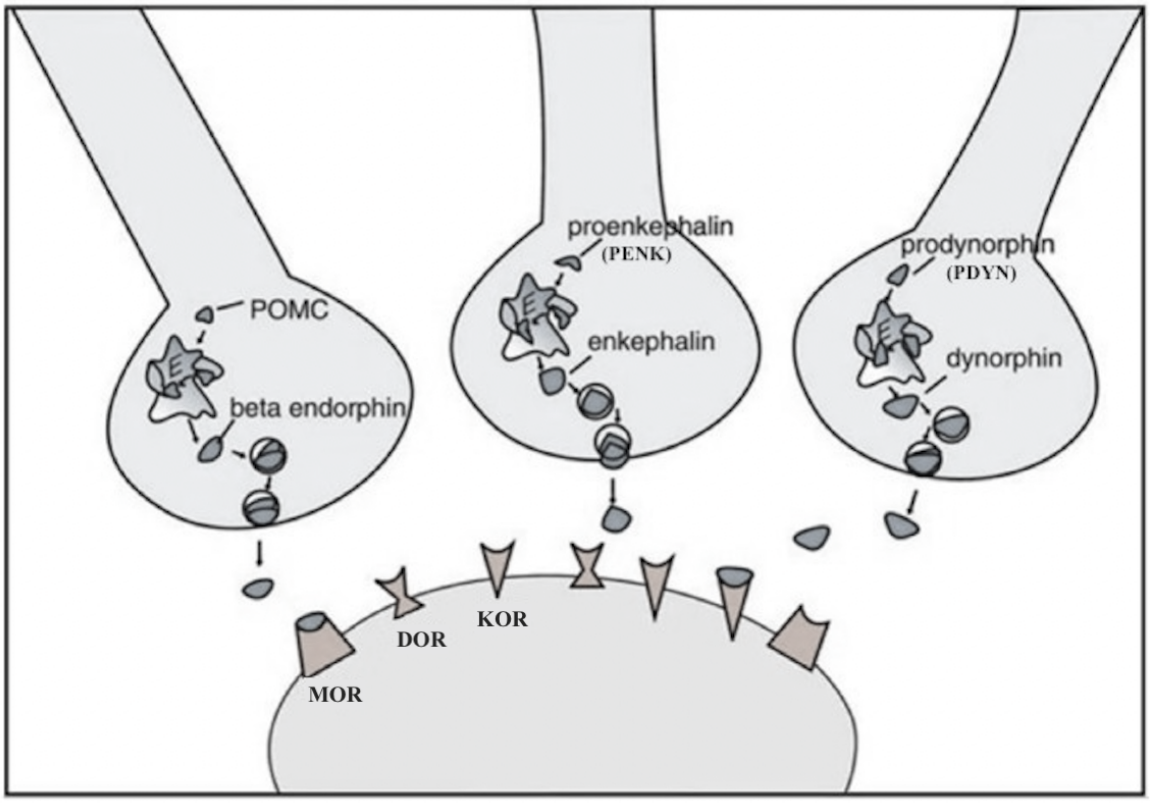

Genes encoding opioid-related peptides:	Main peptide:	Receptor:	Effects:
POMC	beta-endorphin	μ (MOR)	Euphoria Constipation
	met-enkephalin		Analgesia Respiratory depression
Proenkephalin (PENK)	met-enkephalin leu-enkephalin	δ (DOR)	Euphoria Analgesia
Prodyrnophin (PDYN)	dynorphin A or B neoendorphin	κ (KOR)	Dysphoria Analgesia

Figure 1.1: The endogenous opioid neurotransmitters and their receptors. The dynorphins, derived from PDYN, bind to KOR, whereas the endorphins, derived from POMC, bind to MOR. The enkephalins, derived from PENK, bind mostly to DOR, apart from met-enkephalin, which binds to both MOR and DOR. The effect of the binding is also listed to the right. The figure is obtained and modified from (26).

1.1.2 Morphine

Morphine is a natural alkaloid found in the opium poppy plant and was discovered in the early 19th century by Friedrich Sertüner, a German pharmacist who worked with opium (27). He managed to isolate morphine from the poppy plant, and morphine quickly became more commonly used for pain management because of its high potency compared with opium (11). Today, morphine is often prescribed for postoperative pain or pain associated with other medical conditions and is administered as tablets, injections, drops and mixtures in Norway (28, 29). In the serum, 0.12 μM is the upper reference limit after a 100 mg oral administration (30), although concentrations up to 0.27 μM have been observed (31). It is an agonist with a high affinity to MOR and is metabolised through phase 2 glucuronidation in the liver, brain, and kidneys (32, 33). Morphine is often used as the standard for opioid analgesics, and painkillers tend to be compared with morphine (8). In this study, morphine is used as a gold standard, as its effectiveness and use have been studied for a long time. The structure, molecular weight and the logP are presented in Figure 1.2.

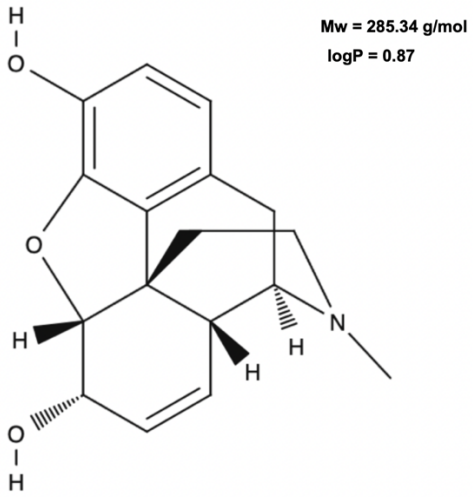

Figure 1.2: The structure of morphine. The molecular weight of morphine is 285.34 g/mol, and logP is 0.87 (34).

1.1.3 Methadone

Methadone is a synthetic opioid that is commonly used in OMT in Norway (14). It has a longer half-life than many other opioids and is a better substitute for heroin as it prevents withdrawal symptoms for longer. The half-life of methadone is longer than that of buprenorphine, which is another opioid used for the treatment of opioid dependence (35). Methadone is a full opioid agonist of MOR, whereas buprenorphine is only a partial opioid agonist. Notably, methadone differs from other opioids in that it is also an N-methyl-D-aspartate (NMDA) receptor antagonist (14, 36). Due to these differences, methadone is often preferred by patients, whereas buprenorphine is the preferred choice for prescribing doctors (14).

According to Fürst laboratory, the serum concentration in patients using methadone for OMT should be around 600-1200 nmol/L (0.6-1.2 μM) (37). Plasma-peak concentration when taken orally is around 2.5-4.4 hours (38, 39). The structure, molecular weight and logP of methadone are illustrated in Figure 1.3. The main metabolising enzyme of methadone is CYP3A4, which mediates oxidation and creates the main metabolite EDDP (2-Ethylidene-1,5-Dimethyl-3,3-Diphenylpyrrolidine) (40).

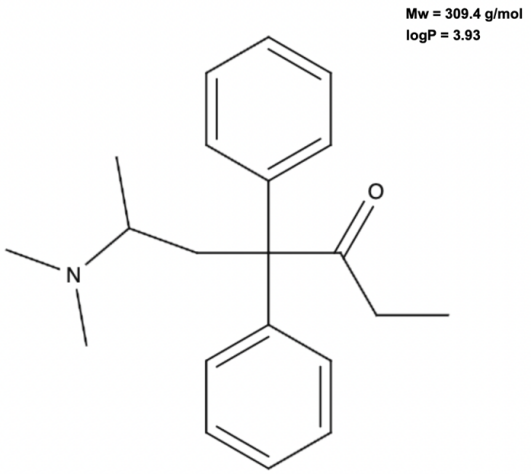

Figure 1.3: The structure of methadone. The molecular weight of methadone is 309.4 g/mol, and logP is 3.93 (41).

1.2 Opioids during pregnancy

Opioid use during pregnancy is associated with a range of negative effects on newborns, such as developing neonatal abstinence syndrome (42). Research has shown that foetal exposure to opioids during pregnancy can cause changes in brain structure and function, which can impact cognitive, behavioural, and emotional functioning. Additionally, studies have shown that foetal opioid exposure is associated with an increased risk of neurodevelopmental disorders such as autism and attention deficit hyperactivity disorder (ADHD) (43, 44). Opioids have been observed to rapidly pass the placenta, taking less than an hour to do so (45), and they cross the blood-brain barrier (BBB) of the foetus (46). Both methadone and morphine cross the placenta and enter the foetal bloodstream (47), which leads to rapid exposure of the foetus. Although there is a risk associated with the use of methadone during pregnancy, it is the better option for both the mother and child compared with continuing heroin use (48).

Because of the complexity of brain development, using clinical cohorts to understand the effects of opioid exposure during pregnancy is difficult (49). Additionally, opioid abuse is often associated with malnutrition and low socioeconomic status (50, 51), which may act as confounding factors. Therefore, animal studies are required. Prenatal morphine exposure has been linked to impaired memory in female rats (52), and in rat embryos, it has been linked to disruption of the migration and survival of neurons (53). Moreover, exposure has been linked to the alteration of the opioid receptor density (46). Nevertheless, further research is needed to better understand the exact mechanisms of how opioids affect neuronal development.

1.3 Development of the nervous system

Embryonic development starts at conception and lasts through gestational week 8 (54). During this time, the central nervous system (CNS) starts developing (54), with the first critical event being the formation of the neural tube – also known as neurulation (55). Putting it simply, there are four main processes that are crucial for the development of the nervous system: cell proliferation, differentiation, migration, and apoptosis. The development is a complex system, and the time for each process can influence the later developmental events (56). This also makes the development of the CNS very vulnerable. In the third week of gestation, neural progenitor cells start differentiating. On embryonic day 42, neurons start forming, and around mid-gestation, the process is almost finished (57). During this time, the

cells proliferate, differentiate, and migrate to the forebrain, midbrain, and hindbrain. After differentiating into neurons, they become postmitotic and unable to proliferate (54). Apoptosis serves to eliminate excess neurons (58) and occurs both pre- and postnatally (59). Another important part of the development is synaptogenesis. Since neurons rely on synapses to relay information, synaptogenesis plays a significant role in the proper functioning of the brain. A timeline of the development is presented in Figure 1.4. Chapter 1.3.2 provides more information on various molecules and receptors that are critical for neurodevelopment.

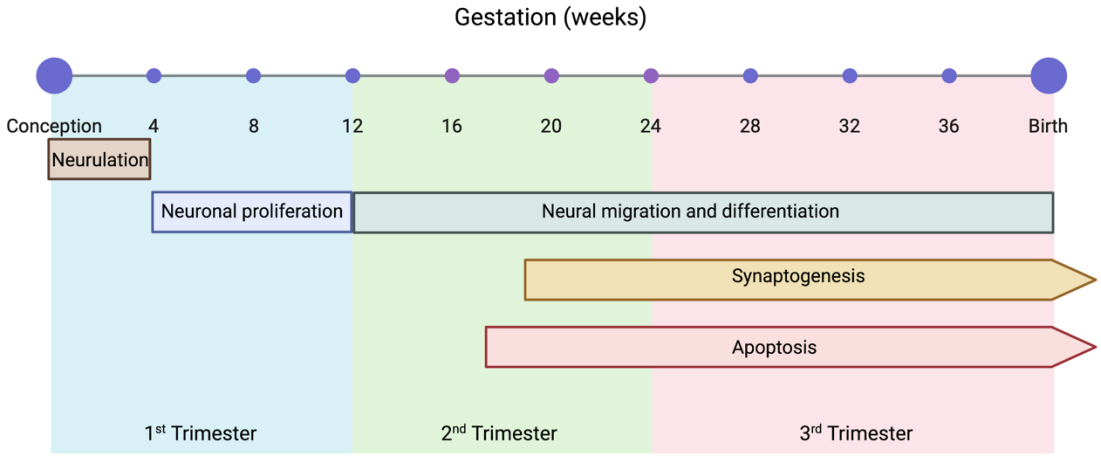

Figure 1.4: A schematic timeline of the important aspects of the development of the CNS during the human gestation period. During the first four weeks, neurulation commences. Proliferation is important in the first trimester, and neuronal migration, differentiation, synaptogenesis and apoptosis are important in the second and third trimesters. Arrows on synaptogenesis and apoptosis indicate that this continues after birth. The figure was made with Biorender and is based on a figure from (60).

1.3.1 The cerebellum

The cerebellum, situated under the occipital lobe, is the largest part of the hindbrain (61, 62). Although it constitutes only 10% of the total weight of the brain, it contains over half of its neurons. Among these, cerebellar granule neurons are the most abundant, constituting 90% of all cerebellar neurons and forming the brain's largest homogeneous neuronal population (63). The cerebellum mainly regulates movement-related functions such as posture, balance, and coordination (64) but also contributes to cognitive processes such as language, attention, emotion, and executive functions (65, 66). Furthermore, the similarity of the cerebellum across species and the presence of all stages of development in a small time window makes it an excellent model for toxicology studies (67).

The cerebellum has three distinct layers in the cortex; the molecular layer (ML), the Purkinje cell layer (PCL) and the internal granular layer (IGL). During development, the cerebellum also includes a temporary layer known as the external germinal layer (EGL), which disappears postnatally (58). This is where progenitor granule cells are produced before they migrate to the ML (68). The cells then migrate to the PCL, where they differentiate before migrating further into the IGL. In the IGL, the cells mature into cerebellar granule neurons. The layers of the adult cerebellum are presented in Figure 1.5.

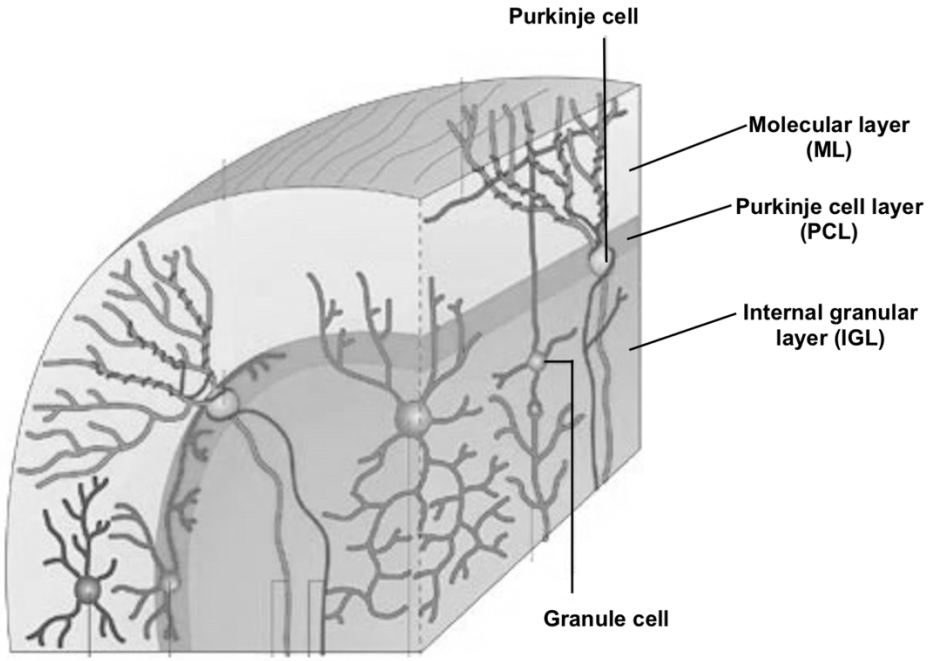

Figure 1.5: The adult cerebellar cortex and its three distinct layers. The cortex is made up of the molecular layer (ML), Purkinje cell layer (PCL) and internal granular layer (IGL). A Purkinje cell can be seen in the PCL, and a granule cell in the IGL. The figure is obtained and modified from (69).

1.3.2 Receptors and molecules important for neuronal development

The opioid receptors and the NMDA receptor have been linked to controlling various processes in neurodevelopment. Sustained signalling through the opioid receptors is associated with reductions in proliferation, survival, neuronal plasticity, and differentiation (16). The NMDA receptor is a glutamatergic receptor important for neuronal plasticity, differentiation, migration, and synaptogenesis (70, 71). The NMDA receptor consists of three subunits: GluN1, GluN2 and GluN3 (72). Subunit GluN2 is coded by four genes, where one of them is GluN2B (73). At the end of gestation, GluN2B expression is high compared with

the other subunits, whereas expression of the other subunits increases postnatally (70). This makes GluN2B a relevant subunit to study during neurodevelopment.

Brain-derived neurotrophic factor (BDNF) and its receptor tyrosine kinase B (TrkB) is associated with neuronal differentiation (74), maturation (75), and survival (76). The binding of BDNF to TrkB is also associated with the production of cAMP response-element binding protein (CREB) (77). This protein family is divided into many subtypes, with one of them being CREB1. CREB is a transcription factor involved in regulating the expression of genes (78) and cellular processes like proliferation and survival (79).

Neurotrophin receptor $p75^{NTR}$ is associated with survival and apoptosis in the CNS, therefore contributing to the development and maintenance of the nervous system (80, 81). The $P75^{NTR}$-Trk complex supports pro-survival and pro-growth signalling when mature neurotrophins bind. However, if a pro-neurotrophin, such as pro-BDNF, binds to the $P75^{NTR}$-sortilin complex, it leads to signalling pathways of apoptosis and death (80, 82).

In toxicology studies, it is important to determine what regulates the toxic effects on neuronal development. By blocking signals that promote survival and apoptosis, one can study if this causes any changes in the effect of the drug. In this case, it is interesting to study if opioids affect BDNF expression and if the addition of an inhibitor of TrkB while being exposed to the opioids may affect the survival of the cells. Such an inhibitor is, for instance, ANA-12, a TrkB receptor antagonist, and inhibits receptor activation caused by BDNF binding (83). When adding an inhibitor of $P75^{NTR}$, such as TAT-Pep5, the signalling pathway that leads to apoptosis is inhibited (84). This makes it possible to study the effects of drugs when an important receptor regulating apoptosis is blocked. If the blocking of this receptor reverses the toxic effect of a drug, it might indicate that apoptosis due to the toxicity is regulated by $p75^{NTR}$. A simplified illustration of the signalling through the $p75^{NTR}$ and TrkB receptors can be seen in Figure 1.6.

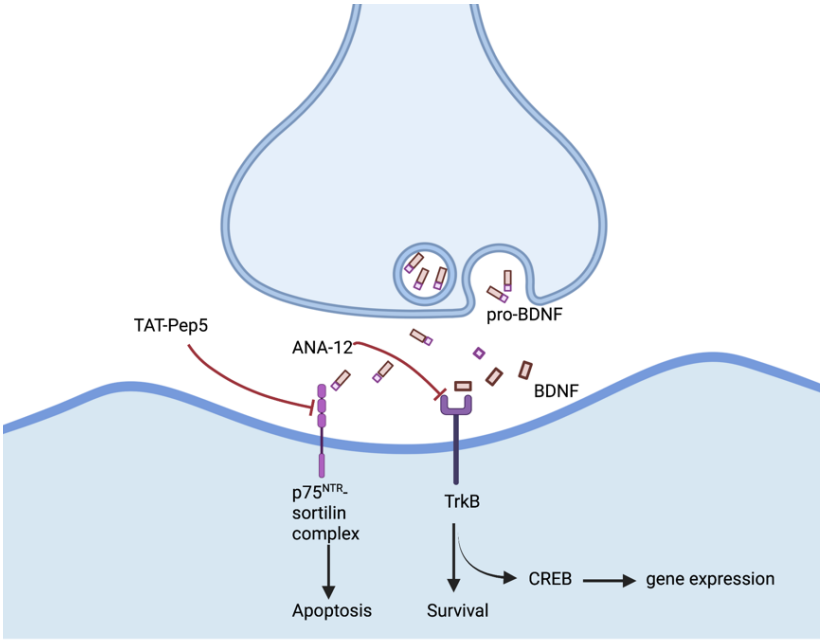

Figure 1.6: A simplified illustration of the TrkB receptor and p75^{NTR} signalling. Pro-BDNF binds to the p75^{NTR}-sortilin complex, which promotes apoptosis. This receptor can be inhibited by TAT-Pep5. BDNF binds to the TrkB receptor, which promotes survival and activates a signalling cascade promoting CREB, which will affect gene expression. The TrkB receptor can be inhibited by ANA-12. The illustration was made with Biorender.

1.3.3 The blood-brain barrier

The blood vessels of the brain are lined with endothelial cells that regulate the entry of substances into the brain. These cells are distinguished from other endothelial cells by their tight junctions, which limit the movement of ions and molecules between the blood and the brain, and constitute the blood-brain barrier (BBB) (85). Although the BBB is not impenetrable, the transport of molecules across it is restricted to certain types. These include small lipophilic molecules that can cross by passive diffusion, molecules that are actively transported across the membrane, and molecules that use receptor-mediated transport (86). Another important aspect of the BBB is that it is high in p-glycoprotein, which is an efflux pump and is considered an important restricting factor in the uptake of drugs into the brain (87). Before the BBB is fully developed, the permeability to the brain is higher. This can result in higher concentrations of drugs in the developing brain of the foetus when the mother takes opioids during pregnancy.

Methadone and morphine, which are relatively small and lipophilic, cross the BBB through passive diffusion driven by the concentration gradient between the blood and the brain (86). The ability of a drug to diffuse passively across the BBB can be determined by Lipinski's Rule of Five, which takes into account the molecular weight, logP, hydrogen bond acceptors, and hydrogen bond donors of a substance (88). The rules are that molecules should not have >10 hydrogen bond acceptors, >5 hydrogen bond donors, a molecular weight >500 Da and a logP >5 (89). It has been observed that opioids with higher logP values have higher concentrations in the brain (88, 90), ideally between 1.5 to 2.5.

1.4 Model systems

1.4.1 The chicken model

When conducting animal research, it is important to consider the ethical implications of animal experimentation, as the animals may be subjected to various procedures that may cause pain, distress, or harm. Therefore, researchers must strive to minimise the impact of animal research by adhering to the principles of the Three Rs - reduction, replacement, and refinement (91). One way to minimise the impact is to use alternative animal models that reduce the number of animals involved or avoid using certain animals altogether. For example, the chicken model can be a useful alternative to other animal models in studying the teratogenic effects of opioids, as it allows for an exact number of eggs to be ordered and avoids exposing the mother to experimentation.

The chicken model has been extensively used for studying teratogenicity and developmental toxicology. Compared to humans, chickens have a shorter gestation period and faster development of the cerebellum (92). The chicken hatches after 21 days of incubation, whereas the human gestation takes approximately 40 weeks. Towards the end of gestation, both humans and chickens experience rapid cerebellar development, but the chicken cerebellum develops at a faster rate, illustrated in Figure 1.7. This results in the chicken having a more morphologically developed cerebellum than the human foetus at the end of gestation.

The presence of MOR, DOR, and KOR (93, 94), as well as the expression of the PENK gene (95), makes the chicken model a valuable tool in studying the teratogenicity of opioids. Furthermore, the expression of the NMDA receptor and CYP3A4 enzyme makes this model

particularly useful for investigating the toxic and pharmacokinetic effects of methadone (92, 96). In addition, the chicken model is useful for the study of opioids as it can be employed for both *in vivo* and *in vitro* exposures. The cells for the cerebellum cultured *in vitro* display similarities to those present in the EGL and gradually differentiate into cells resembling those found in the IGL. This makes the *in vitro* model a useful tool for studying exposure during development.

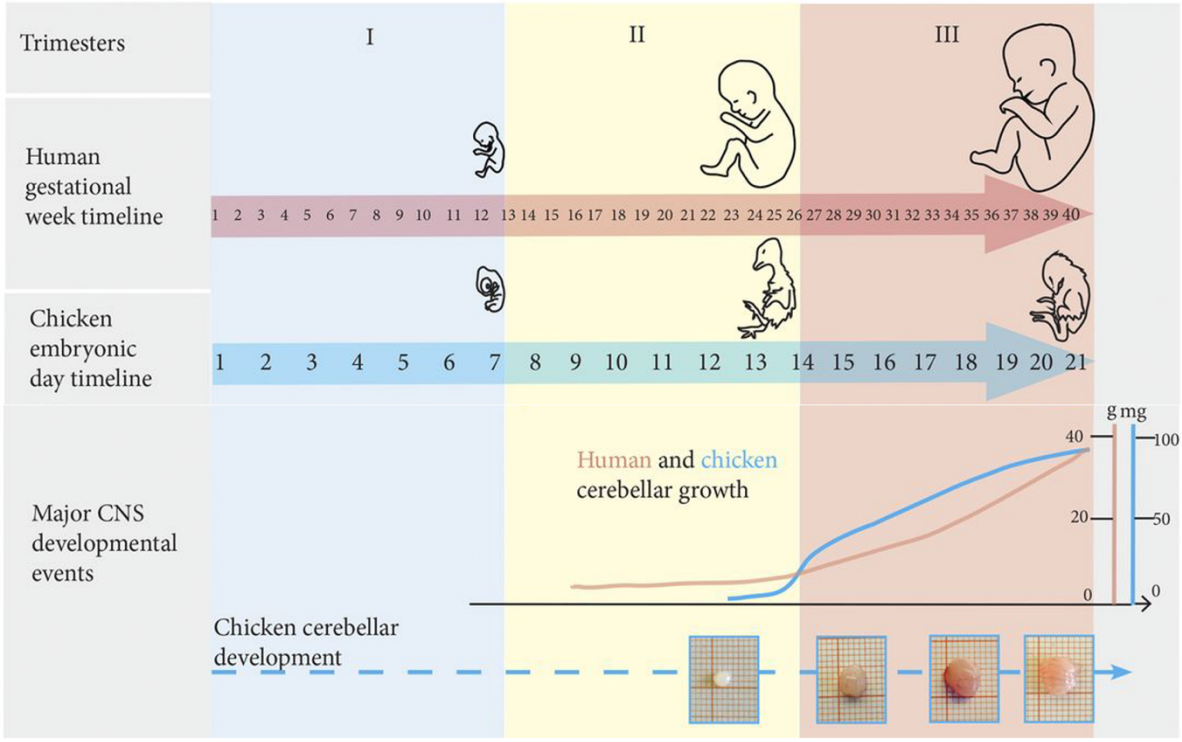

Figure 1.7: The development of the human and chicken embryo. The development of the cerebellum in chickens is faster than in humans, and the gestation period is shorter. The figure is obtained and modified from (92).

1.4.2 PC12 cells

The PC12 cell line, derived from a rat adrenal medulla pheochromocytoma, is an established immortalised cell line that has been extensively used in neurotoxicity research (97). These cells are easily maintained and proliferate rapidly. Moreover, they can be differentiated into sympathetic ganglion neurons with nerve growth factor (NGF), which induces neurite outgrowth and stops cell proliferation. Upon differentiation, the PC12 cells exhibit characteristics similar to dopaminergic neurons (97). Additionally, the cell line expresses KOR, as well as the genes encoding PENK and PDYN (98). However, the model lacks

knowledge of the presence of MOR and DOR, resulting in MOR usually being transfected into the cell line if needed (99, 100).

1.5 The aim of the study

Although some effects of methadone on neuronal development have been observed postnatally, its impact on early neuronal development has not been thoroughly studied. To gain a better understanding of the potential effects of methadone on human neuronal development, further research is necessary. Studying the effects of methadone and morphine in a wider range of models, including animal and *in vitro* models, could enhance the applicability of the findings to human neuronal development and help to identify any species-specific differences. The aim of the thesis is to study the effect of methadone and morphine on neuronal development *in vitro*, as well as to establish methadone concentrations *in vivo*. The hypothesis is that methadone exposure affects neuronal development.

The secondary aims are:

- Examining the effects of methadone and morphine on neuronal viability.
- Examining the effects on neurite outgrowth and synaptogenesis.
- Examining the expression of genes encoding proteins important for signalling pathways and metabolism; MOR, DOR, KOR, PENK, PDYN, BDNF, CREB1, GluN2B, and CYP3A4.
- Determining the distribution of methadone and the main metabolite EDDP in the chicken embryo.

2 Materials and methods

2.1 Products and materials.

General laboratory equipment, such as pipettes, distilled water, Milli-Q water (MQ water), etc., is not listed in Table 2.1 and Table 2.2.

Table 2.1 Chemicals and biological products	
Product:	**Producer:**
2-Mercapotethanol 50 mM, Gibco™	Thermo Fisher Scientific, Rockford, USA
Acetonitrile (ACN)	Thermo Fisher Scientific, Rockford, USA
Ammonium formate, VWR®	Avantor, Radnor, USA
ANA-12 (SML0209)	Sigma Aldrich, St. Louis, USA
Anti-MAP2 antibody, chicken, (ab5392)	Abcam, Cambridge, UK
Anti-PSD95 antibody [7E3-1B8] - Synaptic Marker, mouse, (ab13552)	Abcam, Cambridge, UK
Anti-Synaptophysin (SYP) antibody, rabbit, (ab14692)	Abcam, Cambridge, UK
Basal Medium Eagle (BME), Gibco™	Thermo Fisher Scientific, Rockford, USA
Bovine Serum Albumin (BSA) (Lyophilized powder)	Cytiva, Logan, USA
Bovine Serum Albumin Solution (BSA), 35%, Merck.	Sigma Aldrich, St. Louis, USA
Buffer RLT Plus RNeasy® Plus lysis buffer	Qiagen, Hilden, Germany
Buffer RPE Wash buffer	Qiagen, Hilden, Germany
Buffer RW1 Wash buffer	Qiagen, Hilden, Germany
$CaCl_2$	Sigma Aldrich, St. Louis, USA
Chicken serum, Gibco™	Thermo Fisher Scientific, Rockford, USA
DAPI Solution (1 mg/mL) (62248)	Thermo Fisher Scientific, Rockford, USA
Deoxyriconuclease I (DNase) from bovine pancreas	Sigma-Aldrich, St. Louis, USA
Dimethyl sulfoxide (DMSO)	Sigma-Aldrich, St. Louis, USA

DPBS 1x (PBS+), + $MgCl_2$ + $CaCl_2$, Dulbecco's Phosphate buffered Saline, Gibco™	Sigma Aldrich, St. Louis, USA
Dulbecco's Modified Eagle Medium (DMEM), Gibco™	Thermo Fisher Scientific, Rockford, USA
EDDP perchlorate	Chiron AS, Trondheim, Norway
EDDP-d3 perchlorate	Chiron AS, Trondheim, Norway
Fetal bovine serum (FBS)	Biowest, Nuaillé, France
Formaldehyde solution 4 %	Sigma-Aldrich, St. Louis, USA
Goat anti-chicken IgY H&L DyLight 488 (ab96951)	Abcam, Cambridge, UK
Goat anti-mouse IgG H&L DyLight 550 (ab96880)	Abcam, Cambridge, UK
Goat anti-Rabbit IgG H&L DyLight 650 (ab96902)	Abcam, Cambridge, UK
H-Transferrin	Sigma Aldrich, St. Louis, USA
High Capacity RNA-to-cDNA Kit	Thermo Fisher Scientific, Rockford, USA
Horse serum, Gibco™	Thermo Fisher Scientific, Rockford, USA
Hydrogen peroxide solution 30 % (H_2O_2)	Sigma-Aldrich, St. Louis, USA
Insulin I5500, from bovine pancreas	Sigma-Aldrich, St. Louis, USA
L-Glutamine	Sigma-Aldrich, St. Louis, USA
Methadone hydrochloride	Chiron AS, Trondheim, Norway
Methadone-13C6 hydrochloride	Chiron AS, Trondheim, Norway
Methanol (MeOH) LiChrosolv®, Supelco®	Sigma Aldrich, St. Louis, USA
$MgSO_4$	Sigma-Aldrich, St. Louis, USA
Nerve Growth Factor (NGF)	Sigma Aldrich, St. Louis, USA
Nitric acid (HNO_3), VWR®	Avantor, Radnor, USA
$p75^{NTR}$ Signaling Inhibitor, Cell-permeable, TAT-Pep5	Sigma Aldrich, St. Louis, USA
Penicillin-Streptomycin (10000 U/mL / 10000 µg/mL), Gibco™	Thermo Fisher Scientific, Rockford, USA
Poly-L-lysine hydrobromide (PLL)	Sigma-Aldrich, St. Louis, USA
Potassium chloride (KCl)	Sigma-Aldrich, St. Louis, USA

*Power*SYBR® green PCR Master Mix (4367659)	Thermo Fisher Scientific, Rockford, USA
Putrescine	Sigma-Aldrich, St. Louis, USA
RNase-Free Water	Qiagen, Hilden, Germany
RT buffer Mix (2X)	Thermo Fisher Scientific, Rockford, USA
RT Enzyme Mix (20X)	Thermo Fisher Scientific, Rockford, USA
Sodium pyruvate, Gibco	Thermo Fisher Scientific, Rockford, USA
Sodium selenite (Na_2SeO_3)	Sigma-Aldrich, St. Louis, USA
Thiazolyl Blue Tetrazolium Bromide, MTT (3-(4,5-dimethylthiazol-2-yl)-2,5-diphenyltetrazolium bromide)	Sigma-Aldrich, St. Louis, USA
Triiodo-L-thyronine sodium salt (T_3)	Sigma Aldrich, St. Louis, USA
Triton X-100 solution, 10%, BioUltra	Sigma Aldrich, St. Louis, USA
Trypsin from bovine pancreas	Sigma-Aldrich, St. Louis, USA
Trypsin inhibitor (soybean)	Sigma-Aldrich, St. Louis, USA

Table 2.2 Instruments and equipment	
Product:	**Producer:**
2720 Thermal cycler, Applied Biosystems®	Thermo Scientific, Waltham, USA
96-well plate (0.1 ml) for qPCR	BIOplastics BV, Landgraaf, Netherlands
Allegra X-15R Centrifuge	Beckman Coulter, Indianapolis, USA
Aquite UPLC® BEH C18 1.7 µM, 2.1x50mm	Waters, Milford, USA
Aquity UPLC® with Xevo TQ-S Triple Quadrupole Mass Spectrometer	Waters, Milford, USA
Captiva EMR – Lipid, 40 mg	Agilent Technologies, Santa Clara, California, United States
Cell culture plate, 6 well	Sarstedt, Nümbrecht, Germany
CellInsight CX7 Laser	Thermo Scientific, Bothell, USA
CFX96™ Touch Real-Time PCR Detector System	Bio-Rad Laboratories, Hercules, USA
CLARIOstar® plate reader	BMG Labtech, Ortenberg, Germany

Corning® BioCoat® Poly-D-Lysine 96-Well Plates	Corning, New York, USA
PELLET PESTLE® Cordless motor	Kimble Chase, Vineland, USA
IncuCyte®	Essen BioScience, USA
U-100 Insulin syringe (0.5 ml)	B. Braun, Melsungen, Germany
Kubota 2010 Centrifuge	Kubota Corp., Japan
Laminar flow hood (Holten LaminAir, model 1.2)	Eco Holten AS, Denmark
LightCycler® 480 Sealing Foil	Roche, Basel, Switzerland
Multi-Tube Vortexer (VX-2500), VWR®	Avantor, Radnor, USA
Multiply®-µStrip 0.2 ml chain	Sarstedt, Nümbrecht, Germany
NanoDrop™ Lite Spectrophotometer	Thermo Fisher Scientific, Rockford, USA
Neubauer 0.100 mm Tiefe Depth Profondeur	Assistant, Germany
Nunc™ Cell culture flask (75 cm^2)	Thermo Scientific, Waltham, USA
Nunc™ Clear 96-well Plates	Thermo Scientific, Waltham, USA
OvaEasy 380 Advance EXII incubator	Brinsea, Weston-super-Mare, UK
RNeasy® Plus Mini Kit (250)	Qiagen, Hilden, Germany
ROTINA 420R Centrifuge	Hettich, Tuttlingen, Germany
SPE Dry 96 Solvent Evaporator	Biotage, Uppsala, Sweden
Sterile filter (0.2 µm)	Whatman, Germany
Sub Aqua 12 water bath	Grant Instruments, Royston, UK
TPP® tissue culture plates, 96-well plate	Sigma Aldrich, St. Louis, USA
Whirl mixer	Terumo lab AS, Sweden

2.2 PC12 cells

The immortalised PC12 cell line consists of cells derived from a rat pheochromocytoma in the adrenal medulla (97). The cells were maintained in PC12-medium (Appendix A, Table 7.1) and split into new passages twice a week. When splitting, the cells were dislodged by hitting the sides of the cell culture flask. This eliminated the need for trypsin, which might be beneficial for the cell culture as trypsin is known to have damaging effects on cells after long-term exposure (101). After dislodging the cells, 10-15% of the cell suspension was transferred to a new flask or back to the old flask. The passages used in these experiments ranged from P5 to P9. A detailed protocol for splitting the cells into new passages can be found in Appendix B 8.1.

The cells were used for experiments in 96-well plates with a density of $7 \cdot 10^4$ cells/mL. The density of the cells from the flask was calculated by counting the cells in a Neubauer haemocytometer and then diluted to the desired density. Then the cells were seeded onto the plate with 0.2 mL in each well, equivalent to 14,000 cells in each well. A detailed protocol for splitting the cells and seeding them onto plates can be found in Appendix B 8.2. Some cells were left undifferentiated, and others were differentiated with nerve growth factor (NGF) while being exposed to drugs. The differentiated cells required a different medium that contained only 2% horse serum and no foetal bovine serum. The recipe for this can be found in Appendix A, Table 7.2.

This cell line was exposed to methadone before or during differentiation. Some cells were also exposed to the drugs with 2% horse serum (HS) media without NGF and foetal bovine serum (FBS) as a control (Appendix A, Table 7.2 without NGF). A control with regular PC12 media was also used. The methadone concentrations used were 100 µM, 10 µM and 1 µM. This was made from 100 mM stocks with the drug dissolved in MQ water.

2.3 The chicken embryo

Fertilised eggs from the chicken species *Gallus gallus domesticus* of the strain Ross 308, ordered from Nortura Samvirkekylling (Våler in Solør, Norway), were used for harvesting tissue and making cell culture. The eggs were incubated in an OvaEasy 380 Advance EXII

incubator at 45% humidity and 37.5°C with periodic cooling to simulate the hen leaving the eggs. With the automatic tilting feature, the incubator also imitates the brooding of a hen. All exposures *in ovo* were done before embryonic day 14 (E14), which is before the embryos are defined as animals in the EU Directive 2010/63/EU. Untreated animals are not covered by this regulation.

2.3.1 Preparation of chicken granule neurons for *in vitro* exposure

Eggs on E17 were submerged in ice for 7 minutes to anaesthetise them before decapitation. Removal of the cerebellum, as seen in Figure 2.1, was done under a laminar flow hood. A detailed protocol can be found in Appendix B 8.3. When plating the chicken granule neurons (CGNs), the cells were maintained in CGN plating medium (Appendix A Table 7.3). Solutions for exposure were made with the CGN feeding medium (Appendix A Table 7.4).

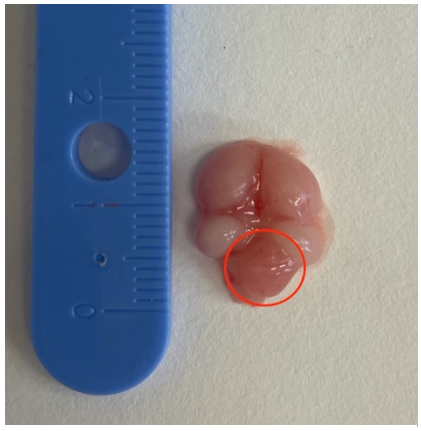

Figure 2.1: Chicken brain at embryonic day 17. The markings on the ruler to the left show the size in cm. The cerebellum is marked with a red circle.

Five different solutions were used in the preparation of the cells, and the recipes for these can be found in Appendix A, Table 7.5. The solutions are rich in bovine serum albumin (BSA), Krebs-Ringer solution, calcium, and magnesium because they provide a stable pH value and environment, as well as help maintain normal cell function. Micronutrients like calcium and magnesium are important in many cellular and biological processes (102). Krebs-Ringer solution is a saline solution, which provides the cells with fluids and salts that resemble bodily fluids and maintains normal osmolarity (103). In addition, the Krebs-Ringer solution acts as a buffer because of its physiologic pH of 7.4 and provides the cells with nutrition in the form of glucose. BSA has antioxidant properties and stabilises components in the cell culture, such as fatty acids, hormones, peptides, and amino acids (104). Solution 2 contains the enzyme trypsin, which causes enzymatic dissociation of the tissue. The trypsin cleaves peptide bonds, which helps release the cells from the tissue (105). Solution 3 contains a trypsin inhibitor to stop the enzymatic reaction to prevent the trypsin from destroying the cells. It also contains DNase, an enzyme that breaks down DNA (106). This is added to prevent cell clumping, as the stickiness of the free DNA in the cell culture causes cells and debris from cell lysates to aggregate (107).

After counting and diluting the cell suspension at the end of the preparation, the cells were seeded with a density of 1.5-1.7·10^6 cells/mL onto plates that were coated with poly-L-lysine (PLL) in advance. PLL provides an increased number of cationic binding sites for the negatively charged cell membranes (108). This improves cell attachment to the surface of the plates used, which is useful in protocols that include many steps where the cells can loosen unintentionally. A detailed protocol for coating with PLL can be found in Appendix B 8.4.

2.3.2 Injection *in ovo* for the distribution study

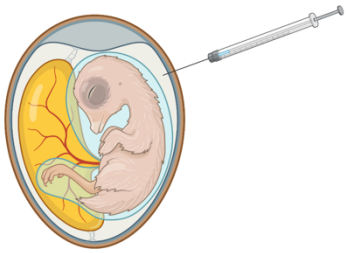

Figure 2.2: An illustration of the egg being injected at a suitable injection site. Note the injection being administered at the blunt end. Created with BioRender.com.

Injections in the eggs were done on E13. Detection of the embryo was done by candling the egg. If the embryo was determined viable, a suitable injection site was marked. A suitable injection site is determined by finding a spot to inject onto the chorioallantoic membrane, avoiding the large visible blood vessels. Moreover, the injection site should be close to smaller vessels to ensure an even distribution of the drug. Previously, injections have been administered at the pointed end of the egg. However, all injections in this study were administered in the blunt end of the egg while exercising caution to prevent injection of the air sac. This is illustrated in Figure 2.2. Before injecting, all eggs were weighed to calculate the injection volume, as the protocol is to inject 1 µL for every gram the egg weighs. Methadone (20 mg/kg) dissolved in saline was injected. A detailed protocol for *in ovo* injection can be found in Appendix B 8.5.

For the distribution study, eggs in triplicates were injected 24, 18, 12, 8, 7, 6, 5, 4, 3, 2, 1 and 0.5 hours before harvesting brains, lungs, and yolks. The first injections were done 2 hours before the last injections, except for the 18-hour time point. The injection for the 18-hour time point was done 7 hours after the first injections so that the harvesting of the tissue did not end up in the middle of the night. The experiment was done with two batches of eggs, bringing the total number of biological replicates to six per time point.

2.4 MTT in PC12 cells and chicken granule neurons

PC12 cells and chicken granule neurons were seeded onto 96-well plates with a density of 7·10^4 cells/mL and 1.5-1.7·106 cells/mL, respectively. A detailed protocol can be found in Appendix B 8.2 and 8.3. The cells were then exposed to 100 µM, 10 µM or 1 µM methadone

or morphine. Cells were also exposed to the inhibitors ANA-12 and TAT-Pep5, both in the presence and absence of the highest concentration of the drugs.

MTT (long name 3-(4,5- Dimethylthiazol-2-yl)-2,5-diphenyltetrazolium bromide) assays were used to measure the viability of the cells (109). Viable cells with active metabolism in the mitochondria will metabolise MTT and reduce them to formazan. DMSO (dimethyl sulfoxide) was used to dissolve the formazan crystals, which makes it possible to measure the absorbance (110). The plates were incubated for 3 hours at 37°C and 5% CO_2 after adding the MTT medium (Appendix A, table 7.6). Then the plates were incubated in DMSO for 30 minutes before measuring the absorbance at 570 nm using a CLARIOstar® plate reader. Dead cells will not metabolise MTT. An increased production of formazan crystals is correlated with the quantity of cells with functional mitochondria and the level of mitochondrial activity within those cells. A detailed protocol on this can be found in Appendix B 8.6.

2.5 IncuCyte

Chicken granule neurons were seeded onto 96-well TPP plates with a density of $1.7 \cdot 10^6$ cells/mL. These plates have wells with a flat bottom, and the plastic is completely transparent, which is crucial for clear pictures of neurite outgrowth. The cells were then exposed to 100 µM, 10 µM or 1 µM of methadone or morphine. Some were also exposed to the inhibitors TAT-Pep5 and ANA-12, both in the presence or absence of simultaneous exposure to the highest concentration of the opioids. A detailed protocol on how the cells were seeded onto the plate can be found in Appendix B 8.3. The plates were then transported to the IncuCyte® machine borrowed at the National Institute of Occupational Health. The plates were put in the machine and the bottom vessel was filled with autoclaved distilled water. The incubator was set at 37°C and 5% CO_2. Pictures were taken every four hours for 72 hours in total.

2.6 RT-qPCR in chicken granule neurons

Chicken granule neurons were seeded onto 6-well plates with a density of $1.7 \cdot 10^6$ cells/mL. See Appendix B 8.3 for details. The cells were exposed to 100 µM, 10 µM or 1 µM of methadone or morphine for 72 hours. Lysis of the cells was done with the RLT Lysis buffer from the RNeasy® Plus Mini kit (Appendix A, Table 7.7). A detailed protocol for this can be found in Appendix B 8.7. RNA from the samples was isolated by using the same kit and a

detailed protocol for this can be found in Appendix B 8.8. NanoDrop™ Lite Spectrophotometer was used to measure the RNA concentration and purity degree in the samples before dilution. Absorbance was set to 260/280 nm, and purity degrees ranged from 1.99 to 2.41. A value of approximately 2.0 is regarded as "pure" RNA (111). Purity degrees higher than 2.11 were only observed in the samples exposed to 100 µM methadone. Conversion from RNA to cDNA was done in qPCR tubes, and the enzyme master mix used for this can be found in Appendix A, Table 7.8. In the 96-well qPCR plates, 3 µL of the samples were added to each well. The rest of the samples were frozen at -20°C. The SYBR® Green master mix was made by mixing SYBR® Green with reverse primer and forward primer for the studied genes (Appendix A Table 7.9). The plate was then sealed with LightCycler® 480 sealing foil and centrifuged with ROTINA 420R at 1000 rpm for 1 minute before doing RT-qPCR. A detailed protocol for the conversion and analysis with RT-qPCR can be found in Appendix B 8.9.

GAPDH was used as an internal control. By adding the housekeeping gene, it is possible to normalise the amount of RNA added to every reaction (112). RT-qPCR is a quantitative method, and normalising the amount is crucial for reliable results. The level of expression of the selected genes was determined through the calculation of relative quantification between the selected genes and the housekeeping gene. The selected genes were MOR, DOR, KOR, PENK, PDYN, BDNF, CREB1, GluN2B and CYP3A4.

2.7 High-content imaging in chicken granule neurons

A pilot on high-content imaging was conducted in CGNs to assess the synapses. Chicken granule neurons were seeded onto Corning® BioCoat® Poly-D-Lysine 96 Well plates at a density of $1.7 \cdot 10^6$ cells/mL. The cells were exposed to the control containing 1 ‰ MQ water or two concentrations of methadone or morphine (1 µM, 10 µM). After 72 hours, the cells were fixed using 4% formaldehyde and stored in PBS at 4°C until staining. The protocol from the Norwegian Institute of Public Health (NIPH) is to store the cells in PBS+ (PBS with calcium and magnesium). However, the PBS used in this pilot did not contain magnesium or calcium. The protocol for fixation can be found in Appendix B 8.10.1. The immunostaining was done with the help of Agata Antonina Rita Impellizzeri at the NIPH. The protocol for this is derived from the standard operating procedure (SOP) from NIPH and can be found in Appendix B 8.10.2. A permeabilisation buffer was used to permeabilise the cells and stain

intracellular antigens (Appendix A, Table 7.10). To reduce unspecific binding of the antibodies, a blocking buffer was used (Table 7.11). The primary antibodies used were microtubule-associated protein 2 (MAP2), postsynaptic density protein 95 (PSD95) and synaptophysin (SYP), and concentrations can be found in Appendix A, Table 7.12. The secondary antibodies used were 4′,6-diamidino-2-phenylindole (DAPI), goat-anti-chicken IgY, goat anti-mouse IgG, and goat anti-rabbit IgG, and concentrations can be found in Appendix A, Table 7.13. SYP is a pre-synaptic marker, while PSD95 is a post-synaptic marker. MAP2 is a marker for neurite outgrowth, and DAPI identifies nuclei (113). With these markers, it is possible to quantify the synapses. The high-content imaging was done in CellInsight® CX7 Laser.

2.8 Preparation of whole brains, lungs, and yolk from chickens for kinetics

2.8.1 Homogenisation of the tissue

The tubes with the tissue were snap-frozen immediately after harvesting and stored at -80°C until homogenisation. Frozen tissue was weighed in Eppendorf tubes. For the brains and lungs, MQ-water was added in a 1:1 ratio. For the yolks, MQ-water was added with a ratio of 1:2 (yolk:water). The tissue was then homogenised using an electric homogeniser with a plastic pistil. 50 µL of each homogenate was added to kinetics tubes, snap-frozen in liquid nitrogen, and stored at -80°C until further sample preparation. A detailed protocol can be found in Appendix B 8.11.

2.8.2 Sample preparation

MQ water, an internal standard, ammonium formate buffer and/or standards were added to controls, tissue controls, standards, 0-samples, and the harvested tissue samples. An overview of each sample and the concentrations for the standards and controls can be found in Appendix A, Table 7.14 and 7.15, respectively. The sample preparation was done at the Department of Forensic Science at Oslo University Hospital by Elisabeth Nerem. A detailed protocol for this can be found in Appendix B 8.12 and is derived from the department's protocol. The ammonium formate buffer in the protocol is added to the tissue samples to compensate for the ammonium formate buffer in the standards. Tissue components were

removed during centrifugation, and Captiva EMR was used to remove any remaining protein and lipids from the samples.

2.8.3 LC-MS-MS

To analyse the samples, ultra-high-performance liquid chromatography with tandem mass spectrometry (LC-MS-MS), in Acquity UPLC with Xevo TQ-S triple quadrupole MS, was used. LC-MS-MS is a qualitative and quantitative analysing technique. Firstly, the components of the sample are separated using liquid chromatography (LC). The samples are first sent through an LC column, which in this case was an Aquity UPLC® BEH C18 1.7 µm column (2.1x50 mm). The LC column is the stationary phase, and the samples are sent through it by the mobile phase flowing through at high pressure. The components in the samples interact with the stationary and mobile phases in different ways, depending on the size, charge (ionisation), and level of hydrophobicity, which then separates the components. Secondly, the samples are sent to the mass spectrometer. Here the mobile phase with the components is nebulised and ionised with electrospray ionisation (ESI), which charges the particles (precursor ions). The ions are then sent through three quadrupoles; two mass filters with electromagnetic fields and one collision cell in between (114). A specific precursor ion is selected based on the mass-charge ratio (*m/z*) in the first quadrupole. Only the targeted ion is allowed to pass when sending the precursor ions through. After this, the ions are sent to the second quadrupole – the collision cell, where the ions are fragmented into daughter ions by colliding with an inert gas. The last quadrupole targets specific daughter ions, which are then quantified (115). The principle for the MS-MS after LC is illustrated in Figure 2.3.

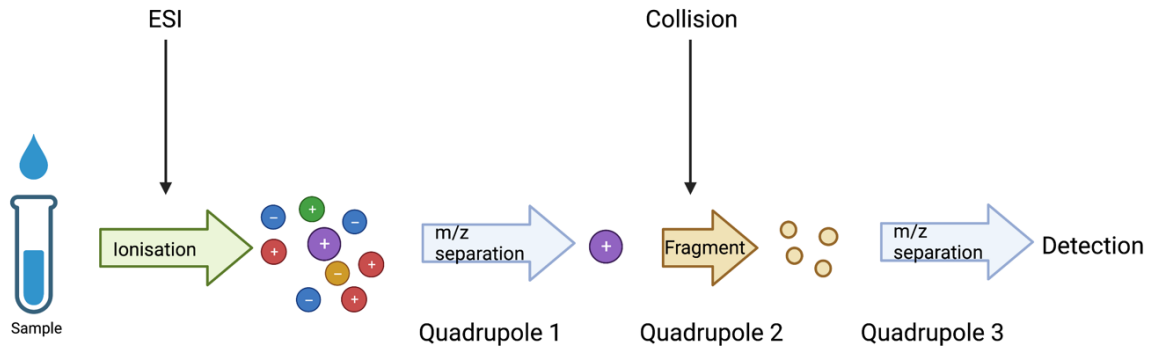

Figure 2.3: The principle for tandem mass spectrometry in Xevo TQ-S triple quadrupole MS. The figure was created with Biorender and is based on the figure in (116).

2.9 Statistics

Statistics and graphical presentations were done in GraphPad Prism 9 (Graph-Pad Software, La Jolla, CA, USA). One-way Analysis of Variance (ANOVA) was used for data with normal (Gaussian) distribution, followed by a Dunnett's *post hoc* for multiple comparisons. The non-parametric test Kruskal-Wallis by ranks (One-Way ANOVA) was used for data assumed not to have a normal distribution, followed by Dunn's *post hoc* test for multiple comparisons. To compare two groups with each other, a student t-test or Mann-Whitney's test was used. P-values < 0.05 were regarded as statistically significant.

3 Results

3.1 Viability

3.1.1 Viability of chicken granule neurons determined with MTT assay

To determine the effect of methadone and morphine on the CGNs viability, an MTT assay was utilised. The cells were exposed to 1, 10 or 100 µM methadone or morphine 24 hours after plating. Some cells were also exposed to the inhibitors TAT-Pep5 (called P75i in the figure, 100 nM) or ANA-12 (10 µM) in the presence or absence of 100 µM methadone or morphine. Approximately 68 hours after exposure, MTT was used to analyse the viability. Hydrogen peroxide (H_2O_2) was used as a positive control for cell death. The negative control was used to measure 100% viability, where the cells were exposed to feeding media with 1 ‰ MQ water to account for the effect of the solvent on viability.

Figures 3.1A and B show the results for the CGNs' viability after methadone and morphine exposure, respectively. Cells exposed to morphine did not show any significant change in viability, whereas a significant reduction in cells exposed to 100 µM methadone was observed, both in the presence and absence of inhibitors. The inhibitors alone showed no significant change in viability, although the graph for ANA-12 tends to be reduced slightly. The viability of the cells exposed to 100 µM methadone was reduced by approximately 60-70%. ANA-12 decreased the viability further, whereas no change was observed with TAT-Pep5. The positive control for cell death reduced the viability by 99%. P-values < 0.05 were regarded as statistically significant.

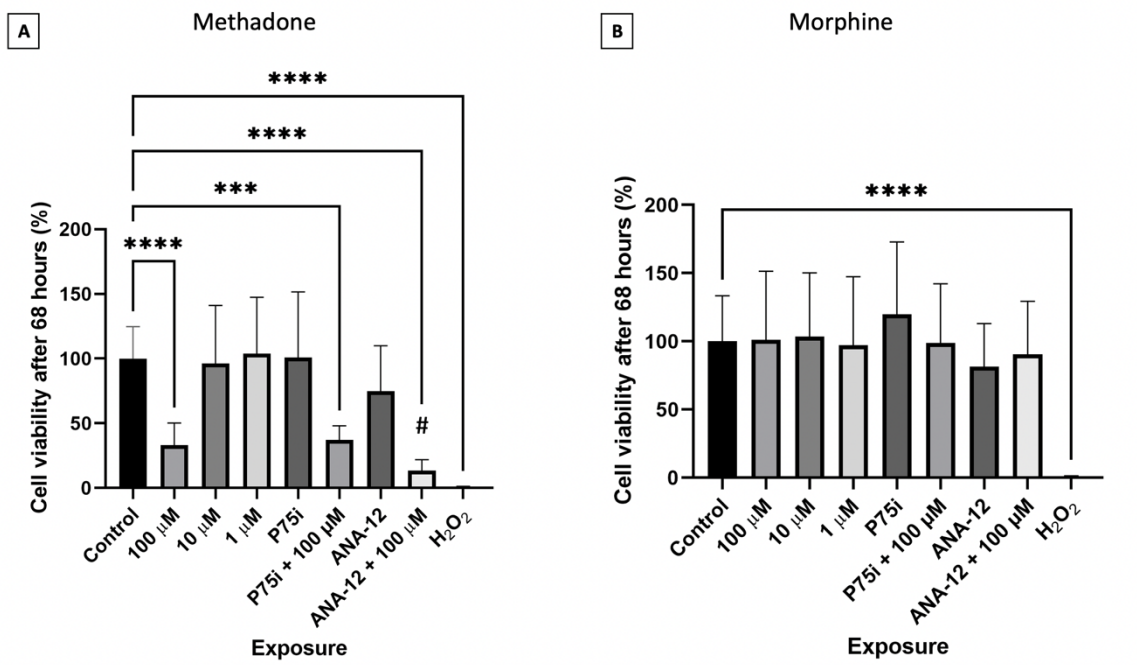

Figure 3.1: The viability of chicken granule neurons was reduced with 100 µM methadone, both in the presence and absence of inhibitors.

The chicken granule neuron cultures were exposed to methadone (1, 10 or 100 µM) or morphine (1, 10 or 100 µM) dissolved in MQ water the day after plating. Cells were also exposed to the inhibitors TAT-Pep5 (P75i, 100 nM), or ANA-12 (10 µM) in the presence or absence of 100 µM methadone. The viability was measured using an MTT assay three days (68 hours) after exposing the cells. The results are presented as the mean + SD of six and eight technical replicates from four biological replicates. All data is normalised to the control (100% viability). **A)** MTT assay results with the methadone exposures compared with the control. **B)** MTT assay results with the morphine exposures compared with the control. Three outliers were removed from **A** with ROUT (Q=1). Statistical differences were determined using Kruskal-Wallis One-Way ANOVA, followed by Dunn's *post hoc* test. Significance is denoted by $p<0.05$ (*), $p<0.01$ (**), $p<0.001$ (***) and $p<0.0001$ (****). Note the #-marking in **A**, which denotes a statistical difference between 100 µM methadone alone and in the presence of ANA-12. This was calculated using Mann-Whitney's test.

3.1.2 Viability of methadone-exposed PC12 cells determined with MTT assay

The effect of methadone on viability in PC12 cells was also studied using an MTT assay. The effect of undifferentiated cells with normal growth environment and undifferentiated cells with less growth factor was studied. Cells were also exposed to methadone during differentiation with NGF. Hydrogen peroxide (H_2O_2) was used as a positive control for cell death.

Figure 3.2A-C shows the viability of PC12 cells after methadone exposure in three different media environments. The highest concentration of methadone (100 µM) reduced the viability in all three environments, as shown in the figure. Methadone at 10 µM in the media with the low concentration of horse serum and the absence of NGF also showed a significant reduction in viability, as shown in Figure 3.2B.

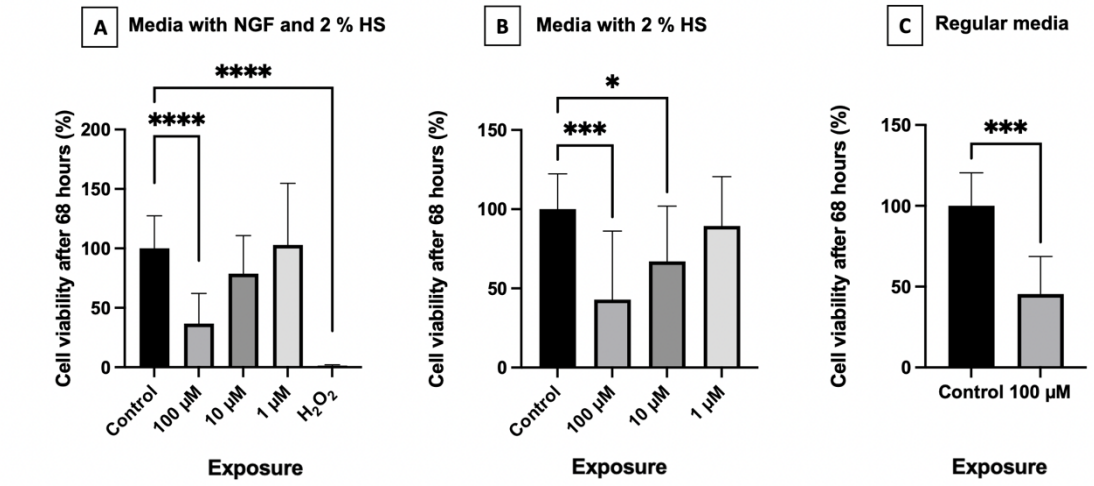

Figure 3.2: The viability of differentiated and undifferentiated PC12 cells was reduced by 100 µM methadone. The cells were exposed to methadone (1, 10 or 100 µM) in three different media environments. **A)** The media in the exposures was the PC12 differentiation medium with NGF (5 ng/mL) and a low concentration of horse serum (2%). Cells were exposed to 1, 10 and 100 µM of methadone during differentiation. **B)** The media used was similar to the PC12 differentiation medium, excluding NGF. The undifferentiated cells were exposed to 1, 10 and 100 µM of methadone. **C)** The media used was the regular PC12 media with higher concentrations of FBS (10%) and HS (5%). The undifferentiated cells were only exposed to 100 µM methadone. All values are presented as the mean + SD relative to the corresponding media control of eight technical replicates from three biological replicates. Two outliers in **C** were removed using ROUT (Q=1). Kruskal-Wallis One-Way ANOVA, followed by Dunn's *post hoc* test, was used to determine statistical differences between the corresponding controls and the methadone exposures. Statistical significance was denoted by $p<0.05$ (*), $p<0.001$ (***) and $p<0.0001$ (****). Note the difference in the values on the y-axis between the graphs.

3.2 Live-cell imaging of chicken granule neurons

Neurite outgrowth was studied using chicken granule neuron cultures. The cells were prepared from chicken embryos on E17. The day after seeding the cells onto 96-well plates, the cells were exposed to saline (0.9% NaCl), methadone (1, 10 and 100 µM) or morphine (1, 10 and 100 µM). The inhibitors TAT-Pep5 (called P75i in the figures,100 nM) and ANA-12 (10 µM) in the presence or absence of 100 µM methadone or morphine were also studied. The same day the cells were exposed, live-cell imaging with IncuCyte was used to assess neurite outgrowth visually.

3.2.1 Neurite length was reduced in chicken granule neurons exposed to 100 µM methadone

Figure 3.3A-C shows the change in neurite length in chicken granule neurons every four hours over the course of 72 hours after methadone exposure. Figure 3.3A shows a graph of all the exposures. Figure 3.3B shows the three concentrations of methadone compared with the control. The same figure shows that the graph for 100 µM methadone is much lower than the control. In comparison, the two other concentrations of methadone also tend to be lower in a dose-dependent manner, but to a lesser extent. Figure 3.3C shows the second control and the inhibitors both in the presence and absence of 100 µM methadone. Here all the exposures with 100 µM methadone are much lower than the second control. The neurite length in the cells exposed to the inhibitors alone did not tend to be changed compared with the control.

Specific time points were selected to present the neurite outgrowth and statistics. Figure 3.4A-D shows the change in neurite length when exposed to the three concentrations of methadone at 0, 24, 48 and 68 hours after exposure. The neurite length was significantly reduced by 100 µM methadone at 24 hours and onwards. Figure 3.5A-D shows the change in neurite length when exposed to the inhibitors TAT-Pep5 or ANA-12 in the presence or absence of 100 µM methadone. The neurite length of the cells exposed to the inhibitors in the presence of 100 µM methadone was significantly reduced from 24 hours and onwards. At 0 hours, the neurite length of cells exposed to TAT-Pep5 and 100 µM methadone was significantly reduced when compared with the second control, but not significantly changed when compared with 100 µM methadone alone. Neurites and cell bodies for the different exposures are pictured in Figure 3.6A-L at 0, 24 and 68 hours. Neurites and cell bodies at 48 hours are not included in the figure.

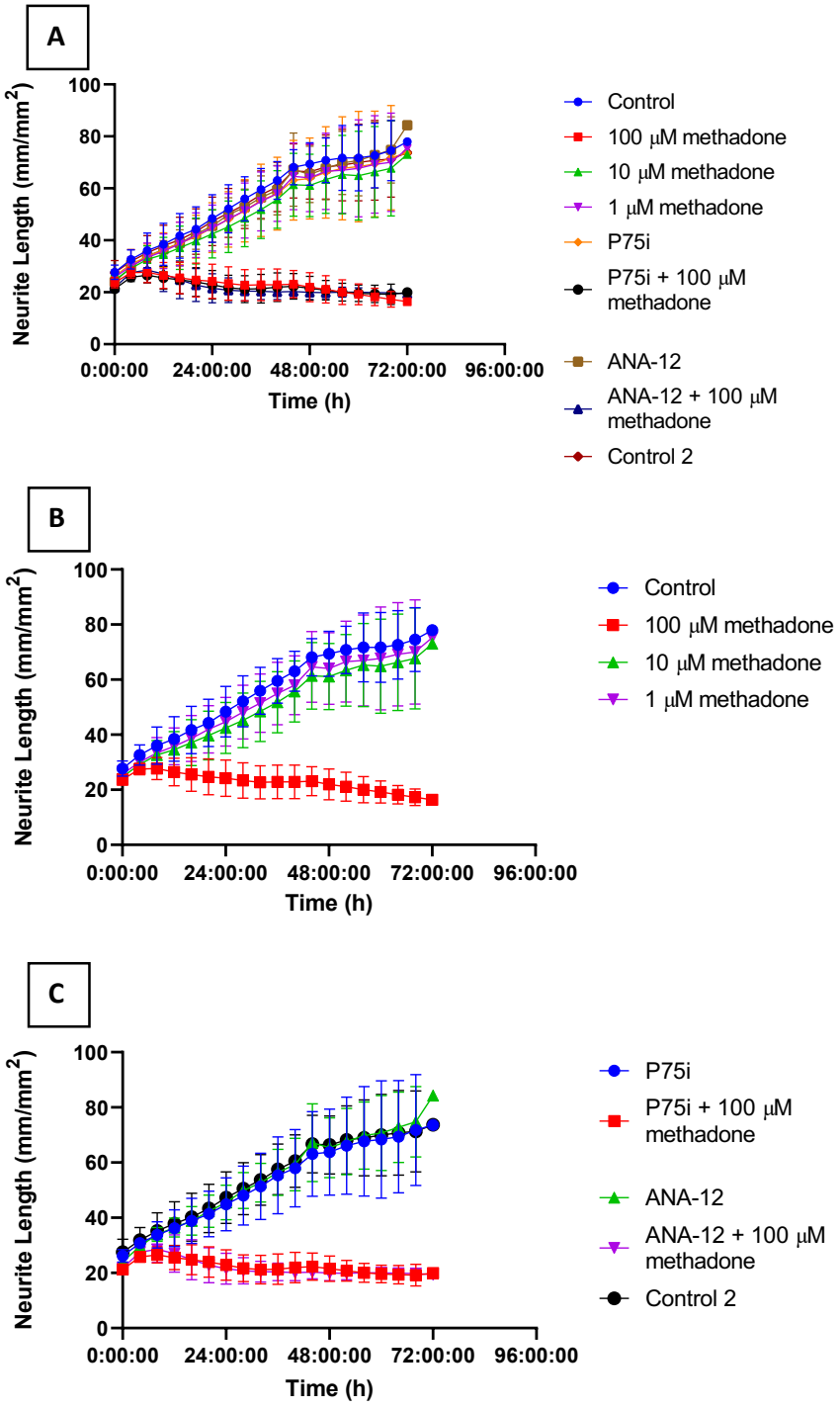

Figure 3.3: Neurite length in chicken granule neurons was reduced by 100 µM methadone. The cells were exposed to methadone (1, 10 and 100 µM) and analysed using IncuCyte's live-cell imaging. Some cells were also exposed to the inhibitors TAT-Pep5 (P75i, 100 nM), or ANA-12 (10 µM) in the presence and absence of 100 µM methadone. The values are presented as the mean ± SD of neurite length at different time points in three biological replicates. Each biological replicate had six technical replicates of each exposure. **A)** Neurite length for all exposures. **B)** Neurite length in cells exposed to 1, 10 and 100 µM methadone. **C)** Neurite length in cells exposed to the inhibitors in the presence and absence of 100 µM methadone.

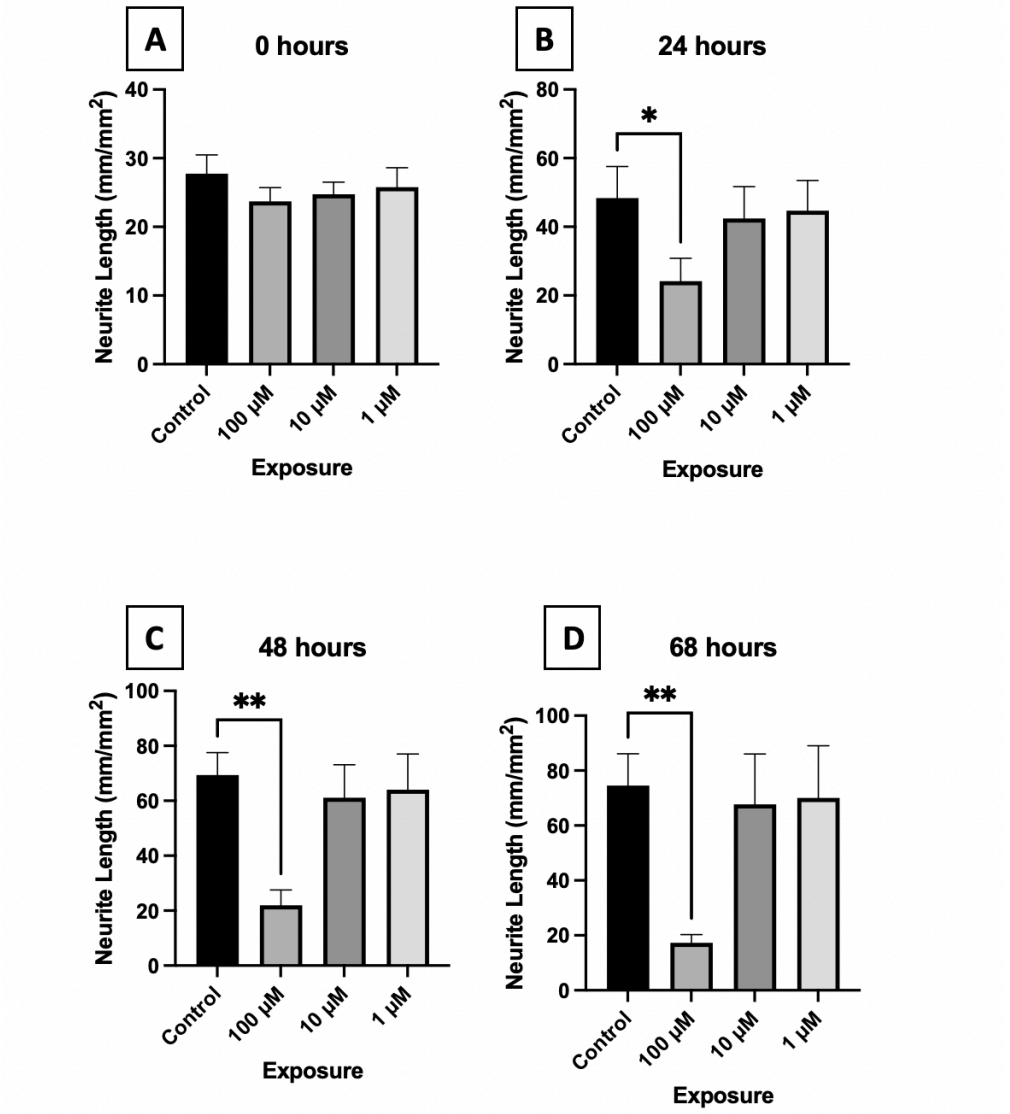

Figure 3.4: Neurite length was reduced by 100 µM methadone after 24 hours. Neurite length is presented as the mean of three different biological replicates + SD at **A)** 0 hours, **B)** 24 hours, **C)** 48 hours and **D)** 68 hours. Statistical difference between the concentrations and the control was analysed using One-Way ANOVA, followed by Dunnett's *post hoc* test for multiple comparisons. Statistical significance is noted by $p<0.05$ (*) and $p<0.01$ (**). Note the difference in the values on the y-axis between the graphs.

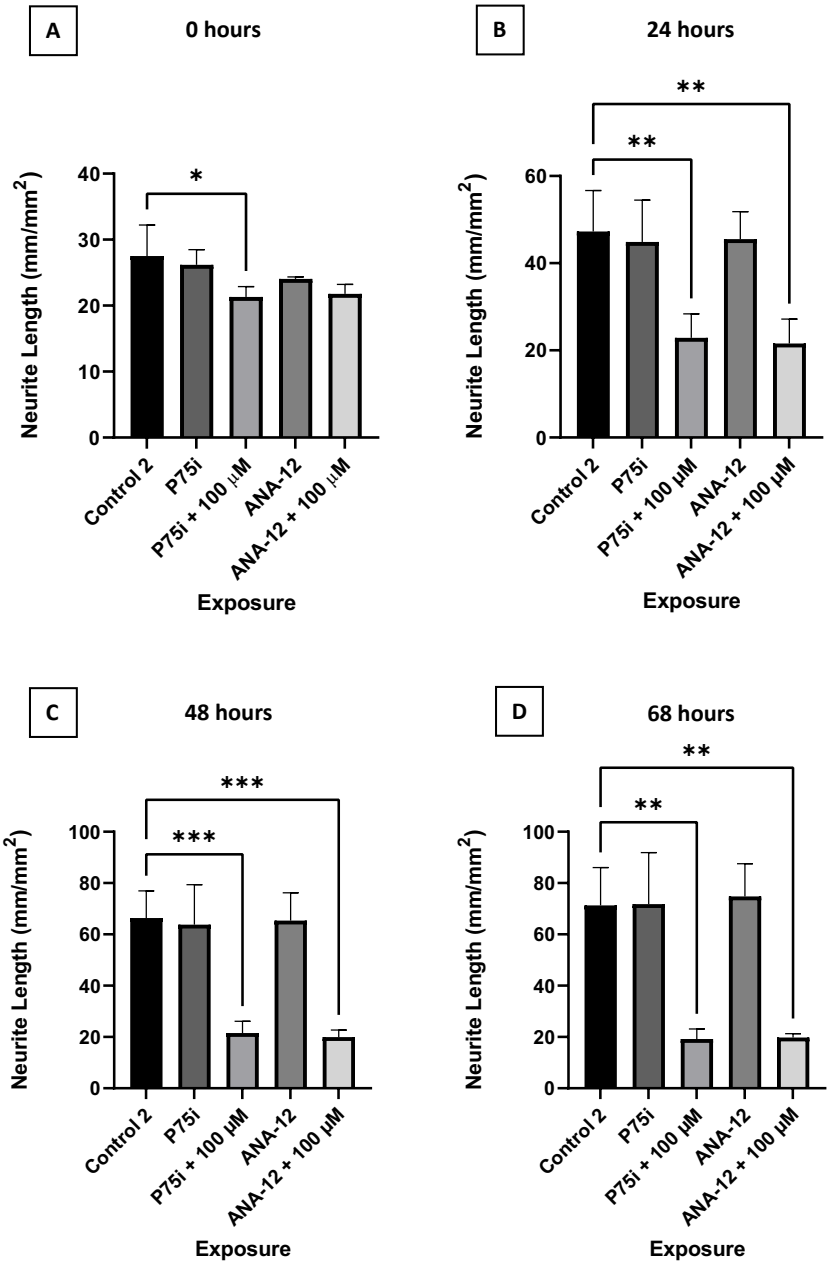

Figure 3.5: Neurite length was reduced by 100 µM methadone in the presence of the inhibitors TAT-pep5 (P75i) and ANA-12. Neurite length is presented as the mean of three different biological replicates + SD at **A)** 0 hours, **B)** 24 hours, **C)** 48 hours and **D)** 68 hours. Statistical difference between the exposures and the control was analysed using One-Way ANOVA, followed by Dunnett's *post hoc* test for multiple comparisons. Statistical significance is noted by $p<0.05$ (*), $p<0.01$ (**), and $p<0.001$ (***). The neurite lengths for cells exposed to 100 µM methadone alone were 23.7, 24.2, 21.9 and 17.3 mm/mm^2 at 0, 24, 48 and 68 hours, respectively. There was no significant difference between the cells exposed to 100 µM methadone compared with 100 µM methadone in the presence of the inhibitors and is therefore not presented in the graph. This was also analysed using One-Way ANOVA, followed by Dunnett's *post hoc* test. Note the difference in the values on the y-axis between the graphs.

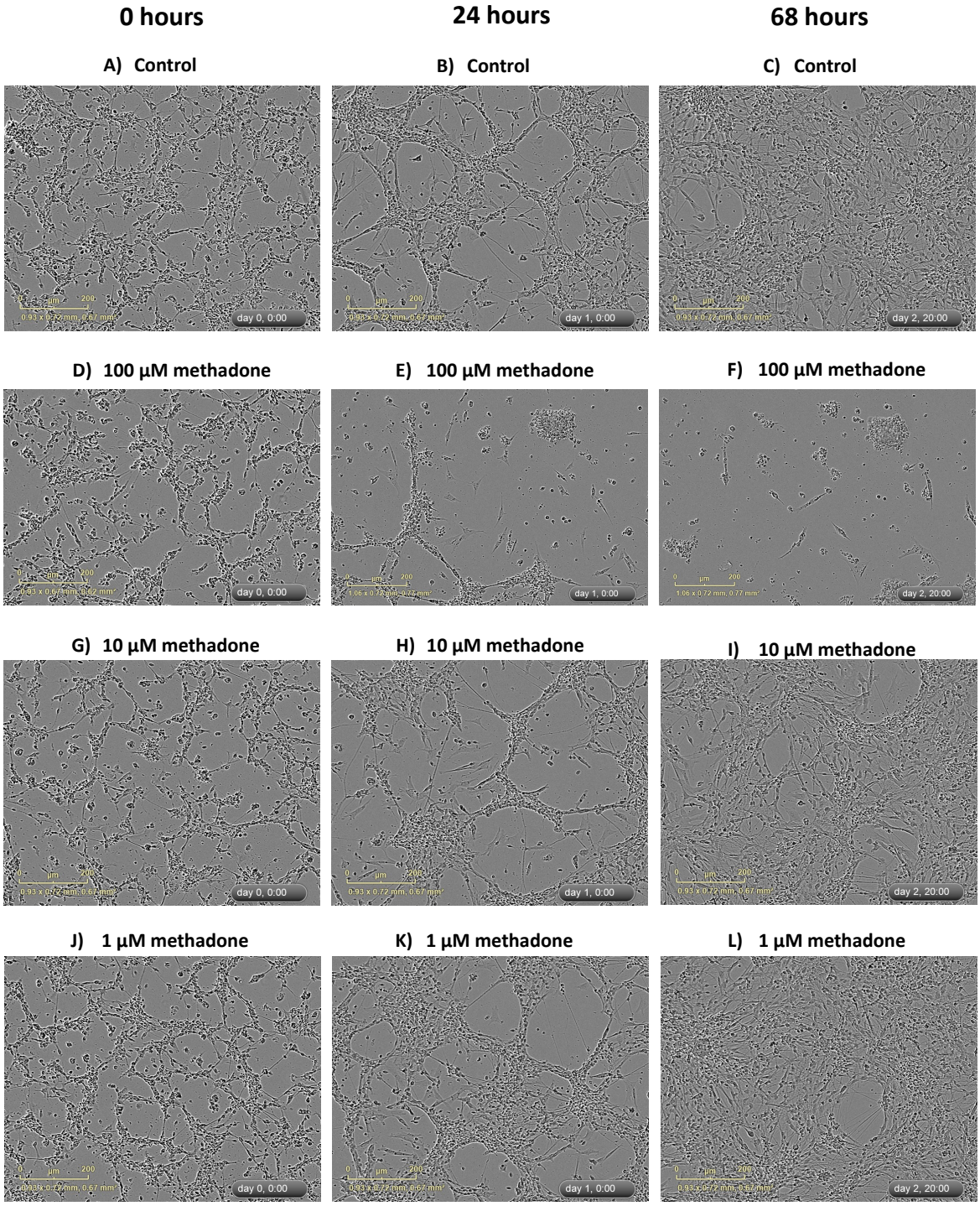

Figure 3.6: Live-cell images of CGNs exposed to methadone (1, 10 and 100 µM) and the control. CGNs from chicken cerebella (E17) were exposed to methadone (1, 10 or 100 µM) the day after plating. The analysis with IncuCyte was started immediately after exposure and continued for 72 hours. Each row of images represents a different exposure. The scale can be seen to the left, whereas the time point is presented to the right in each image. **A, D, G, J)** cells on day 0, 0 hours = 0 hours. **B, E, H, K)** cells on day 1, 0 hours = 24 hours. **C, F, I, L)** cells on day 2, 20 hours = 68 hours.

3.2.2 Neurite length was not significantly reduced in chicken granule neurons exposed to 100 µM morphine

Figure 3.7A-C presents the neurite length in chicken granule neurons every four hours over the course of 72 hours after being exposed to 1, 10 or 100 µM of morphine, including inhibitors TAT-Pep5 (called P75i in the figure, 100 nM) and ANA-12 (10 µM) in the presence or absence of 100 µM morphine. Figure 3.7A shows all exposures and controls in one graph, while Figure 3.7B shows the control and the three concentrations of morphine alone. In the latter, the curve for 100 µM morphine tended to be lower than the control and the two other concentrations. Morphine at 10 µM and 1 µM also tended to have a reduced neurite length in a non-dose-dependent manner. Figure 3.7C shows the graphs for the second control and the inhibitors in the presence and absence of 100 µM morphine.

In Figure 3.8A-D, neurite lengths at 0, 24, 48 and 68 hours after exposure were chosen to present the statistical differences between the control and the three concentrations of morphine. There was a statistical difference in the neurite length at 48 hours in the cells exposed to 100 µM morphine compared with the control, as presented in Figure 3.8. The other chosen time points did not show a statistically significant reduction, but the columns for 100 µM morphine in B, C and D all tend to be lower than the control. Figure 3.9A-D shows the change in neurite length when exposed to the inhibitors TAT-Pep5 or ANA-12 in the presence or absence of 100 µM methadone. There was no statistical change in neurite length when exposed to the inhibitors in the presence or absence of 100 µM morphine, when comparing them with the second control and 100 µM morphine alone. Neurites and cell bodies for the different exposures are pictured in Figure 3.10A-L at 0, 24 and 68 hours. Neurites and cell bodies at 48 hours are not included in the figure.

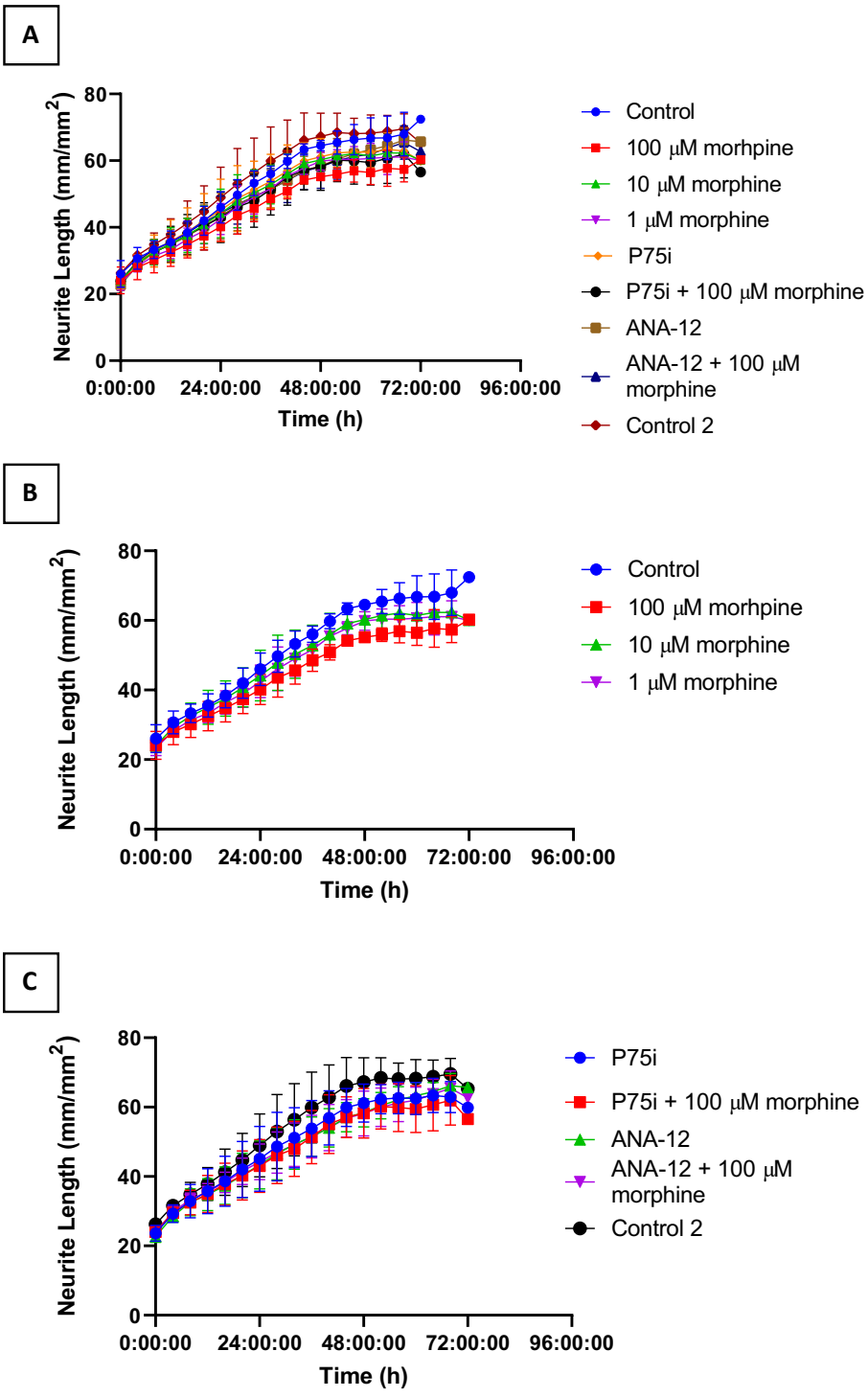

Figure 3.7: Neurite length in chicken granule neurons was slightly affected after morphine exposure. The cells were exposed to morphine (1, 10 and 100 µM) and analysed using IncuCyte's live-cell imaging. Some cells were also exposed to the inhibitors TAT-Pep5 (P75i in the figure, 100 nM), or ANA-12 (10 µM) in the presence or absence of 100 µM morphine. The values are presented as the mean of neurite length ± SD at different time points in three biological replicates. Each biological replicate had six technical replicates of each exposure. **A)** Neurite length for all exposures. **B)** Neurite length in cells exposed to 1, 10 and 100 µM morphine. **C)** Neurite length in cells exposed to the inhibitors in the presence and absence of 100 µM morphine.

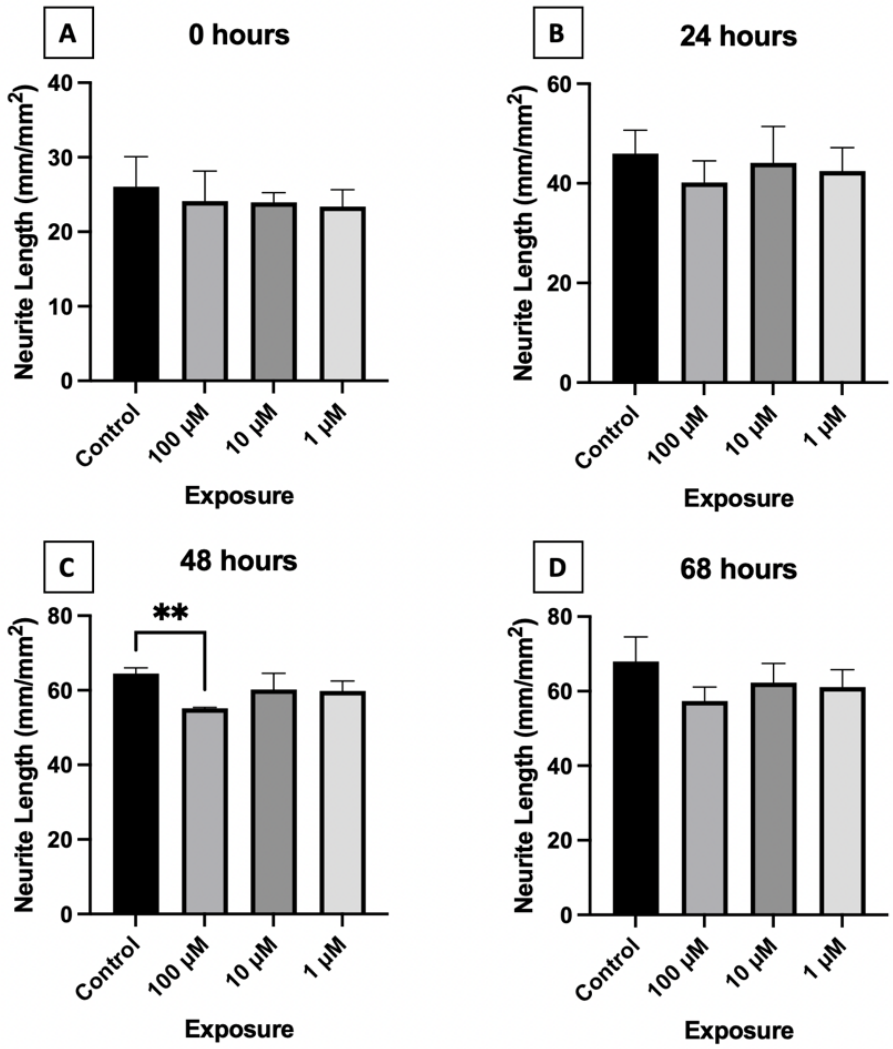

Figure 3.8: Neurite length in chicken granule neurons was reduced at 48 hours when exposed to 100 µM morphine. Neurite length is presented as the mean of three different biological replicates + SD at **A)** 0 hours, **B)** 24 hours, **C)** 48 hours and **D)** 68 hours. Statistical difference between the exposures and the control was analysed using One-Way ANOVA, followed by Dunnett's *post hoc* test for **A-C** and Kruskal-Wallis One-Way ANOVA, followed by Dunn's post hoc for **D**. Statistical significance is noted by $p<0.01$ (**). Note the difference in the values on the y-axis between the graphs.

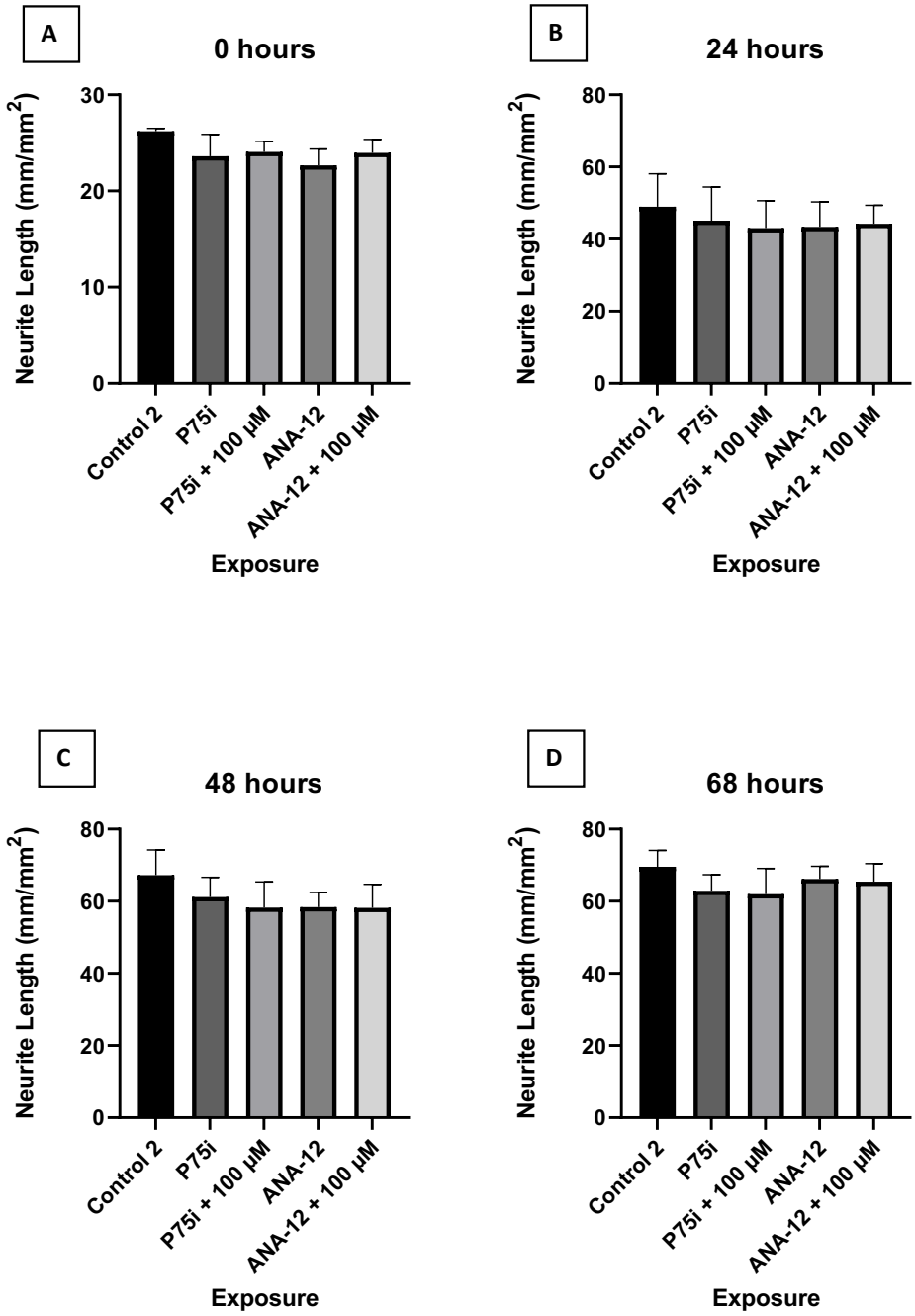

Figure 3.9: Neurite length was not reduced by 100 µM morphine in the presence of the inhibitors TAT-pep5 (P75i) and ANA-12. Neurite length is presented as the mean of three different biological replicates + SD at A) 0 hours, B) 24 hours, C) 48 hours and D) 68 hours. Statistical difference between the exposures and the control was analysed using One-Way ANOVA, followed by Dunnett's *post hoc* test. The mean neurite length of 100 µM morphine alone was 21.9 mm/mm^2 at 48 hours but is not presented in this figure as there was no significant difference between the cells exposed to 100 µM morphine compared with 100 µM morphine in the presence of the inhibitors. This was also analysed using One-Way ANOVA, followed by Dunnett's *post hoc* test. Note the difference in the values on the y-axis between the graphs.

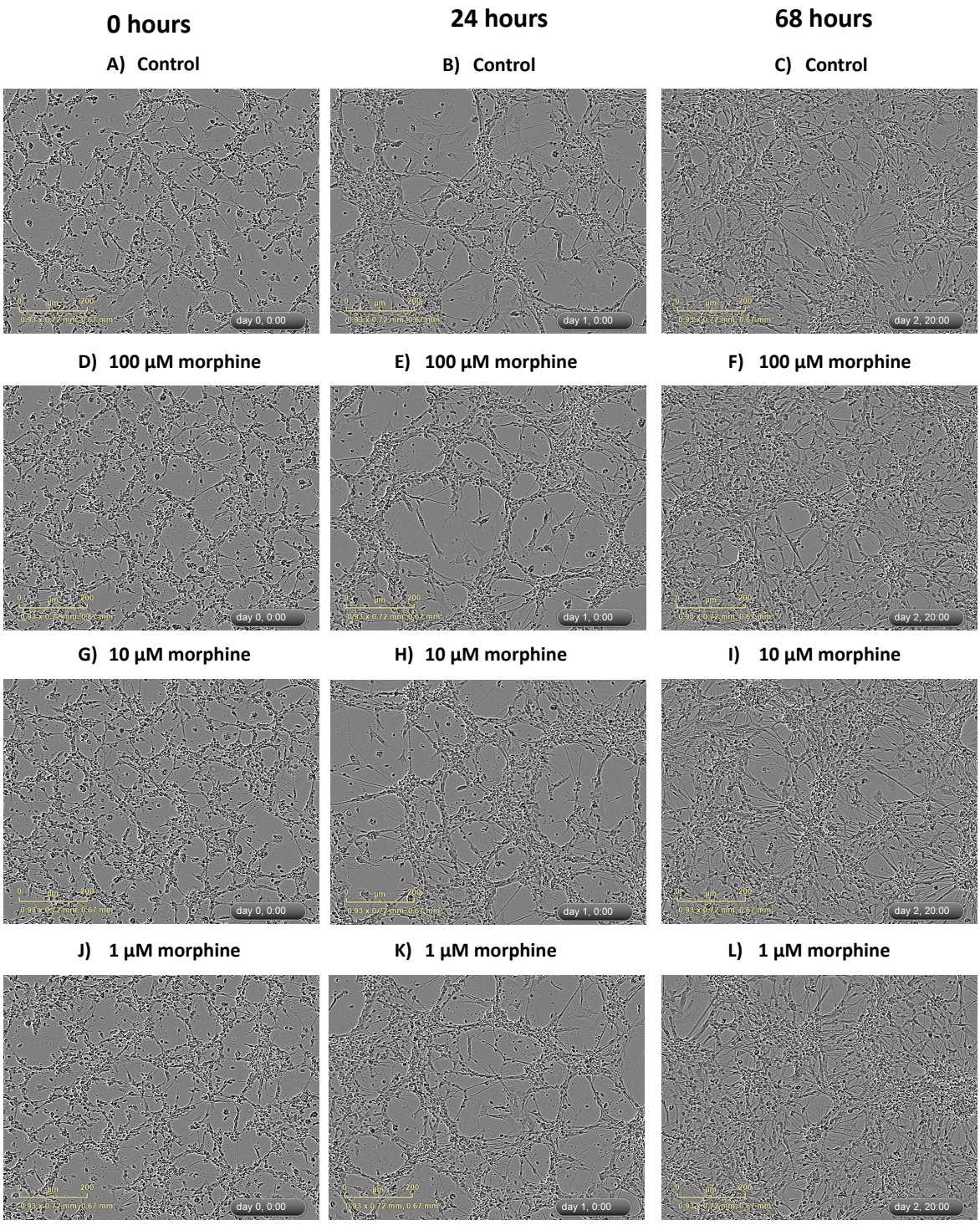

Figure 3.10: Live-cell images of CGNs exposed to morphine (1, 10 and 100 µM) and the control. CGNs from chicken cerebella (E17) were exposed to morphine (1, 10 and 100 µM) the day after plating. The analysis with IncuCyte was started immediately after exposure and continued for 72 hours. Each row of images represents a different exposure. The scale can be seen to the left, whereas the time point is presented to the right in each image. **A, D, G, J)** cells on day 0, 0 hours = 0 hours. **B, E, H, K)** cells on day 1, 0 hours = 24 hours. **C, F, I, L)** cells on day 2, 20 hours = 68 hours.

3.3 Gene expression in chicken granule neurons exposed to methadone and morphine

CGNs exposed to a control containing 1 ‰ of the solvent (MQ water) or three concentrations of methadone (1, 10 or 100 µM) or morphine (1, 10 or 100 µM) were harvested and lysed 72 hours after exposure. The lysates were analysed with RT-qPCR, and all Ct-values were normalised to GAPDH and then normalised to the control using the ddCt-method. RT-qPCR was done once as a pilot.

3.3.1 The opioid receptors

Methadone increased the expression of MOR at 100 µM, as shown in Figure 3.11A. The expression of DOR and KOR were not significantly changed, but the graphs in Figure 3.11B-C show that the 100 µM methadone tended to reduce the expression. None of the morphine concentrations significantly changed the expressions of the opioid receptors, as presented in Figure 3.11D-F. Still, the graph in Figure 3.11D shows a tendency to a dose-response effect of morphine on the MOR gene, where higher concentrations of morphine tended to reduce MOR expression. Note the high standard deviation in all the graphs.

3.3.2 Opioid polypeptide precursors

As shown in Figure 3.12A-B, 100 µM methadone increased the expression of the PDYN gene and reduced the expression of the PENK gene. There was no statistical change for 1 and 10 µM methadone, but the graphs show that there is a dose-response tendency. Figure 3.12C-D show no significant change in the expression of PDYN and PENK after morphine exposure, but there was a dose-response tendency, where higher doses of morphine tend to reduce PDYN expression and increase PENK expression.

3.3.3 BDNF and CREB1

Figure 3.13A-B show a dose-response tendency of reduction in expression of the BDNF and CREB1 gene after methadone exposure, although there is no significant reduction. Note the high standard deviation of the control. Figure 3.13C, where the effect of morphine is presented, does not present a similar dose-response tendency as methadone. Still, it shows a tendency for a slight reduction of BDNF expression for 100 µM and 10 µM morphine. Figure

3.13D does not have a dose-response tendency, but the CREB1 expression tends to increase at all concentrations of morphine. This was, however, not a statistically significant increase.

3.3.4 GluN2B

The expression of GluN2B is significantly reduced with 100 µM methadone, as illustrated in Figure 3.14A. Morphine does not show the same changes in expression, although the graph for GluN2B in Figure 3.14B shows a dose-response tendency to higher gene expression.

3.3.5 CYP3A4

There was a significant 17-fold increase in CYP3A4 expression in the cells exposed to 100 µM methadone. This is illustrated in Figure 3.15A. Morphine did not change the expression of CYP3A4, as shown in Figure 3.15B.

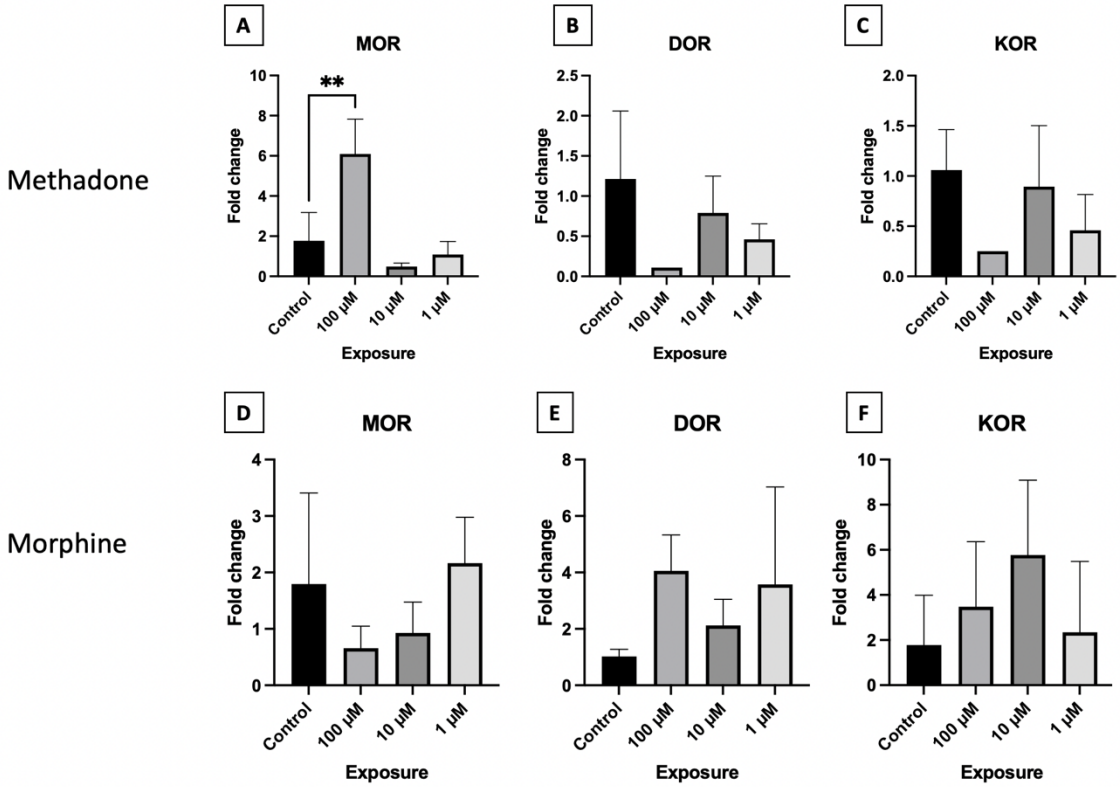

Figure 3.11: Methadone changed the expression of the MOR-gene, but morphine does not. Chicken granule neurons were exposed to 1, 10 and 100 µM methadone or morphine for 72 hours. Cells from one experiment with three replicates of each exposure were studied using RT-qPCR, where the gene expression of MOR, DOR and KOR were studied. Only two replicates of 100 µM methadone were used. Relative fold change in the expression of **A)** MOR, **B)** DOR and **C)** KOR when exposed to methadone. Relative fold change in the expression of **D)** MOR, **E)** DOR, and **F)** KOR when exposed to morphine. The values are normalised with the untreated control and presented as the mean of the fold change + SD. A value equal to 1 indicates no change in gene expression, whilst values above and below 1 indicate upregulation and downregulation of the gene expression, respectively. Statistical analysis was done using One-Way ANOVA, followed by Dunnett's *post hoc* test for multiple comparisons. Statistical significance is shown as $p<0.01$ (**). Note the difference in the values on the y-axis between the graphs.

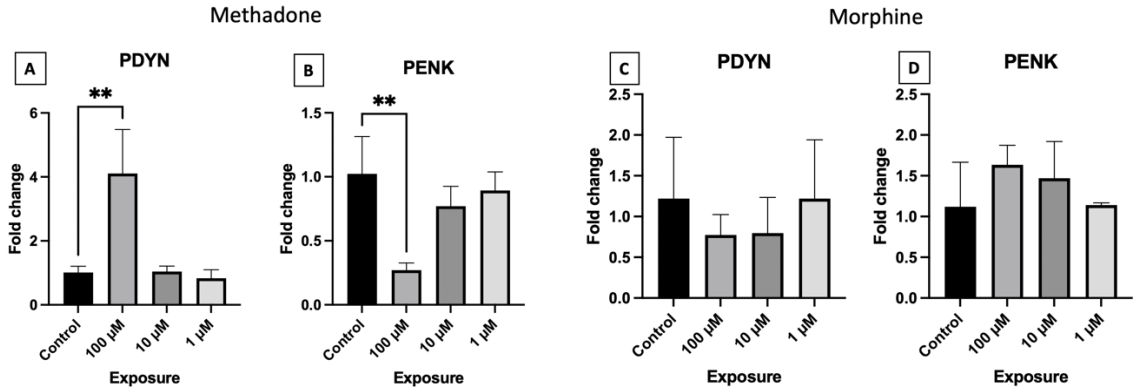

Figure 3.12: PDYN and PENK expression was changed by the highest concentration of methadone but not by morphine. Chicken granule neurons were exposed to 1, 10 and 100 µM methadone or morphine for 72 hours. Cells from one experiment with three replicates of each exposure (two replicates of 100 µM methadone) were studied using RT-qPCR, where PDYN and PENK gene expression were studied. Relative fold change in the expression of **A)** PDYN and **B)** PENK when exposed to methadone. Relative fold change in the expression of **C)** PDYN and **D)** PENK when exposed to morphine. The values are normalised with the untreated control and presented as the mean of the fold change + SD. A value equal to 1 indicates no change in gene expression, whilst values above and below 1 indicate upregulation and downregulation of the gene expression, respectively. Statistical analysis was done using One-Way ANOVA, followed by Dunnett's *post hoc* test for multiple comparisons. Statistical significance is shown as $p<0.01$ (**). Note the difference in the values on the y-axis between the graphs.

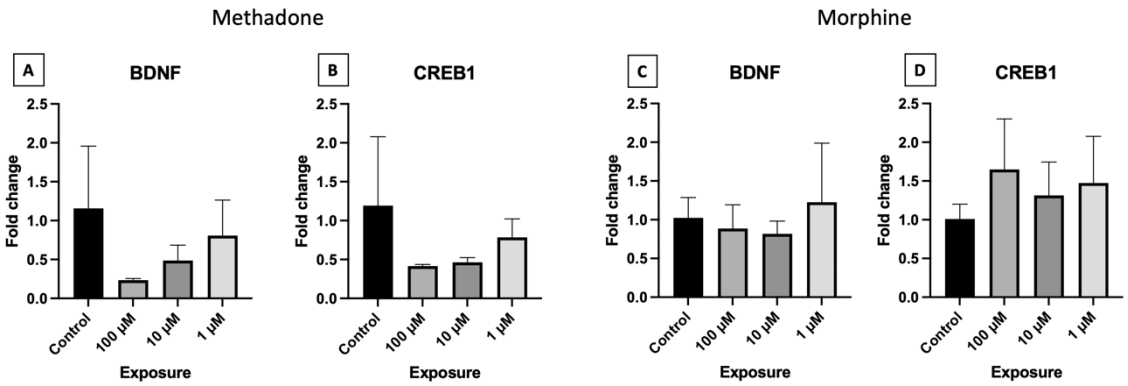

Figure 3.13: There was no significant change in BDNF and CREB1 gene expression in chicken granule neurons exposed to methadone or morphine. Chicken granule neurons were exposed to 1, 10 and 100 µM methadone or morphine for 72 hours. Cells from one experiment with three replicates of each exposure (two replicates of 100 µM methadone) were studied using RT-qPCR, where BDNF and CREB1 gene expression were studied. Relative fold change in the expression of **A)** BDNF and **B)** CREB1 when exposed to methadone. Relative fold change in the expression of **C)** BDNF and **D)** CREB1 when exposed to morphine. The values are normalised with the untreated control and presented as the mean of the fold change + SD. A value equal to 1 indicates no change in gene expression, whilst values above and below 1 indicate upregulation and downregulation of the gene expression, respectively. Statistical analysis was done using One-Way ANOVA, followed by Dunnett's *post hoc* test for multiple comparisons.

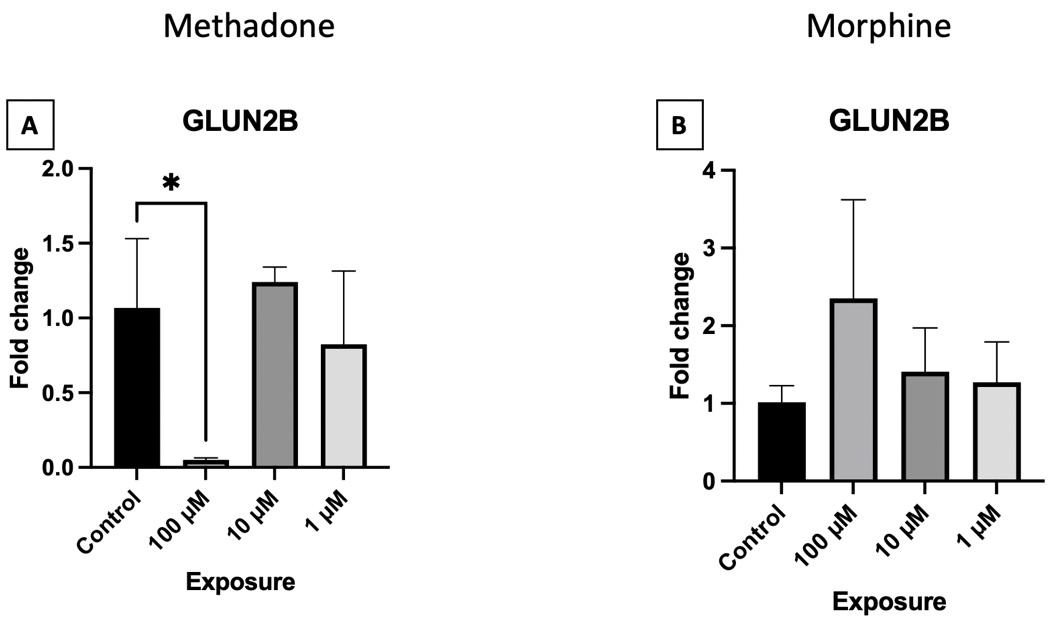

Figure 3.14: Methadone, but not morphine, changed the GluN2B gene expression. Chicken granule neurons were exposed to 1, 10 and 100 µM methadone or morphine for 72 hours. Cells from one experiment with three replicates of each exposure (two replicates of 100 µM methadone) were studied using RT-qPCR, where GluN2B gene expression was studied. Relative fold change in the expression of **A)** GluN2B when exposed to methadone and **B)** GluN2B when exposed to morphine. The values are normalised with the untreated control and presented as the mean of the fold change + SD. A value equal to 1 indicates no change in gene expression, whilst values above and below 1 indicate upregulation and downregulation of the gene expression, respectively. Statistical analysis was done using One-Way ANOVA, followed by Dunnett's *post hoc* test for multiple comparisons. Statistical significance is shown as $p<0.05$ (*). Note the difference in the values on the y-axis between the graphs.

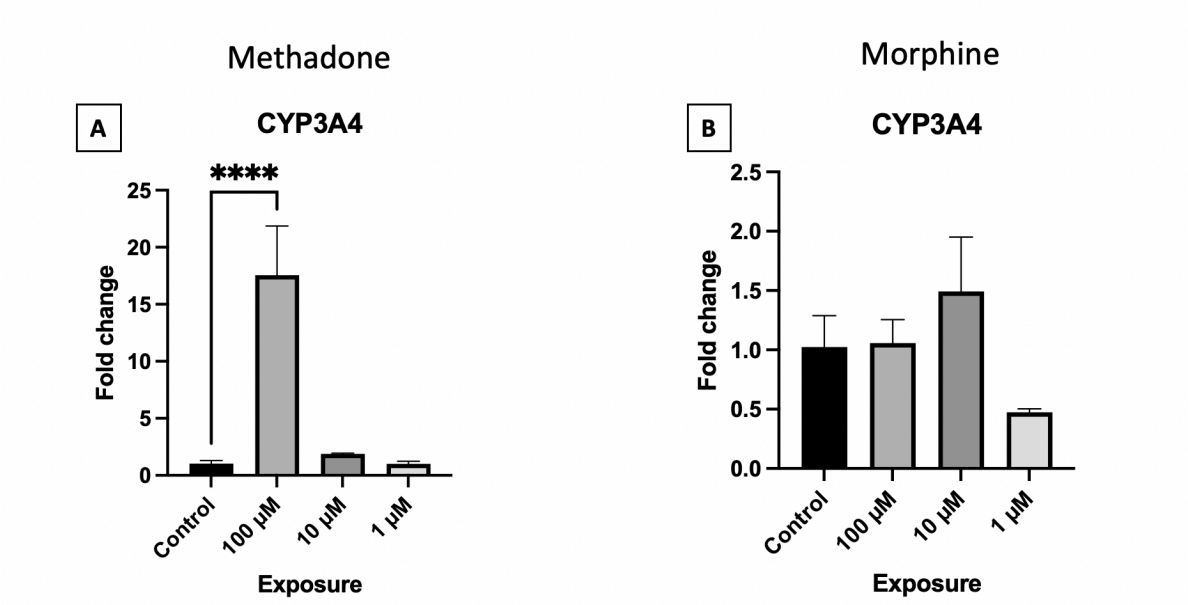

Figure 3.15: Methadone, but not morphine, changed the CYP3A4 gene expression. Chicken granule neurons were exposed to 1, 10 and 100 µM methadone or morphine for 72 hours. Cells from one experiment with three replicates of each exposure (two replicates of 100 µM methadone) were studied using RT-qPCR, where CYP3A4 gene expression was studied. Relative fold change in the expression of **A)** CYP3A4 when exposed to methadone and **B)** CYP3A4 when exposed to morphine. The values are normalised with the untreated control and presented as the mean of the fold change + SD. A value equal to 1 indicates no change in gene expression, whilst values above and below 1 indicate upregulation and downregulation of the gene expression, respectively. Statistical analysis was done using One-Way ANOVA, followed by Dunnett's *post hoc* test for multiple comparisons. Statistical significance is shown as $p<0.0001$ (****). Note the difference in the values on the y-axis between the graphs.

3.4 High-content imaging of chicken granule neurons

A pilot for high-content imaging was done using chicken granule neurons. The cells were exposed to a control containing 1 ‰ MQ water or exposed to methadone (1 or 10 µM) or morphine (1 or 10 µM) the day after seeding them onto 96-well plates. After 72 hours, the cells were fixed using formaldehyde and stored in PBS until immunostaining. The cells were stained with DAPI, MAP2, PSD95 and SYP at the Norwegian Institute of Public Health.

A composite image of stains of DAPI, MAP2, PSD95 and SYP can be seen in Figure 3.16. Examples of costains of PSD95 and SYP are marked with a grey circle in the figure. No qualitative difference between the exposures was observed, and quantitative differences were not calculated. Images of the cells with the different exposures can be found in Appendix C, Figures 9.1-9.5, where the figures include separate images of the expression of DAPI, MAP2, PSD95 and SYP, including a composite image.

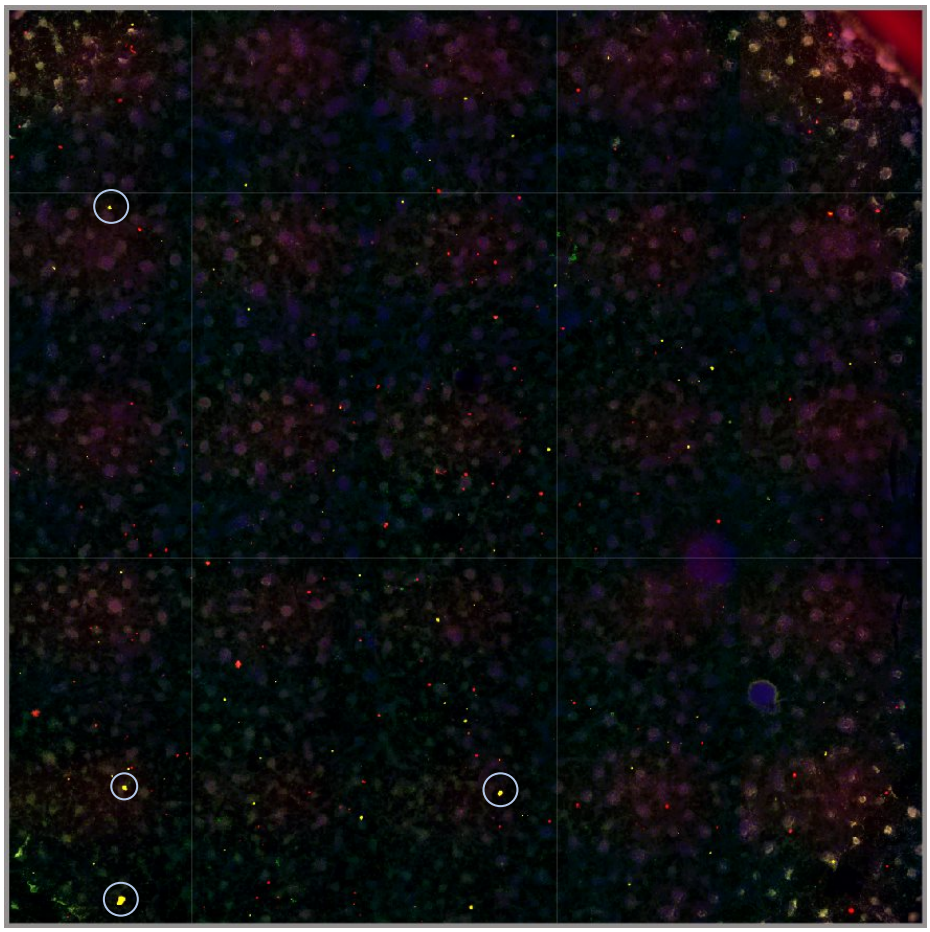

Figure 3.16: A composite high-content image of CGNs exposed to the control. This is a representative image of CGNs after staining. All stains are included in the image. Blue=DAPI, green=MAP2, red=PSD95 and yellow=SYP. The grey circles mark areas with overlapping stains of PSD95 and SYP. Note that not all overlapping stains have been marked.

3.5 Pharmacokinetics and distribution of methadone and its metabolite EDDP to the brain, lungs, and yolk

Eggs with embryos at E13 were injected with 20 mg/kg methadone, and the brains, lungs, and yolks were harvested at 0.5, 1, 2, 3, 4, 5, 6, 7, 8, 12, 18, and 24 hours after the injection. For every time point, six eggs were injected.

3.5.1 Methadone concentration in the brain, lungs, and yolk

To illustrate the peaks and means for each tissue, the curves are separated into brain, lungs, and yolk in Figure 3.17A, B and C, respectively. Figure 3.17D shows the methadone concentrations for all three tissues in one graph. The methadone concentration in the brain was significantly higher at all time points when compared with the lungs. This was determined using a student's t-test for every time point and is not presented in the figure. For methadone measured in the yolk, the mean concentration at three hours was higher compared with the lungs and brain, as illustrated in Figure 3.17C-D. The yolk had a higher concentration of methadone at all time points after three hours. Note the high standard deviations in the yolk graph.

3.5.2 Pharmacokinetics of methadone in the brain and lungs

The observed maximum concentration (C_{max}) of methadone in the brain was 210 µM, and the time of maximum concentration (T_{max}) was 1 hour after injection. The area under the curve (AUC) was determined to be 828.4 (µM·hour) using the trapezoid rule in GraphPad. The other pharmacokinetic parameters were determined using non-linear regression in GraphPad with One-Phase Decay. The half-life ($T_{1/2}$) was measured to be 2.1 hours. These pharmacokinetic parameters are presented in Table 3.1.

The observed C_{max} of methadone in the lungs was 87 µM, and the T_{max} was 0.5 hours. The measured $T_{1/2}$ was 1.4 hours. AUC was estimated to be 304.2 (µM·hour). All pharmacokinetic parameters for the lungs are presented in Table 3.2.

The fitted line in the non-linear regression for the brain and lungs are illustrated in Figure 3.18A-B. The R^2 for the brain and lungs were 0.90 and 0.87, respectively, and the plots for the non-fitted curves are also included in the figure. The curves fit the plots quite well.

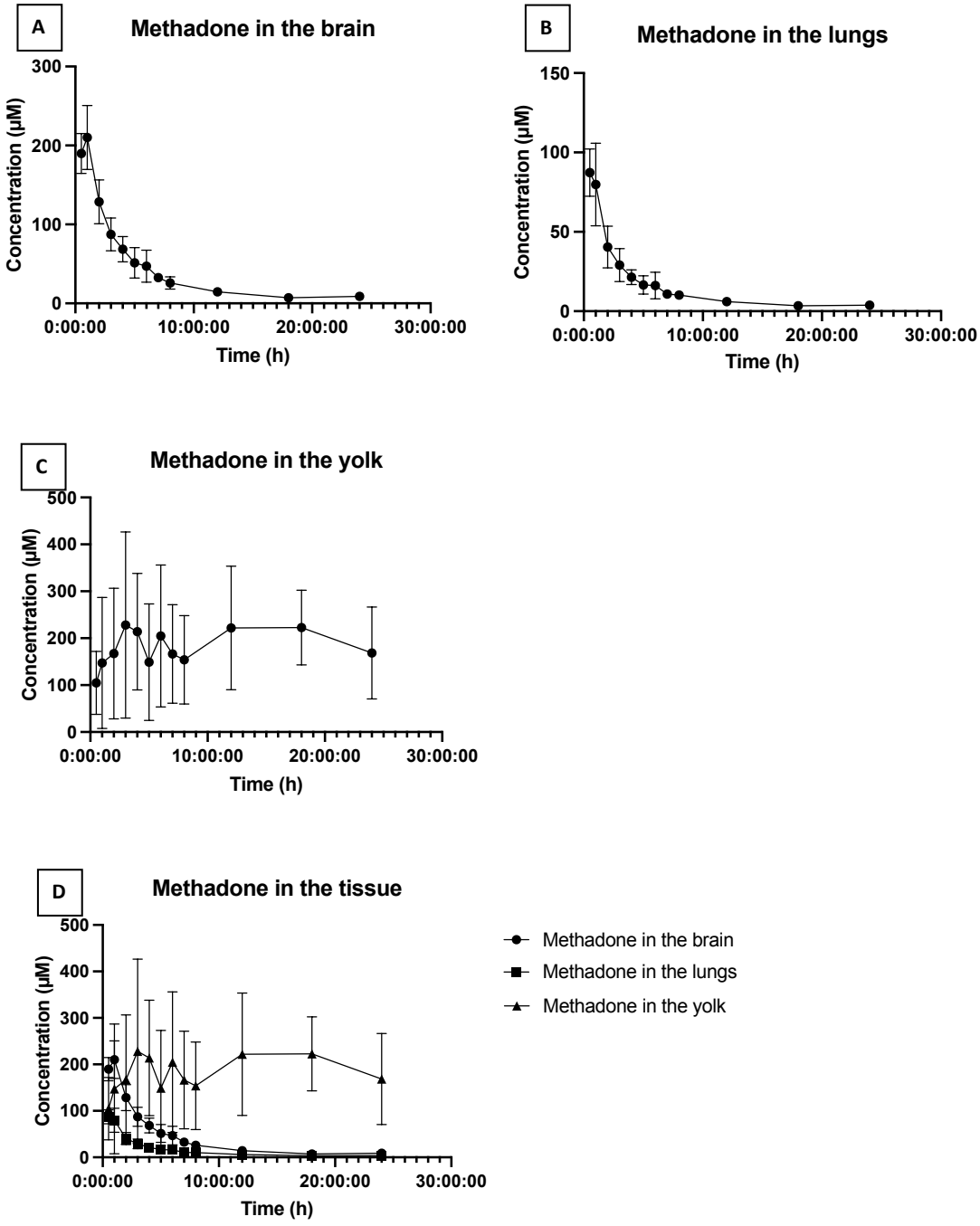

Figure 3.17: Methadone concentration (µM) in the three tissues at specific time points. Eggs with embryos at E13 were injected with 20 mg/kg methadone. The whole brain, lungs, and a part of the yolk were harvested 0.5, 1, 2, 3, 4, 5, 6, 7, 8, 12, 18 and 24 hours after the injections. The concentration in the tissue was measured using LC-MS-MS. Methadone concentration in the **A)** brain, **B)** lungs, and **C)** yolk. **D)** Methadone concentration in all three tissues, presented in one graph. n=6 at 0.5, 1, 3, 4, 5, 6, and 12 hours and n=5 at 2,7, 8, 18 and 24 hours for **A**. n=6 at 1, 3, 4, 5, 6, and 12 hours, n=5 at 2, 7, 8, and 24 hours and n=4 at 0.5 and 18 hours for **B**. n=5 at 0.5 hours and n=6 at 1-24 hours for **C**. A lung at the 18-hour point was not harvested, and one homogenate from the lungs and yolk at 0.5 hours could not be analysed. Five outliers from **A** and five outliers from **B** were removed using Grubbs (alpha=0.05). The values are shown as the mean concentration ± SD. Note the difference in the values on the y-axis in each graph.

Table 3.1 Pharmacokinetic parameters of methadone in the brain on E13		
Parameter	**Determined**	**Generated**
C_{max} (μM)	210	
T_{max} (hours)	1	
AUC (μM x hour)		828.4
$T_{1/2}$ (hours)		2.1

Table 3.2 Pharmacokinetic parameters of methadone in the lungs on E13		
Parameter	**Determined**	**Generated**
C_{max} (μM)	87.34	
T_{max} (hours)	0.5	
AUC (μM x hour)		304.2
$T_{1/2}$ (hours)		1.4

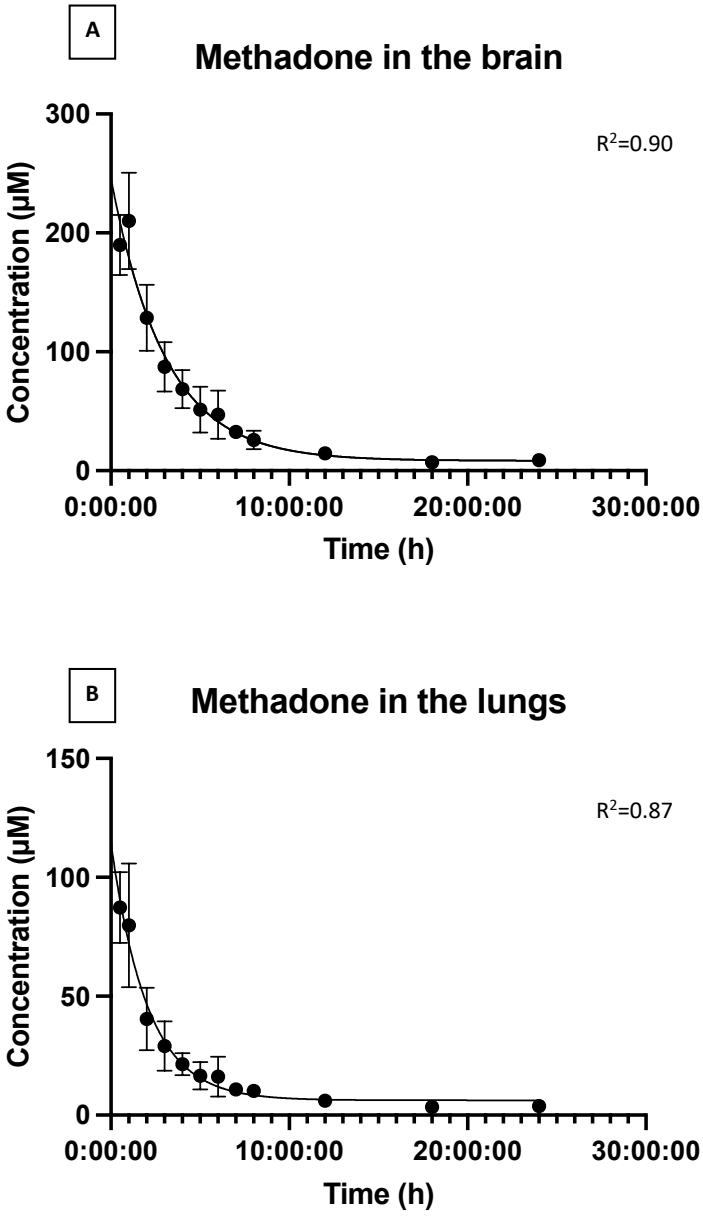

Figure 3.18: The nonlinear fitted curve of the brain and lungs with the original points plotted. A) The fitted curve of methadone in the brain, R^2=0.90. **B)** The fitted curve of methadone in the lungs, R^2=0.87. The curves were made with non-linear regression.

3.5.3 Distribution of the main metabolite of methadone, EDDP, in the brain, lungs, and yolk

The concentration of the main metabolite EDDP in the brain, lungs and yolk is presented in Figure 3.19. The three curves are separated in Figure 3.19A, B and C to make it easier to read the concentrations. Figure 3.19D shows the EDDP concentrations for all three tissues in one graph. EDDP concentrations in the yolk are substantially higher than in the brain and lungs. Concentrations in the lungs were significantly higher at 0.5-4 hours and at 6 hours ($p < 0.05$) and was measured using a student's t-test for every time point. This is not presented in the figure. A graph with both EDDP and methadone in the tissue could not be made due to the considerable difference in concentration. Pharmacokinetic parameters were not calculated for the EDDP curves.

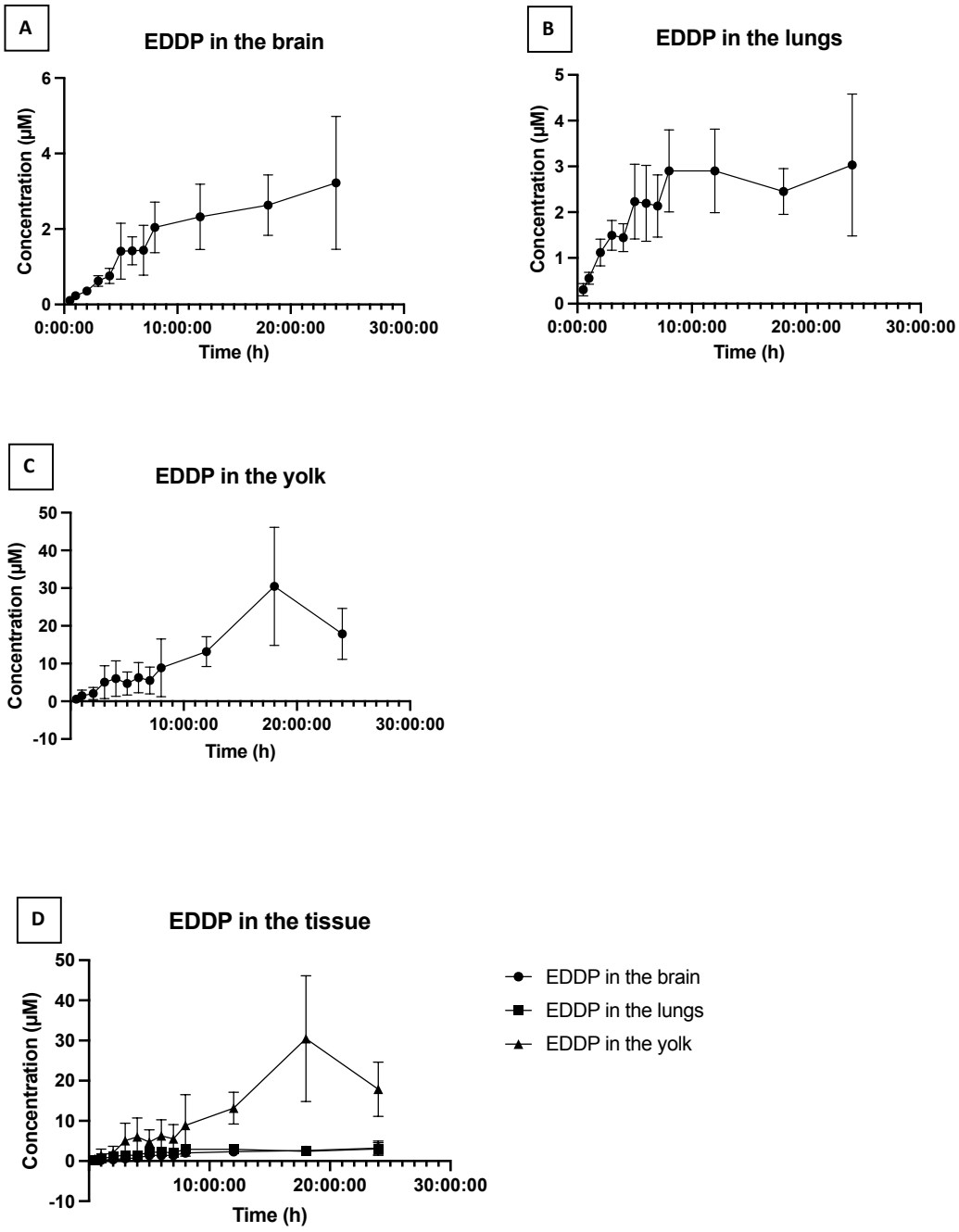

Figure 3.19: Concentrations of the main metabolite EDDP (µM) in the three tissues at specific time points. Eggs with embryos at E13 were injected with 20 mg/kg methadone. The whole brain, lungs, and a part of the yolk were harvested 0.5, 1, 2, 3, 4, 5, 6, 7, 8, 12, 18 and 24 hours after the injections. The EDDP concentration in the tissue was measured using LC-MS-MS. EDDP concentration in the **A)** brain, **B)** lungs, and **C)** yolk. **D)** EDDP concentration in all three tissues, presented in one graph. n=5 at 18 hours and n=6 at all other time points for **A**. n=4 at 18 hours, n=5 at 0.5 hours and n=6 at all other time points for **B**. n=5 at 0.5, 7, 12 and 18 hours and n=6 at all other time points for **C**. A lung at the 18-hour point was not harvested, and one homogenate from the lungs and yolk at 0.5 hours could not be analysed. One outlier in **A**, one outlier in **B** and three outliers in **C** were removed using Grubbs (alpha=0.05). The values are shown as the mean concentration ± SD. Note the difference in the values on the y-axis in each graph.

4 Discussion

4.1 The model systems

4.1.1 The *in vivo* model

The similarities between human and rodent anatomy, physiology and genetics are some of the reasons why rodents, like rats and mice, often are the preferred choice when studying toxicity (117). However, rodent models have a few disadvantages compared with the chicken model. The chicken model is less expensive and easier to maintain. Compared with rats and mice, which need food, water and a suitable environment that satisfies their needs, embryonic chickens only need the right temperature, humidity, and a machine to mimic the brooding of a hen. This is due to the embryo being nutritionally self-sufficient, requiring much less maintenance and resources than rodent models (92).

Notably, the chicken model offers a few advantages over rodents. Firstly, the mother is not exposed, and the embryo is a lot more accessible than rodent embryos (118). Secondly, all eggs and embryos are statistically independent, and the number of animals is easy to determine. Additionally, the embryos originate from different mothers, which takes genetic variability into account. Furthermore, when conducting teratogenic studies, exposing chicken embryos is likely to cause less stress than exposing rodent embryos through the mother. These factors lead to the fulfilment of two of the three Rs: reduction and refinement.

Embryonic development in chickens is faster than that of humans, with hatching occurring 21 days after incubation. Moreover, the developmental process in chickens has been extensively studied and can be compared to human development (119). However, the experiments cannot translate directly to human embryos, as the chicks are exposed directly to the drugs, whereas human and rodent embryos are exposed through the mother. In other words, the chicken model does not consider the effect of the mother's metabolism (92). Nevertheless, this can also be an advantage, as the metabolites are commercially available. This offers a possibility to study the independent effect of the metabolites and drugs.

Unlike humans and rodents, gestation in chickens is a closed system, but if the egg contains various compartments for metabolites, waste, and toxins, it may have similarities to an open system. This was the basis for including the yolk in the distribution study. The different compartments in the chicken egg are the yolk inside the vascularised yolk sac, amniotic fluid, albumen, and the allantois inside the chorioallantoic membrane (CAM). The allantois is responsible for the elimination of urinary waste products, while the yolk is the source of nutrients in avian embryos. The CAM performs numerous functions, such as facilitating gas exchange and maintaining homeostasis (120). These three compartments together share similarities with the human placenta. The anatomy of the embryonic egg and its compartments are illustrated in Figure 4.1.

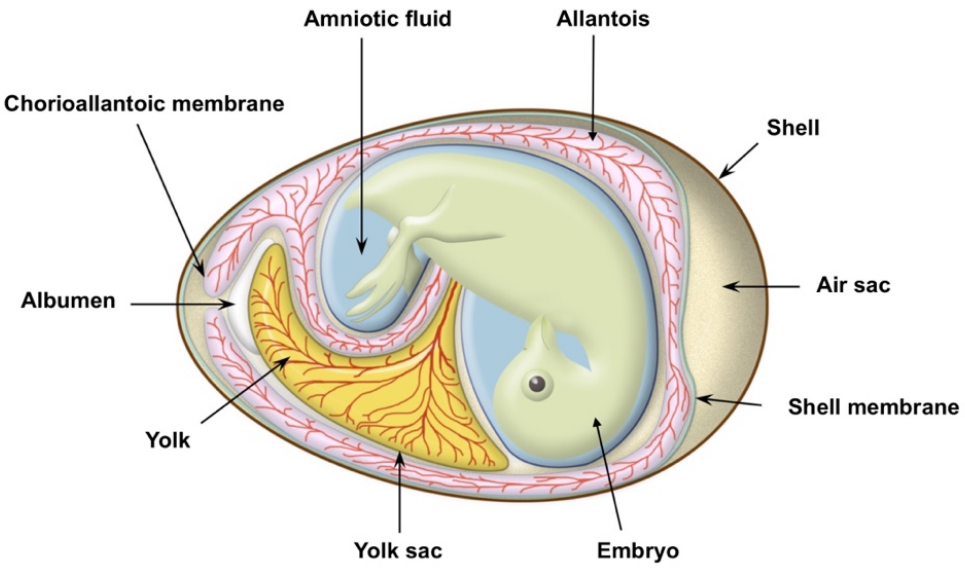

Figure 4.1: An illustration of a fertilised chicken egg on E16. The main compartments of the egg surround the embryo. The figure is obtained and modified from (121).

The injection of drugs into the allantoic cavity leads to exposure of CAM. This membrane is a product of the allantoic membrane fusing with the chorion and is highly vascularised (120). The chorion is also a compartment in the egg, but because of its fusion with CAM, it is difficult to pinpoint its exact location in Figure 4.1. The aim of the injections was to expose the CAM, which leads to a bioavailability that is similar to that of a topical administration (122). However, the injection process can be problematic as it is difficult to determine precisely whether the injection is made into the chorion or the allantois. An inaccurate injection can adversely impact the results of a distribution study.

To improve the accuracy of distribution studies in the chicken model, earlier time points should be included to account for the rapid uptake of drugs to the brain, such as methadone. However, a potential challenge with earlier time points is the chosen anaesthesia with hypothermia, which may slow down embryo metabolism and potentially affect brain uptake. Lower uptake in cells due to lower temperature has been shown in previous studies (123, 124). This could result in an underestimation of the true uptake levels. This raises the question of how the model can be improved. The understanding of embryonic pain in the chicken embryo is not yet definitive, and it is argued that it is impossible for the embryos to perceive pain in the early stages of incubation (92). From E8 to E15, an understanding of the embryonic chick's pain perception is lacking (92, 125), which leads to the question of whether the embryos in this distribution study, which were decapitated at E13 and E14, need anaesthesia. However, in the present study, the embryos were exposed to methadone, which has analgesic effects, so one can argue that anaesthesia may be unnecessary.

4.1.2 The *in vitro* models

To avoid animal exposure to the drugs, one can use cell cultures. Cell cultures can be primary cell cultures, like the chicken granule neurons, or immortalised cell lines, like the rat pheochromocytoma PC12 or the human neuroblastoma SH-SY5Y. An advantage of primary cells is that if they show the same results as *in vivo* models, it is less of a burden on the animals to do experiments *in vitro*. Instead of exposing the animals to the drugs, the cells can be exposed directly, resulting in adverse effects on the animals being avoided. Moreover, *in vitro* models provide the opportunity to experiment with inhibitors of important signalling pathways. Acquiring authorisation to administer these inhibitors *in vivo* is more challenging than obtaining permission to administer drugs. This is due to drugs having undergone thorough research and documentation to ensure they are non-hazardous to humans and animals. In contrast, inhibitors are usually solely intended for experimental purposes, and *in vitro* experiments do not need authorisation for the use of these.

PC12 cells are often chosen as a model to study neurotoxicity (97). Immortalised cell lines have several advantages compared with primary cell cultures, as they are more cost-effective and easier to use (126). The cells also proliferate, which means that studies can be done several times from the same cell line. However, one must be aware that high passage numbers

can result in the cells developing spontaneous changes that affect the phenotype (127). The cells are cancerous before differentiation and do not possess neurites but can produce neurites after differentiation. Differentiation can easily be done by adding NGF to the medium, and it takes about 2-3 days before they are differentiated (97). Since there is a difference in phenotype between differentiated and undifferentiated cells, investigating whether this can affect the results is worth considering.

4.2 Choice of exposures

Both methadone and morphine are classified as opioids, but their area of use is very different. Since morphine often is regarded as the golden standard for opioids and their effects, it was used as a golden standard in these experiments as well. In Norway, the serum concentration of methadone for patients in OMT should range from 0.6-1.2 µM (37). Morphine does not have the same strict guidelines for serum concentration as methadone, so a clinically relevant concentration is based on the minimum effective concentration and other therapeutic concentrations. A study from 1985 determined the minimum effective plasma concentration to be 0.07-0.14 µM (20-40 ng/mL) (128). In 2015, a study of cancer patients receiving morphine observed the median concentration of morphine to be 0.27 µM (31).

According to the guide on safety pharmacological studies made by ICH/EMA (CPMP/ICH/539/00), *in vitro* and *in vivo* studies should be designed to study the relationship between concentration and the effect of pharmaceuticals (129). The same guide emphasises that the concentrations used should increase the chance of observing an effect. This includes concentrations that are above the therapeutic range to uncover pharmacodynamic variability between species and models that can affect the response (129).

The three concentrations of methadone (1, 10 and 100 µM) were chosen because they meet the requirements of concentrations in the ICH guideline and because the concentrations have shown significant differences in results done by previous master's students (130, 131). The morphine concentration, however, does not meet these requirements, as the range used does not include a therapeutic concentration. The lowest concentration is still ten times higher than the minimum effective range for plasma concentration mentioned earlier. These concentrations were used in all *in vitro* exposures except exposures before high-content

imaging. Because the highest concentration of methadone was deemed toxic for the CGNs, this concentration was excluded from the pilot.

Methadone and morphine were dissolved in MQ water. To eliminate the potential effect of water on the osmolarity in the growth environment, 1000x stocks of the pharmaceuticals were used. This resulted in the cells only being exposed to 1 ‰ MQ water at the highest, and to account for any potential effects, all controls contained 1 ‰. However, an effect on osmolarity caused by such a small amount is highly unlikely.

For the distribution study, a methadone concentration of 20 mg/kg was chosen because of its use in previous studies (130, 132). However, some studies have shown that concentrations as low as 0.8 mg/kg egg have affected the chicken embryo's development (133). In these studies, methadone was injected for several days and is, therefore, not completely comparable to our study. Methadone was dissolved in saline (0.9% NaCl) to eliminate the risk of changing the osmolarity of the egg, which can further affect the development of the embryo. The distribution study was not meant to study the effects within the therapeutic range. Additionally, the embryos were only exposed briefly, for a maximum of 24 hours, before harvesting the tissue. Therefore, the concentration was deemed suitable for this experiment.

The inhibitors were chosen to assess the effect they had on neurite outgrowth and viability. The concentration for ANA-12 (10 μM) was based on previous studies where the inhibitor blocked BDNF-induced neurite outgrowth (83) and is within the IC_{50} values (134). Given that methadone has been shown to decrease cell viability at high concentrations (130, 135, 136), it was deemed appropriate to study the effect of adding an inhibitor for a receptor involved in apoptotic signalling. The $p75^{NTR}$-sortilin complex mediates apoptotic signalling (80), and therefore the $p75^{NTR}$ inhibitor TAT-Pep5 was chosen. A TAT-Pep5 concentration of 100 nM was chosen, as it is deemed effective (137).

ANA-12 and TAT-Pep5 were dissolved in DMSO. DMSO is deemed to be toxic for cells at a concentration of 0.5-1% (138, 139). However, even lower concentrations (0.1-0.001%) have been linked to enhancing proliferation in GSF3.2 cells (139). The inhibitors in the present experiments were used to expose CGNs, and the highest DMSO concentration in these experiments was 1‰. The effect of DMSO might be different in other cell lines, and therefore, a control with DMSO should have been included in the experiments.

4.3 *In vitro* methods

4.3.1 MTT assay

The MTT assay is a widely recognised method for assessing cell viability; however, it comes with a few disadvantages (140). It was observed that after adding MTT, the CGNs became less adherent, making them susceptible to aspiration during the removal of the MTT solution. This may lead to potential variability in the number of remaining cells, which can affect the analysis. When the CGNs were seeded with a lower density, improved adhesion of the cells to the plate was observed. Another disadvantage of the method is that the MTT assay does not measure cell death; it measures mitochondria activity (140). Due to this, it is important to note that not all results can be attributed to cell death or reduced viability but rather to reduced cell activity or proliferation. This can lead to inaccurate conclusions being drawn. Therefore, the MTT assay should be done alongside other ways to measure cell death or proliferation. Cell death can be confirmed by using trypan blue, which will stain the dead cells, whereas the viable cells will remain unstained (141).

4.3.2 RT-qPCR

While the significance of the results obtained through RT-qPCR in this study is limited, there is potential for improvement in the method. The lack of statistical significance in most of the results may be due to the variation in the control. This could be attributed to the use of an inappropriate housekeeping gene. The choice of housekeeping gene is crucial since some genes are more suitable in the chicken model than others (142). Furthermore, using a single housekeeping gene may result in larger errors when compared to using several genes (143). To address this issue, it is recommended to use more than one housekeeping gene, and to select genes that are appropriate for the specific model used. In avian animal models, studies have identified ACTB (actin beta) and GAPDH as the most unstable housekeeping genes (142, 144). The studies also recommended using 18S ribosomal RNA as the housekeeping gene; therefore, this should be used in future research. Additionally, RT-qPCR does not provide information on the downstream effects of change in gene expression. However, this can be studied using a western blot analysis which can verify the RT-qPCR results.

4.4 Biological findings

4.4.1 Viability and neurite outgrowth

The MTT assay determined that the viability of both PC12 cells and CGNs was significantly decreased when exposed to 100 μM methadone. Viability was further reduced with simultaneous exposure to ANA-12, which might be an indication of synergism. The TrkB receptor is important for cell survival due to BDNF binding to the receptor, promoting plasticity and survival (75). Therefore, ANA-12 blocks a signalling pathway of cell survival, exacerbating the toxic effects of methadone. To date, no previous research has investigated the potential synergistic effect of ANA-12 and methadone in combination. However, the effect of ANA-12 alone in the human medulloblastoma cell lines UW228 and D283 has been studied, resulting in decreased cell viability after 72 hours of exposure (145). Although the viability of the cells was not significantly reduced by ANA-12 alone in our study, this might explain the observed tendency towards a slight reduction.

The $p75^{NTR}$ inhibitor TAT-Pep5 did not reverse the effect of methadone on viability, which may suggest an alternative pathway is regulating cell death or that the inhibitory concentration used was insufficient. In previous research with TAT-Pep5, the concentration used was 10 μM (84, 146, 147), whereas a study in SH-SY5Y cells showed effective inhibition at 1 μM and 500 nM (148). These concentrations are significantly higher than the 100 nM deemed effective by the supplier (137). Further studies on this should therefore be conducted.

In terms of the MTT assay results in PC12 cells, all three media environments demonstrated a reduction in cell viability upon exposure to 100 μM methadone. Furthermore, when the undifferentiated cells were exposed to 10 μM methadone in a low serum environment, a significant decrease in cell viability was observed compared to the control group. Cells cultured in differentiation media supplemented with NGF have an increased amount of growth factors compared to cells grown in low serum media alone. NGF has been linked to increased cell survival and proliferation (149, 150). The regular media contains FBS, which has been shown to increase proliferation in various cell lines (151, 152, 153). Therefore, it is plausible that the observed decline is not due to apoptosis but rather a reduction in proliferation caused by the low serum environment. Another possibility is that the combined effect of methadone and a low serum environment may produce a synergistic outcome.

However, an interesting observation is that there is no apparent difference between the differentiated and undifferentiated PC12 cells in this study. This raises the question of whether it is necessary to differentiate the cells to study their viability, as the results indicate that the differentiation process did not make the cells more susceptible to toxic effects.

The effect of methadone on viability has also been shown previously, although in different cell lines. A study done in SH-SY5Y cells showed that a concentration of 500 µM methadone resulted in 40% cell death (136), however, they assessed it using lactate dehydrogenase activity and not MTT. An MTT study in LN229 glioblastoma cells showed a significant reduction in cell viability when exposed to 65 µM methadone (135). The big difference in the concentrations resulting in a significant reduction in viability may be caused by the difference in the methods, but the differences in the models used could also play a part. Therefore, it was interesting to evaluate the effect on viability in both PC12 cells and CGNs. Interestingly, they exhibited similar results. As previously stated, the PC12 model lacks information on the presence of MOR, which has resulted in many studies transfecting the receptor. If there is a lack of MOR in the model, similar results between the CGNs and PC12 cells may indicate that the toxicity is mediated through a different pathway. Additionally, further studies with concentrations of methadone between 10 and 100 µM should be conducted to determine the IC_{50} values.

Neurite length in the CGNs exposed to 100 µM methadone was significantly decreased. However, these results are likely due to this concentration of methadone reducing the viability and not because the cells develop shorter neurites. Analysis of the IncuCyte images revealed an evident contrast between the control and 100 µM methadone-treated cells. The cells exposed to 100 µM methadone displayed distinct morphological differences, indicating cell death. Therefore, the reduced neurite length is most likely due to cell death. The cells exposed to 1 and 10 µM methadone showed no statistically significant reduction in neurite length. However, the curves tend to be lower than the control for these concentrations. The cells exposed to 10 µM methadone seem to have shorter neurites compared with 1 µM in general, and the lowest concentration gave shorter neurites than the control. This might imply that there is a response in neurite length when exposed to higher, non-toxic concentrations. However, more experiments with additional concentrations between 10 and 100 µM methadone are needed to reach statistical power. Additionally, further evaluation of what has

caused the decrease in neurite length can be done by analysing cell body clusters and cell body cluster areas.

At 48 hours, there was a significant reduction in neurite length in cells exposed to 100 µM morphine. Unlike methadone, this is not likely caused by cell death, as the MTT assay shows no significance or tendency to reduce viability for any of the concentrations of morphine. This claim is supported by the live-cell images, which show no apparent morphological changes when comparing morphine-treated cells with the control. However, like methadone, the curves for 1 and 10 µM morphine tend to be lower than the control, although not statistically significant. Contrary to this observed trend, a previous study conducted in differentiated PC12 cells showed that 10 µM morphine does not affect neurite outgrowth (154). Additionally, ultra-low concentrations of morphine have been shown to increase neurite outgrowth, though these concentrations are considerably lower than the ones in the present study (155). Given that the concentrations used in the present study exceed clinical concentrations, investigating lower concentrations may be of interest to future research.

In addition to the effect of methadone and morphine on neurite length, the effect on synaptogenesis was studied using high-content imaging. When synaptogenesis was studied, 100 µM methadone and morphine exposure were excluded. The exposure with 100 µM methadone was excluded due to the significant cell death observed with the MTT assays, resulting in a substantial reduction in neurite length during live-cell imaging. The absence of neurites and viable cells undermines the relevance of studying synaptogenesis, particularly from a quantitative perspective. Nevertheless, even at lower concentrations, quantitative results could not be obtained due to the high density of the cells. From the lack of clear synapses stained in the images, the theory is that a lot of them are situated inside the cell clusters. Consequentially, it was challenging to determine any qualitative differences between the exposures. A lower density is therefore required to produce both quantitative and qualitative results.

4.4.2 Gene expression in the chicken granule neurons

Since prolonged signalling through the opioid receptors has been linked to an effect on several processes involved in neurodevelopment (16), studying the gene expression of MOR, DOR and KOR was relevant. The MOR expression increased significantly in cells exposed to

100 µM methadone, whereas morphine exposure tended towards a dose-response reduction. The effect on KOR and DOR expression remains inconclusive in the present study. Interestingly, the effect of 100 µM methadone contradicts previous studies. In a study involving human pre-term and full-term immune cells, methadone and morphine exposure resulted in a decline in MOR expression, while KOR and DOR expression remained unchanged (156). They also did a western blot analysis, which resulted in 10 µM methadone and morphine decreasing the protein expression of MOR (156). Changes in the expression and location of MOR may be linked to the mechanism behind developing tolerance to opioids (157, 158). Therefore, the increased expression of MOR in the present study is unexpected. However, both 10 µM methadone and 10 µM morphine tended to decrease MOR expression in the present study. Statistical power might be reached with more experiments.

Due to methadone and morphine binding to the same receptors as endogenous opioid peptides (21), it was relevant to study the effect of the precursors of these. PDYN and PENK gene expression was increased and reduced by 100 µM methadone, respectively. The results also indicated a possible dose-response relationship, with higher concentrations increasing PDYN and decreasing PENK. Morphine showed the opposite dose-response trend. No studies on the correlation between PENK and methadone were found. However, a study of SH-SY5Y cells exposed to opioids showed that methadone increases PDYN expression, while morphine initially increases and then decreases PDYN expression after 72 hours (159). This is in accordance with the findings of the present study. However, a study of repeated morphine exposure in mice shows the opposite effect (160). Therefore, this needs more studying.

The study also aimed to investigate the impact of opioids on the genes encoding BDNF and CREB1, as they are important signalling pathways for development (74-79). In the present findings, methadone appears to have a dose-response relationship in the expression of BDNF and CREB1, where higher concentrations lead to greater reductions in expression. However, there were no dose-response trends in the morphine findings. In previous research conducted on rats (161), it was discovered that exposure to methadone and morphine resulted in a significant decrease in the expression of CREB and BDNF genes. This is in accordance with a study of patients receiving methadone maintenance treatment, where BDNF concentrations in the serum were significantly reduced after 12 weeks of treatment (162).

It was relevant to investigate whether opioid exposure affects the expression of the GluN2B gene, given that methadone is an NMDA-receptor antagonist (36). Interestingly, the GluN2B expression tends to be increased by 100 µM morphine, despite morphine not binding to the NMDA receptor. This result was, however, not statistically significant. In contrast, 100 µM methadone significantly decreased the expression of the GluN2B gene. A decreased expression of the gene is likely to result in less GluN2B protein; however, this is not necessarily the case. In a study by our group, chicks injected with 20 mg/kg methadone or morphine at E13 or E14 did not show a significant change in GluN2B protein in western blotting (132). However, these data cannot be compared directly, as CGNs were used for RT-qPCR, while cerebella were used for western blotting. Alterations in GluN2B expression may have an impact on neurodevelopment, as this subunit of the NMDA receptor undergoes changes in its expression levels during development and is associated with processes such as neuronal migration and differentiation (70, 71). Therefore, this should be studied further.

Methadone is mainly metabolised by the enzyme CYP3A4 (40), whereas morphine is mainly metabolised through phase 2 glucuronidation (33). CYP enzymes have been detected in the brain of various species, including dogs, rodents, monkeys, and humans (163). The expression of local CYP enzymes has been linked to the potential effect of local metabolism and efficacy in the brain (164). However, no studies of the CYP3A4 expression in neurons have been conducted, which may be due to the low levels of CYP enzymes in the brain compared to the liver. A study done in human hepatocytes measured that the expression of CYP3A4 mRNA was increased 3-fold when exposed to 10 µM methadone (165) and is concluded to be an autoinduction. A significant increase in the expression of CYP3A4 was not observed at 10 µM in the present study. However, the cells exposed to 100 µM had a 17-fold increase in CYP3A4 gene expression. While no studies on the effect of morphine on CYP3A4 were found, it is expected that morphine does not alter CYP3A4 expression, as it is not metabolised by it and neither induces nor inhibits the enzyme. This is in accordance with the findings of the present study.

4.4.3 Distribution of methadone and its metabolite in the chicken model

The distribution study revealed that methadone rapidly distributes to the brain, lungs, and yolk of the chicken embryo. A similar distribution study of methadone was done in a previous master's thesis in the group, where they did concentration measurements at 6 hours and

onwards (130). However, a further investigation of the peak was needed, as the concentrations from 0 hours to 6 hours were unknown. Therefore, it was interesting to study earlier time points, especially around the 6-hour time point where morphine has its peak (T_{max}) in chicken embryos (131). The T_{max} of methadone in the present study turned out to be around 1 hour, which is vastly different from the T_{max} of morphine. The reason for this might be explained by Lipinski's Rule of Five and the existence of a BBB (88). Methadone has no hydrogen bond donors, whereas morphine has two. This chemical property of methadone increases the logP value, which means that methadone is more lipophilic than morphine. As previously stated, lipophilicity is an important factor that can influence passive diffusion across the BBB. This has also been proven in previous studies. A distribution study done in rats concluded that methadone would have a faster uptake in the brain than morphine after an intravenous injection (90), and higher logP values have been shown to result in a faster distribution to the brain (88).

There are also other factors from the present study that can indicate the existence of a BBB. The C_{max} of methadone (210 µM) in the brain is significantly higher than in the lung (87 µM), and $T_{1/2}$ in the brain was longer than in the lungs (2.1 vs 1.4 hours). Notably, the slope of the methadone concentration curve in the lungs decreased immediately, whereas the concentration of methadone in the brain appeared to increase from 30 minutes to 1 hour. The fact that the T_{max} of the brain arrived later than that of the lungs suggests that the BBB is developing. However, the existence of a BBB is expected to cause a higher concentration in the lungs than in the brain, as shown when comparing the measured concentrations in studies in mice and rats (166, 167). This was also the case in a previous master's thesis (130), but it is the opposite of what was shown in the present study. The lungs have a much lower concentration in the present study at 6 hours. However, the peak of the lungs might be earlier than measured, which may be why the concentration is lower than the concentration in the brain. Nevertheless, this does not explain why the concentration was lower than in the previous study. Therefore, the difference in the concentration between these studies might be due to differences in the method, for instance, the time of day for injecting or the injection site. As stated previously, it is difficult to determine exactly where the drug is injected, which can potentially lead to differences in the distribution.

Another indication of a developing BBB is explained by the distribution of the main metabolite EDDP. EDDP seems to accumulate in all three tissues but at different rates. The

concentrations of EDDP during the first four hours are significantly lower in the brain than in the lung. This might indicate that the drug is metabolised peripherally, most likely in the liver, and is distributed rapidly to the lungs. Additionally, it takes longer for the concentrations of EDDP to reach the same concentrations as the lungs, which might indicate the existence of a developing BBB.

Based on the theory that the BBB develops rapidly at E13 and E14, the 18-hour time point raised concerns as methadone was administered later in the day compared to the other time points. While a delayed injection at this point could potentially affect the results, there is no indication from the curve that this has occurred. Studies using horseradish peroxidase (HRP) in embryonic chicks revealed that the BBB impedes HRP passage to the brain at E10 (168), and the BBB was fully developed in the cerebellum at E15 (169). Another study established that the BBB almost completely blocked HRP at E14, while smaller molecules (<1.000 Da) could still permeate. Additionally, the permeability of HRP was fully blocked at E18 (170). Based on these studies, it is likely that the BBB matures between E10 and E18. Since methadone is a smaller molecule than HRP, it is reasonable to expect it to cross the BBB at similar rates within a few hours at E13.

The drug distribution study in the chicken embryo may have been affected by other factors. Firstly, the yolk may act as a reservoir for drug accumulation, potentially leading to an increase in concentration in other organs and tissues over time due to the yolk being the source of nutrition (171). An accumulation of endogenous metabolites in the yolk has been shown in previous studies (171), which also seems to be the case for the EDDP metabolite and methadone in the present study. Secondly, as shown with the MTT assay, the viability of the cells was significantly decreased when exposed to 100 µM methadone. This raises the question of whether the concentration of methadone can affect the distribution since the observed C_{max} was 210 µM. Lastly, the RT-qPCR results showed increased CYP3A4 gene expression at 72 hours of exposure to 100 µM methadone. This raises the question of whether this can affect EDDP distribution. However, the high concentration of methadone *in vivo* may not last long enough to cause an effect.

4.5 Future perspectives

The RT-qPCR experiment conducted in this study served as a pilot, and further research is necessary to investigate the effects of methadone and morphine in greater depth. Although the graphs show some interesting changes and trends, the findings require validation through more biological and technical replicates. These genes encode different proteins that can be analysed using western blot, however, only some have been studied so far. Therefore, to obtain a greater understanding of the effects of the opioids, western blots should be conducted together with qPCR. It is important to note that all qPCR results presented in this study are from CGNs exposed to methadone and morphine. By administering *in ovo* injections in further studies, we could also examine if there is any variation in the results between *in vitro* and *in ovo* exposures.

In the distribution study, the precise peak of methadone might not yet be determined, and obtaining earlier time-point data could assist in determining this. However, to obtain accurate results at earlier time points, it is necessary to refine the protocol for euthanasia to eliminate potential adverse effects on the distribution in the current method. Additionally, since harvesting lung tissue at E14 is challenging, an alternative or additional approach could be to harvest other organs in the embryo, such as the liver, to refine the distribution study further. This can also provide further insights into the metabolism of methadone in the chicken embryo.

More studies in different types of cell cultures are needed to enhance the applicability of the results to humans. This includes studying the effects in, e.g., SH-SY5Y cells and further studies in PC12 cells. For instance, PC12 cells can be differentiated even longer before exposure or exposed for an even longer period while differentiating to see further effects. This can also be done to study the difference in the behaviour of fully differentiated, undifferentiated, or cells during differentiation. To determine the effect of the differentiation process, live-cell and high-content imaging in PC12 can be utilised. Additionally, further live-cell imaging can be used to validate the results of opioid exposure in the chicken granule neurons.

5 Conclusion

The MTT assay revealed that 100 µM methadone was toxic to cells. The $p75^{NTR}$ receptor may not be involved in the apoptosis caused by methadone exposure, but inhibiting the TrkB receptor may worsen the toxic effect. The cell death caused by methadone affected the studies of neurite outgrowth, as the neurites were lost. Lower and more clinically relevant concentrations of methadone did not show any toxic effects. Morphine did not appear to be toxic to the cells, but after 48 hours of exposure to 100 µM morphine, neurite length was significantly reduced. Due to the high cell density, it was not possible to determine the effect of methadone and morphine on synaptogenesis, which requires further study.

The RT-qPCR pilot gave insights into potential changes in gene expression due to methadone and morphine exposure. However, only 100 µM methadone showed significant changes in the expression of MOR, PDYN, PENK, GluN2B, and CYP3A4. No significant changes were found in the expression of BDNF and CREB1. Due to the high variability in the data, possible significant changes might have been concealed. Further research can assist in revealing effects that reach statistical power.

Methadone was rapidly distributed to the brain and lungs of the embryo and appeared to accumulate in the yolk. Higher concentrations of methadone were found in the brain compared to the lungs. The concentration of the metabolite EDDP increased in all tissues up to 24 hours, and the concentrations in the lungs were higher than in the brain during the first four hours. This may suggest the presence of a blood-brain barrier undergoing development and that metabolism occurs peripherally. Nevertheless, additional studies are required to validate these findings.

6 References

1. Kornør H, Flodgren GM, Mosdøl A, Strømme H, Holte HH. Nedtrapping av buprenorfin eller metadon for gravide i legemiddelassistert rehabilitering (LAR). Folkehelseinstituttet; 2018. Report No.: RL023.
2. Helsedirektoratet. Legemiddelassistert rehabilitering (LAR) [Internet]. Oslo: Helsedirektoratet; 2022 [updated June 13 2022; cited 2022 September 7th]. Available from: https://www.helsenorge.no/rus-og-avhengighet/legemiddelassistert-behandling-lar/.
3. Bech AB, Bukten A, Philipp Lobmaier P, Skeie I, Lillevold PlH, Clausen T. Statusrapport 2021: Siste år med gamle LAR-retningslinjer. Oslo: Senter for rus- og avhengighetsforskning (SERAF); 2022. Report No.: 2.
4. Helsedirektoratet. Gravide i legemiddelassistert rehabilitering (LAR): Nasjonal faglig retningslinje. Anbefalinger om prevensjon og familieplanlegging, legemiddelvalg og legemiddeldose (2019) [Internet]. Oslo: Helsedirektoratet; 2019 [updated August 9 2022; cited 2022 September 7th]. Available from: https://www.helsedirektoratet.no/retningslinjer/gravide-i-lar/anbefalinger-om-prevensjon-og-familieplanlegging-legemiddelvalg-og-legemiddeldose-2019#kvinner-i-legemiddelassistert-rehabilitering-lar-i-fertil-alder-bor-bruke-det-substitusjonslegemiddelet-som-etter-individuell-vurdering-gir-best-behandlingseffekt-ved-ukjent-eller-erfart-likeverdig-behandlingseffekt-bor-buprenorn-foretrekkes.
5. Suarez EA, Huybrechts KF, Straub L, Hernández-Díaz S, Jones HE, Connery HS, et al. Buprenorphine versus Methadone for Opioid Use Disorder in Pregnancy. N Engl J Med. 2022;387(22):2033-44.
6. van der Zande ISE, van der Graaf R, Oudijk MA, van Delden JJM. Vulnerability of pregnant women in clinical research. J Med Ethics. 2017;43(10):657-63.
7. Shafi A, Berry AJ, Sumnall H, Wood DM, Tracy DK. Synthetic opioids: a review and clinical update. Ther Adv Psychopharmacol. 2022;12:20451253221139616.
8. James A, Williams J. Basic Opioid Pharmacology - An Update. Br J Pain. 2020;14(2):115-21.
9. Henderson G, Flower RJ, Ritter JM, Dale MM, Rang HP. Rang and Dale's pharmacology. 8th ed. Edinburgh: Elsevier Churchill Livingstone; 2016.
10. Department of Justice/Drug Enforcement Administration. Synthetic opioids [Internet]. United States Drug Enforcement Administration; 2020 [updated April 2020; cited 2023 April 12th]. Available from: https://www.dea.gov/sites/default/files/2020-06/Synthetic%20Opioids-2020.pdf.
11. National Museum of Drug Enforcement Administration. Opium Poppy [Internet]. 2020 [cited 2023 April 21st]. Available from: https://museum.dea.gov/exhibits/online-exhibits/cannabis-coca-and-poppy-natures-addictive-plants/opium-poppy.
12. Jiang R, Lee I, Lee TA, Pickard AS. The societal cost of heroin use disorder in the United States. PLoS One. 2017;12(5):e0177323.
13. Gjersing L. Skader og problemer knyttet til narkotikabruk [Internet]. Folkehelseinstituttet2018 [updated September 9th 2018; cited 2023 May 10th]. Available from: https://www.fhi.no/nettpub/narkotikainorge/konsekvenser-av-narkotikabruk/skader-og-problemer-knyttet-til-narkotikabruk/.
14. Huseby CH. LAR (legemiddelassistert rehabilitering) [Internet]. Store medisinske leksikon: Store norske leksikon; 2020 [updated May 4th 2020; cited 2023 May 9th]. Available from: https://sml.snl.no/LAR_-_legemiddelassistert_rehabilitering.
15. Chu Sin Chung P, Kieffer BL. Delta opioid receptors in brain function and diseases. Pharmacol Ther. 2013;140(1):112-20.

16. Lutz PE, Kieffer BL. Opioid receptors: distinct roles in mood disorders. Trends Neurosci. 2013;36(3):195-206.
17. Herman TF, Cascella M, Muzio MR. Mu Receptors. StatPearls. Treasure Island (FL): StatPearls Publishing; 2023.
18. Trescot AM, Datta S, Lee M, Hansen H. Opioid pharmacology. Pain Physician. 2008;11(2 Suppl):S133-53.
19. Peng J, Sarkar S, Chang SL. Opioid receptor expression in human brain and peripheral tissues using absolute quantitative real-time RT-PCR. Drug Alcohol Depend. 2012;124(3):223-8.
20. Valentino RJ, Volkow ND. Untangling the complexity of opioid receptor function. Neuropsychopharmacology. 2018;43(13):2514-20.
21. Dhaliwal A, Gupta M. Physiology, Opioid Receptor. StatPearls. Treasure Island (FL): StatPearls Publishing; 2023.
22. Cox BM, Christie MJ, Devi L, Toll L, Traynor JR. Challenges for opioid receptor nomenclature: IUPHAR Review 9. Br J Pharmacol. 2015;172(2):317-23.
23. Fricker LD, Margolis EB, Gomes I, Devi LA. Five Decades of Research on Opioid Peptides: Current Knowledge and Unanswered Questions. Mol Pharmacol. 2020;98(2):96-108.
24. Schwarzer C. 30 years of dynorphins--new insights on their functions in neuropsychiatric diseases. Pharmacol Ther. 2009;123(3):353-70.
25. Zagon IS, Verderame MF, McLaughlin PJ. The biology of the opioid growth factor receptor (OGFr). Brain Res Brain Res Rev. 2002;38(3):351-76.
26. Valbrun LP, Zvonarev V. The Opioid System and Food Intake: Use of Opiate Antagonists in Treatment of Binge Eating Disorder and Abnormal Eating Behavior. J Clin Med Res. 2020;12(2):41-63.
27. Mørland J, Bretteville-Jensen AL. Opium [Internet]. Store medisinske leksikon: Store Norske Leksikon; 2023 [updated January 12th; cited 2023 April 18th]. Available from: https://snl.no/opium.
28. Felleskatalogen. Morfin Orifarm Healthcare [Internet]. Felleskatalogen; 2022 [updated 2022 April 26th; cited 2023 April 10th]. Available from: https://www.felleskatalogen.no/medisin/morfin-orifarm-healthcare-561671.
29. Felleskatalogen. Oramorph Molteni [Internet]. Felleskatalogen; 2020 [updated 2021 January 20; cited 2023 April 10th]. Available from: https://www.felleskatalogen.no/medisin/oramorph-molteni-573631.
30. Helland A, Berg JA, Gustavsen I, Nordal K, Hilberg T, Aronsen L, et al. Serum concentration measurements of addictive drugs. Tidsskr Nor Laegeforen. 2016;136(5):400-2.
31. Lee YJ, Suh SY, Song J, Lee SS, Seo AR, Ahn HY, et al. Serum and urine concentrations of morphine and morphine metabolites in patients with advanced cancer receiving continuous intravenous morphine: an observational study. BMC Palliat Care. 2015;14:53.
32. Christrup LL. Morphine metabolites. Acta Anaesthesiol Scand. 1997;41(1 Pt 2):116-22.
33. Smith HS. Opioid metabolism. Mayo Clin Proc. 2009;84(7):613-24.
34. DrugBank. Morphine [Internet]. [cited 2023 May 8th]. Available from: https://go.drugbank.com/drugs/DB00295.
35. Whelan PJ, Remski K. Buprenorphine vs methadone treatment: A review of evidence in both developed and developing worlds. J Neurosci Rural Pract. 2012;3(1):45-50.
36. Ebert B, Andersen S, Krogsgaard-Larsen P. Ketobemidone, methadone and pethidine are non-competitive N-methyl-D-aspartate (NMDA) antagonists in the rat cortex and spinal cord. Neurosci Lett. 1995;187(3):165-8.

37. Fürst medisinsk laboratorium. S-Metadon [Internet]. Fürst medisinsk laboratorium [cited 2022 September 7th]. Available from: https://www.furst.no/analyse-og-klinikk/analyser/metadon/.
38. Meresaar U, Nilsson MI, Holmstrand J, Anggård E. Single dose pharmacokinetics and bioavailability of methadone in man studied with a stable isotope method. Eur J Clin Pharmacol. 1981;20(6):473-8.
39. Inturrisi CE, Verebely K. The levels of methadone in the plasma in methadone maintenance. Clin Pharmacol Ther. 1972;13(5):633-7.
40. Ferrari A, Coccia CP, Bertolini A, Sternieri E. Methadone--metabolism, pharmacokinetics and interactions. Pharmacol Res. 2004;50(6):551-9.
41. DrugBank. Methadone [Internet]. [cited 2023 May 8th]. Available from: https://go.drugbank.com/drugs/DB00333.
42. Jansson LM, Patrick SW. Neonatal Abstinence Syndrome. Pediatr Clin North Am. 2019;66(2):353-67.
43. Sandtorv LB, Fevang SKE, Nilsen SA, Bøe T, Gjestad R, Haugland S, et al. Symptoms Associated With Attention Deficit/Hyperactivity Disorder and Autism Spectrum Disorders in School-Aged Children Prenatally Exposed to Substances. Subst Abuse. 2018;12:1178221818765773.
44. Ornoy A, Michailevskaya V, Lukashov I, Bar-Hamburger R, Harel S. The developmental outcome of children born to heroin-dependent mothers, raised at home or adopted. Child Abuse Negl. 1996;20(5):385-96.
45. Bhuvaneswar CG, Chang G, Epstein LA, Stern TA. Cocaine and opioid use during pregnancy: prevalence and management. Prim Care Companion J Clin Psychiatry. 2008;10(1):59-65.
46. Fodor A, Tímár J, Zelena D. Behavioral effects of perinatal opioid exposure. Life Sci. 2014;104(1-2):1-8.
47. Mortensen NP, Caffaro MM, Snyder RW, Yueh YL, Fennell TR. Placental trophoblast transfer of opioids following exposures to individual or mixtures of opioids in vitro. Exp Biol Med (Maywood). 2019;244(10):846-9.
48. Di Trana A, La Maida N, Tittarelli R, Huestis MA, Pichini S, Busardò FP, et al. Monitoring Prenatal Exposure to Buprenorphine and Methadone. Ther Drug Monit. 2020;42(2):181-93.
49. Thompson BL, Levitt P, Stanwood GD. Prenatal exposure to drugs: effects on brain development and implications for policy and education. Nat Rev Neurosci. 2009;10(4):303-12.
50. Mahboub N, Rizk R, Karavetian M, de Vries N. Nutritional status and eating habits of people who use drugs and/or are undergoing treatment for recovery: a narrative review. Nutr Rev. 2021;79(6):627-35.
51. Altekruse SF, Cosgrove CM, Altekruse WC, Jenkins RA, Blanco C. Socioeconomic risk factors for fatal opioid overdoses in the United States: Findings from the Mortality Disparities in American Communities Study (MDAC). PLoS One. 2020;15(1):e0227966.
52. Slamberová R, Schindler CJ, Pometlová M, Urkuti C, Purow-Sokol JA, Vathy I. Prenatal morphine exposure differentially alters learning and memory in male and female rats. Physiol Behav. 2001;73(1-2):93-103.
53. Harlan RE, Song DD. Prenatal morphine treatment and the development of the striatum. Regul Pept. 1994;54(1):117-8.
54. Stiles J, Jernigan TL. The basics of brain development. Neuropsychol Rev. 2010;20(4):327-48.
55. Copp AJ, Greene ND, Murdoch JN. The genetic basis of mammalian neurulation. Nat Rev Genet. 2003;4(10):784-93.

56. Nowakowski RS, Hayes NL. CNS development: an overview. Dev Psychopathol. 1999;11(3):395-417.
57. Stiles J. The fundamentals of brain development: Integrating nature and nurture. Cambridge: MA: Harvard University Press; 2008.
58. Marzban H, Del Bigio MR, Alizadeh J, Ghavami S, Zachariah RM, Rastegar M. Cellular commitment in the developing cerebellum. Front Cell Neurosci. 2014;8:450.
59. Rice D, Barone S, Jr. Critical periods of vulnerability for the developing nervous system: evidence from humans and animal models. Environ Health Perspect. 2000;108 Suppl 3(Suppl 3):511-33.
60. Tau GZ, Peterson BS. Normal development of brain circuits. Neuropsychopharmacology. 2010;35(1):147-68.
61. Jansen JKS, Holck P. Lillehjernen [Internet]. Store medisinske leksikon: Store norske leksikon; 2023 [updated March 1st. Available from: https://sml.snl.no/lillehjernen.
62. Jimsheleishvili S, Dididze M. Neuroanatomy, Cerebellum. StatPearls. Treasure Island (FL): StatPearls Publishing; 2023.
63. Contestabile A. Cerebellar granule cells as a model to study mechanisms of neuronal apoptosis or survival in vivo and in vitro. Cerebellum. 2002;1(1):41-55.
64. Beckinghausen J, Sillitoe RV. Insights into cerebellar development and connectivity. Neurosci Lett. 2019;688:2-13.
65. Tanabe H, Kubo D, Hasegawa K, Kochiyama T, Kondo O. Cerebellum: Anatomy, Physiology, Function, and Evolution. 2018. p. 275-89.
66. Koziol LF, Budding D, Andreasen N, D'Arrigo S, Bulgheroni S, Imamizu H, et al. Consensus paper: the cerebellum's role in movement and cognition. Cerebellum. 2014;13(1):151-77.
67. Sultan F, Glickstein M. The cerebellum: Comparative and animal studies. Cerebellum. 2007;6(3):168-76.
68. Lackey EP, Heck DH, Sillitoe RV. Recent advances in understanding the mechanisms of cerebellar granule cell development and function and their contribution to behavior. F1000Res. 2018;7.
69. Apps R, Garwicz M. Anatomical and physiological foundations of cerebellar information processing. Nat Rev Neurosci. 2005;6(4):297-311.
70. Law AJ, Weickert CS, Webster MJ, Herman MM, Kleinman JE, Harrison PJ. Expression of NMDA receptor NR1, NR2A and NR2B subunit mRNAs during development of the human hippocampal formation. Eur J Neurosci. 2003;18(5):1197-205.
71. Jewett BE, Thapa B. Physiology, NMDA Receptor. StatPearls. Treasure Island (FL): StatPearls Publishing; 2023.
72. Monyer H, Sprengel R, Schoepfer R, Herb A, Higuchi M, Lomeli H, et al. Heteromeric NMDA receptors: molecular and functional distinction of subtypes. Science. 1992;256(5060):1217-21.
73. Vyklicky V, Korinek M, Smejkalova T, Balik A, Krausova B, Kaniakova M, et al. Structure, function, and pharmacology of NMDA receptor channels. Physiol Res. 2014;63(Suppl 1):S191-203.
74. Binder DK, Scharfman HE. Brain-derived neurotrophic factor. Growth Factors. 2004;22(3):123-31.
75. Acheson A, Conover JC, Fandl JP, DeChiara TM, Russell M, Thadani A, et al. A BDNF autocrine loop in adult sensory neurons prevents cell death. Nature. 1995;374(6521):450-3.
76. Huang EJ, Reichardt LF. Neurotrophins: roles in neuronal development and function. Annu Rev Neurosci. 2001;24:677-736.

77. Bathina S, Das UN. Brain-derived neurotrophic factor and its clinical implications. Arch Med Sci. 2015;11(6):1164-78.
78. Wang H, Xu J, Lazarovici P, Quirion R, Zheng W. cAMP Response Element-Binding Protein (CREB): A Possible Signaling Molecule Link in the Pathophysiology of Schizophrenia. Front Mol Neurosci. 2018;11:255.
79. Wen AY, Sakamoto KM, Miller LS. The role of the transcription factor CREB in immune function. J Immunol. 2010;185(11):6413-9.
80. Teng HK, Teng KK, Lee R, Wright S, Tevar S, Almeida RD, et al. ProBDNF induces neuronal apoptosis via activation of a receptor complex of p75NTR and sortilin. J Neurosci. 2005;25(22):5455-63.
81. Kraemer BR, Yoon SO, Carter BD. The biological functions and signaling mechanisms of the p75 neurotrophin receptor. Handb Exp Pharmacol. 2014;220:121-64.
82. Nykjaer A, Lee R, Teng KK, Jansen P, Madsen P, Nielsen MS, et al. Sortilin is essential for proNGF-induced neuronal cell death. Nature. 2004;427(6977):843-8.
83. Cazorla M, Prémont J, Mann A, Girard N, Kellendonk C, Rognan D. Identification of a low-molecular weight TrkB antagonist with anxiolytic and antidepressant activity in mice. J Clin Invest. 2011;121(5):1846-57.
84. Head BP, Patel HH, Niesman IR, Drummond JC, Roth DM, Patel PM. Inhibition of p75 neurotrophin receptor attenuates isoflurane-mediated neuronal apoptosis in the neonatal central nervous system. Anesthesiology. 2009;110(4):813-25.
85. Daneman R, Prat A. The blood-brain barrier. Cold Spring Harb Perspect Biol. 2015;7(1):a020412.
86. Groenendaal D, Freijer J, de Mik D, Bouw MR, Danhof M, de Lange EC. Population pharmacokinetic modelling of non-linear brain distribution of morphine: influence of active saturable influx and P-glycoprotein mediated efflux. Br J Pharmacol. 2007;151(5):701-12.
87. Schinkel AH, Wagenaar E, Mol CA, van Deemter L. P-glycoprotein in the blood-brain barrier of mice influences the brain penetration and pharmacological activity of many drugs. J Clin Invest. 1996;97(11):2517-24.
88. Mikitsh JL, Chacko AM. Pathways for small molecule delivery to the central nervous system across the blood-brain barrier. Perspect Medicin Chem. 2014;6:11-24.
89. Benet LZ, Hosey CM, Ursu O, Oprea TI. BDDCS, the Rule of 5 and drugability. Adv Drug Deliv Rev. 2016;101:89-98.
90. Oldendorf WH, Hyman S, Braun L, Oldendorf SZ. Blood-brain barrier: penetration of morphine, codeine, heroin, and methadone after carotid injection. Science. 1972;178(4064):984-6.
91. Kirk RGW. Recovering The Principles of Humane Experimental Technique: The 3Rs and the Human Essence of Animal Research. Sci Technol Human Values. 2018;43(4):622-48.
92. Bjørnstad S, Austdal LP, Roald B, Glover JC, Paulsen RE. Cracking the Egg: Potential of the Developing Chicken as a Model System for Nonclinical Safety Studies of Pharmaceuticals. J Pharmacol Exp Ther. 2015;355(3):386-96.
93. Geladopoulos T, Sakellaridis N, Vernadakis A. Differential maturation of mu and delta opioid receptors in the chick embryonic brain. Neurochem Res. 1987;12(3):279-88.
94. Cserpán E, Tryoen-Tóth P, Bajenaru L, Benyhe S, Maderspach K. Differential expression of the K-2 opioid receptor protein under the effect of opioid agonists in embryonic chick neurons in vitro. Neurobiology (Bp). 1997;5(2):233-48.
95. Maderdrut JL, Merchenthaler I, Sundberg DK, Okado N, Oppenheim RW. Distribution and development of proenkephalin-like immunoreactivity in the lumbar spinal cord of the chicken. Brain Res. 1986;377(1):29-40.
96. Ren J, Yang L, Li Q, Zhang Q, Sun C, Liu X, et al. Global Investigation of Cytochrome P450 Genes in the Chicken Genome. Genes (Basel). 2019;10(8).

97. Wiatrak B, Kubis-Kubiak A, Piwowar A, Barg E. PC12 Cell Line: Cell Types, Coating of Culture Vessels, Differentiation and Other Culture Conditions. Cells. 2020;9(4).
98. Margioris AN, Venihaki M, Stournaras C, Gravanis A. PC12 cells as a model to study the effects of opioids on normal and tumoral adrenal chromaffin cells. Ann N Y Acad Sci. 1995;771:166-72.
99. Niu S, Kuo CH, Gan Y, Nishikawa E, Sadakata T, Ichikawa H, et al. Increase of calmodulin III gene expression by mu-opioid receptor stimulation in PC12 cells. Jpn J Pharmacol. 2000;84(4):412-7.
100. Zarnegar P, Persson AI, Ming Y, Terenius L. Opioid-induced regulation of gene expression in PC12 cells stably transfected with mu-opioid receptor. Neurosci Lett. 2006;396(3):197-201.
101. Lee TJ, Wu T, Kim YJ, Park JH, Lee DS, Bhang SH. Alternative method for trypsin-based cell dissociation using poly (amino ester) coating and pH 6.0 PBS. J Bioact Compat Polym. 2021;36(1):77-89.
102. Arigony AL, de Oliveira IM, Machado M, Bordin DL, Bergter L, Prá D, et al. The influence of micronutrients in cell culture: a reflection on viability and genomic stability. Biomed Res Int. 2013;2013:597282.
103. Bjarnsholt T, Jensen PØ, Alhede M. Revival of Krebs-Ringer balanced salt solution for the investigation of polymorphonuclear leukocytes and Pseudomonas aeruginosa biofilm interaction. Pathog Dis. 2019;77(5).
104. Francis GL. Albumin and mammalian cell culture: implications for biotechnology applications. Cytotechnology. 2010;62(1):1-16.
105. Miersch C, Stange K, Röntgen M. Effects of trypsinization and of a combined trypsin, collagenase, and DNase digestion on liberation and in vitro function of satellite cells isolated from juvenile porcine muscles. In Vitro Cell Dev Biol Anim. 2018;54(6):406-12.
106. Evans CJ, Aguilera RJ. DNase II: genes, enzymes and function. Gene. 2003;322:1-15.
107. Sigma-Aldrich. Cell Clumping Troubleshooting [Internet]. Sigma Aldrich; 2023 [cited 2023 April 6th]. Available from: https://www.sigmaaldrich.com/NO/en/technical-documents/technical-article/cell-culture-and-cell-culture-analysis/mammalian-cell-culture/cell-clumping-troubleshooting.
108. Mazia D, Schatten G, Sale W. Adhesion of cells to surfaces coated with polylysine. Applications to electron microscopy. J Cell Biol. 1975;66(1):198-200.
109. Freimoser FM, Jakob CA, Aebi M, Tuor U. The MTT [3-(4,5-dimethylthiazol-2-yl)-2,5-diphenyltetrazolium bromide] assay is a fast and reliable method for colorimetric determination of fungal cell densities. Appl Environ Microbiol. 1999;65(8):3727-9.
110. Twentyman PR, Luscombe M. A study of some variables in a tetrazolium dye (MTT) based assay for cell growth and chemosensitivity. Br J Cancer. 1987;56(3):279-85.
111. Matlock B. Assessment of Nucleic Acid Purity [Internet]. Wilmington, MA. USA: Thermo Fisher Scientific; 2015 [cited 2023 May 6th]. Available from: https://assets.thermofisher.com/TFS-Assets/CAD/Product-Bulletins/TN52646-E-0215M-NucleicAcid.pdf.
112. Livak KJ, Schmittgen TD. Analysis of relative gene expression data using real-time quantitative PCR and the 2(-Delta Delta C(T)) Method. Methods. 2001;25(4):402-8.
113. Lauvås AJ, Lislien M, Holme JA, Dirven H, Paulsen RE, Alm IM, et al. Developmental neurotoxicity of acrylamide and its metabolite glycidamide in a human mixed culture of neurons and astrocytes undergoing differentiation in concentrations relevant for human exposure. Neurotoxicology. 2022;92:33-48.
114. Hansen SH, Pedersen-Bjergaard S. Bioanalysis of pharmaceuticals : sample preparation, separation techniques and mass spectrometry. Chichester: Wiley; 2015.

115. Eurofins EAG Laboratories. Liquid Chromatography Tandem Mass Spectrometry (LC-MS-MS) [Internet]. [cited 2023 May 7th]. Available from: https://www.eag.com/app-note/liquid-chromatography-tandem-mass-spectrometry-lc-ms-ms/#:~:text=Liquid%20Chromatography%20with%20tandem%20mass,of%20triple%20quadrupole%20mass%20spectrometry.
116. Teuscher N. Understanding LC/MS/MS [Internet]. Certara, 2014 [updated July 15th; cited 2023 May 4th]. Available from: https://www.certara.com/knowledge-base/understanding-lcmsms/.
117. Bryda EC. The Mighty Mouse: the impact of rodents on advances in biomedical research. Mo Med. 2013;110(3):207-11.
118. Stark MR, Ross MM. The Chicken Embryo as a Model in Developmental Toxicology. Methods Mol Biol. 2019;1965:155-71.
119. Hamburger V, Hamilton HL. A series of normal stages in the development of the chick embryo. J Morphol. 1951;88(1):49-92.
120. Gabrielli MG, Accili D. The chick chorioallantoic membrane: a model of molecular, structural, and functional adaptation to transepithelial ion transport and barrier function during embryonic development. J Biomed Biotechnol. 2010;2010:940741.
121. Dombre C, Guyot N, Moreau T, Monget P, Da Silva M, Gautron J, et al. Egg serpins: The chicken and/or the egg dilemma. Semin Cell Dev Biol. 2017;62:120-32.
122. Vargas A, Zeisser-Labouèbe M, Lange N, Gurny R, Delie F. The chick embryo and its chorioallantoic membrane (CAM) for the in vivo evaluation of drug delivery systems. Adv Drug Deliv Rev. 2007;59(11):1162-76.
123. Johnson BA, Cheang MS, Goldenberg GJ. Comparison of adriamycin uptake in chick embryo heart and liver cells an murine L5178Y lymphoblasts in vitro: role of drug uptake in cardiotoxicity. Cancer Res. 1986;46(1):218-23.
124. Thors L, Fowler CJ. Is there a temperature-dependent uptake of anandamide into cells? Br J Pharmacol. 2006;149(1):73-81.
125. Zumbrink L, Brening B, Foerster A, Hurlin J, von Wenzlawowicz M. Electrical anaesthesia of male chicken embryos in the second-third of the incubation period in compliance with animal welfare. EuropPoultSci. 2020;84.
126. Kaur G, Dufour JM. Cell lines: Valuable tools or useless artifacts. Spermatogenesis. 2012;2(1):1-5.
127. Radio NM, Freudenrich TM, Robinette BL, Crofton KM, Mundy WR. Comparison of PC12 and cerebellar granule cell cultures for evaluating neurite outgrowth using high content analysis. Neurotoxicol Teratol. 2010;32(1):25-35.
128. Graves DA, Arrigo JM, Foster TS, Baumann TJ, Batenhorst RL. Relationship between plasma morphine concentrations and pharmacologic effects in postoperative patients using patient-controlled analgesia. Clin Pharm. 1985;4(1):41-7.
129. European Medicines Agency. ICH Topic S 7 A - Safety Pharmacology Studies for Human Pharmaceuticals - Step 5 [Internet]. EMA2001 [cited 2023 April 27th]. Available from: https://www.ema.europa.eu/en/documents/scientific-guideline/ich-s-7-safety-pharmacology-studies-human-pharmaceuticals-step-5_en.pdf.
130. Khoder AZ. Fordeling av og nevronal utvikling etter opioider administrert i kyllingembryo [Master's thesis]. Oslo: University of Oslo; 2020.
131. Sulovic A. Mulige nevroutviklingsforstyrrelser av opioider – studier in vivo og i nevronkulturer [Master's thesis]. Oslo: University of Oslo; 2018.
132. Fjelldal MF, Hadera MG, Kongstorp M, Austdal LPE, Šulović A, Andersen JM, et al. Opioid receptor-mediated changes in the NMDA receptor in developing rat and chicken. Int J Dev Neurosci. 2019;78:19-27.

133. Jakubovic A, McGeer EG, McGeer PL. Effects of d1-methadone and morphine on developing chick embryo. Experientia. 1978;34(12):1617-8.
134. Sigma-Aldrich. TrkB Antagonist, ANA-12 [Internet]. Sigma-Aldrich; [cited 2023 May 11th]. Available from: https://www.sigmaaldrich.com/NO/en/product/mm/506304.
135. Kaina B, Beltzig L, Piee-Staffa A, Haas B. Cytotoxic and Senolytic Effects of Methadone in Combination with Temozolomide in Glioblastoma Cells. Int J Mol Sci. 2020;21(19).
136. Perez-Alvarez S, Cuenca-Lopez MD, de Mera RM, Puerta E, Karachitos A, Bednarczyk P, et al. Methadone induces necrotic-like cell death in SH-SY5Y cells by an impairment of mitochondrial ATP synthesis. Biochim Biophys Acta. 2010;1802(11):1036-47.
137. Sigma-Aldrich. p75NTR Signaling Inhibitor, Cell-permeable, TAT-Pep5 [Internet]. Merck [cited 2023 May 2nd]. Available from: https://www.sigmaaldrich.com/NO/en/product/mm/506181.
138. Galvao J, Davis B, Tilley M, Normando E, Duchen MR, Cordeiro MF. Unexpected low-dose toxicity of the universal solvent DMSO. FASEB J. 2014;28(3):1317-30.
139. Singh M, McKenzie KJ, Ma X. Effect of dimethyl sulfoxide on in vitro proliferation of skin fibroblast cells. J Biotech Res. 2017(8):78-82.
140. Ghasemi M, Turnbull T, Sebastian S, Kempson I. The MTT Assay: Utility, Limitations, Pitfalls, and Interpretation in Bulk and Single-Cell Analysis. Int J Mol Sci. 2021;22(23).
141. Strober W. Trypan blue exclusion test of cell viability. Curr Protoc Immunol. 2001;Appendix 3:Appendix 3B.
142. Olias P, Adam I, Meyer A, Scharff C, Gruber AD. Reference genes for quantitative gene expression studies in multiple avian species. PLoS One. 2014;9(6):e99678.
143. Vandesompele J, De Preter K, Pattyn F, Poppe B, Van Roy N, De Paepe A, et al. Accurate normalization of real-time quantitative RT-PCR data by geometric averaging of multiple internal control genes. Genome Biol. 2002;3(7):Research0034.
144. Lenart J, Kogut K, Salinska E. Lateralization of housekeeping genes in the brain of one-day old chicks. Gene Expr Patterns. 2017;25-26:85-91.
145. Thomaz A, Pinheiro KV, Souza BK, Gregianin L, Brunetto AL, Brunetto AT, et al. Antitumor Activities and Cellular Changes Induced by TrkB Inhibition in Medulloblastoma. Front Pharmacol. 2019;10:698.
146. Lemkuil BP, Head BP, Pearn ML, Patel HH, Drummond JC, Patel PM. Isoflurane neurotoxicity is mediated by p75NTR-RhoA activation and actin depolymerization. Anesthesiology. 2011;114(1):49-57.
147. Pearn ML, Hu Y, Niesman IR, Patel HH, Drummond JC, Roth DM, et al. Propofol neurotoxicity is mediated by p75 neurotrophin receptor activation. Anesthesiology. 2012;116(2):352-61.
148. Schallner N, Ulbrich F, Engelstaedter H, Biermann J, Auwaerter V, Loop T, et al. Isoflurane but not sevoflurane or desflurane aggravates injury to neurons in vitro and in vivo via p75NTR-NF-κB activation. Anesth Analg. 2014;119(6):1429-41.
149. Molloy NH, Read DE, Gorman AM. Nerve growth factor in cancer cell death and survival. Cancers (Basel). 2011;3(1):510-30.
150. Roux PP, Barker PA. Neurotrophin signaling through the p75 neurotrophin receptor. Prog Neurobiol. 2002;67(3):203-33.
151. Khasawneh RR, Al Sharie AH, Abu-El Rub E, Serhan AO, Obeidat HN. Addressing the impact of different fetal bovine serum percentages on mesenchymal stem cells biological performance. Mol Biol Rep. 2019;46(4):4437-41.
152. Ryan JM. Effect of different fetal bovine serum concentrations on the replicative life span of cultured chick cells. In Vitro. 1979;15(11):895-9.

153. Kwon D, Kim JS, Cha BH, Park KS, Han I, Park KS, et al. The Effect of Fetal Bovine Serum (FBS) on Efficacy of Cellular Reprogramming for Induced Pluripotent Stem Cell (iPSC) Generation. Cell Transplant. 2016;25(6):1025-42.
154. Yeh GC, Hsieh TH, Chang SF. The negative influence of endogenous opioid receptor activity on the differentiation of the rat pheochromocytoma PC12 cells induced by nerve growth factor. Neurosci Lett. 1998;252(1):25-8.
155. Brailoiu E, Hoard J, Brailoiu GC, Chi M, Godbolde R, Dun NJ. Ultra low concentrations of morphine increase neurite outgrowth in cultured rat spinal cord and cerebral cortical neurons. Neurosci Lett. 2004;365(1):10-3.
156. Chavez-Valdez R, Kovell L, Ahlawat R, McLemore GL, Wills-Karp M, Gauda EB. Opioids and clonidine modulate cytokine production and opioid receptor expression in neonatal immune cells. J Perinatol. 2013;33(5):374-82.
157. Stafford K, Gomes AB, Shen J, Yoburn BC. μ-Opioid receptor downregulation contributes to opioid tolerance in vivo. Pharmacology Biochemistry and Behavior. 2001;69(1):233-7.
158. Bushell T, Endoh T, Simen AA, Ren D, Bindokas VP, Miller RJ. Molecular components of tolerance to opiates in single hippocampal neurons. Mol Pharmacol. 2002;61(1):55-64.
159. Saify K, Saadat M. Expression levels of OPRM1 and PDYN in human SH-SY5Y cells treated with morphine and methadone. Life Sci. 2016;150:39-41.
160. Turchan J, Lasoń W, Budziszewska B, Przewłocka B. Effects of single and repeated morphine administration on the prodynorphin, proenkephalin and dopamine D2 receptor gene expression in the mouse brain. Neuropeptides. 1997;31(1):24-8.
161. Rezai M, Hajizadeh MR, Mahmoodi M, Torabizadeh SA, Karimabad MN. Effect of Methadone Maintenance on Expression of BDNF and CREB Genes in Brain VTA of Male Morphine Treated Rats. Cent Nerv Syst Agents Med Chem. 2021;21(3):181-6.
162. Wang TY, Lee SY, Chang YH, Chen SL, Chen PS, Chu CH, et al. Correlation of cytokines, BDNF levels, and memory function in patients with opioid use disorder undergoing methadone maintenance treatment. Drug Alcohol Depend. 2018;191:6-13.
163. Meyer RP, Gehlhaus M, Knoth R, Volk B. Expression and function of cytochrome p450 in brain drug metabolism. Curr Drug Metab. 2007;8(4):297-306.
164. Ravindranath V. Metabolism of xenobiotics in the central nervous system: implications and challenges. Biochem Pharmacol. 1998;56(5):547-51.
165. Campbell SD, Crafford A, Williamson BL, Kharasch ED. Mechanism of autoinduction of methadone N-demethylation in human hepatocytes. Anesth Analg. 2013;117(1):52-60.
166. Shah NS, Donald AG, Bertolatus JA, Hixson B. Tissue distribution of levo-methadone in nonpregnant and pregnant female and male mice: effect of SKF 525-A 1,2. J Pharmacol Exp Ther. 1976;199(1):103-16.
167. Peters MA, Turnbow M, Buchenauer D. The distribution of methadone in the nonpregnant, pregnant and fetal rat after acute methadone treatment. J Pharmacol Exp Ther. 1972;181(2):273-8.
168. Delorme P, Gayet J, Grignon G. Ultrastructural study on transcapillary exchanges in the developing telencephalon of the chicken. Brain Res. 1970;22(3):269-83.
169. Wakai S, Hirokawa N. Development of the blood-brain barrier to horseradish peroxidase in the chick embryo. Cell Tissue Res. 1978;195(2):195-203.
170. Ribatti D, Nico B, Bertossi M. The development of the blood-brain barrier in the chick. Studies with evans blue and horseradish peroxidase. Ann Anat. 1993;175(1):85-8.
171. Liu H, Ding P, Tong Y, He X, Yin Y, Zhang H, et al. Metabolomic analysis of the egg yolk during the embryonic development of broilers. Poult Sci. 2021;100(4):101014.

172. Barbedo J. Automatic Object Counting In Neubauer Chambers. 2013.

7 Appendix A – recipes

All media were prepared in vertical laminar flow hoods and stored at 2-8°C after preparation.

Table 7.1 PC12 medium		
Reagent:	Final concentration:	Quantity:
Dulbecco's modified eagle medium with L-glutamine (DMEM)	-	500 mL
Fetal bovine serum (FBS)	10%	50 mL
Horse serum (HS)	5%	25 mL
Penicillin-Streptomycin	1%	5 mL
Sodium Pyruvate	1%	5 mL

Table 7.2 PC12 differentiation medium		
Reagent:	Final concentration:	Quantity:
Dulbecco's modified eagle medium with L-glutamine (DMEM)	-	500 mL
Horse serum (HS)	2%	10 mL
Penicillin-Streptomycin	1%	5 mL
Sodium Pyruvate	1%	5 mL
NGF (5 ng/mL) was added to the exposure solutions where the cells were supposed to be differentiated.		

Table 7.3 CGN plating medium		
Reagent:	Final concentration:	Quantity:
BME	-	500 mL
Chicken serum	7.5 %	37.5 mL
KCl	22 mM	825 mg*
L-Glutamine	2 mM	146 mg*
Penicillin-Streptomycin	1%	5 mL
Insulin I5500	100 nM	50 µL from a 1 mM stock (5.7335 mg in 1 mL distilled water)
*Reagents in solid form were dissolved in a few millilitres of BME and sterile filtered before being added to the medium.		

Table 7.4 CGN feeding medium		
Reagent:	Final concentration:	Quantity:
BME	-	500 mL
KCl	22 mM	825 mg*
L-Glutamine	2 mM	146 mg*
Penicillin-Streptomycin	1%	5 mL
H-Transferrin	100 µg/mL	50 mg (from aliquot)
Putrescine	60 nM	4.8 mg*
Insulin I5500	25 µg/mL	12.5 mg (from aliquot)
T_3	1 nM	17 µL (from a 20 µg/mL stock)
Na_2SeO_3	30 nM	150 µL (from a 100 µM stock)
*Reagents in solid form were dissolved in a few millilitres of BME and sterile filtered before being added to the medium.		

Table 7.5 Solutions used in preparation of CGN cell culture		
	Reagent:	Quantity:
Solution 1*	Bovine serum albumin (BSA)	1.50 g
	Krebs-Ringer solution 10x	50 mL
	$MgSO_4$ (3.82 g/100 mL)	4.0 mL
	Distilled water	ad 500 mL
Solution 2	Trypsin	12.5 mg
	Solution 1	50 mL
Solution 3	DNase	3.1 mg
	Trypsin inhibitor	13.0 mg
	$MgSO_4$ (3.82 g/100 mL)	250 µL
	Solution 1	Ad 25 mL
Solution 4	Solution 3	8 mL
	Solution 1	50 mL
Solution 5	$MgSO_4$ (3.82 g/100 mL)	320 µL
	$CaCl_2$ (1.20 g/100 mL)	320 µL
	Solution 1	40 mL
The solutions are made fresh and sterile filtered before use. * Use a magnetic stirrer until BSA is dissolved.		

Table 7.6 MTT medium		
Reagent:	Final concentration:	Quantity:
PC12 medium or CGN feeding medium*	-	10 mL
MTT 5 mg/mL in PBS	0,4545 µg/mL	1 mL
* Use PC12 medium for PC12 cells and CGN feeding medium for CGNs.		

Table 7.7 RLT lysis buffer for RT-qPCR		
Reagent:	Final concentration:	Quantity:
Buffer RLT Plus RNeasy® Plus lysis buffer	-	1 mL
2-Mercaptoethanol 50 mM	0.5 mM	10 µL
Amount needed is calculated before making the mix		

Table 7.8 Enzyme master mix	
Reagent:	Quantity:
2X RT buffer Mix	10 µL
20X Enzyme Mix	1 µL
This is per sample. Total amount needed is calculated before mixing.	

Table 7.9 SYBR® green master mix and primers	
Reagent:	Quantity:
Power SYBR® Green PCR Master Mix	5 µL
Forward Primer	1 µL
Reverse Primer	1 µL
The master mixes are made separately and right before being added to the qPCR plate. Primers are diluted 1:10 in RNase-free before adding them to the mix.	
Genes:	**Primers (F=forward, R=reverse):**
GAPDH	F: 5'-GAT GGG TGT CAA CCA TGA GAA A-3' R: 5'-TGG TGC ACG ATG CAT TGC-3'
MOR	F: 5'-ACT CTG TAG TGT GCG TCG TG-3' R: 5'-CAA GCA GGG TGG GAG AAT GT-3'
DOR	F: 5'-CCT CAT CGC CAT CGT CAT CA-3' R: 5'-GTC CCA GTA GAT GGG AGG GT-3'
KOR	F: 5'-TCC GTA CTC CTC TCA AGG CA-3' R: 5'-CGC CTA ATG CTT CAA CCA GC-3'
PENK	F: 5'-CGA TGC CCT GGC TAA TTC CT-3' R: 5'-TTA CTC CTC GGT AAT GCG CC-3'
PDYN	F: 5'-CAG GGT GCT TTG GTG TAG TGT-3' R: 5'-CAG CTT CAT GCT CCC AGC TT-3'
BDNF	F: 5'-GAA AAG TCT GCA CAT GAG GGC-3' R: 5'-GTG TGG CAT TGC TGT AAG GG-3'
CREB1	F: 5'-TGT AGT TTG ACG CGG TGT GT-3' R: 5'-TAG TTG AAA TCG GTT GCG GG-3'
GluN2B	F: 5'-AGC TAT GGCC CT CAG TCT CA-3' R: 5'-AGA GCA GAC ACC CAT GAA GC-3'
CYP3A4	F: 5'-AAT GGG ACT CCT TCC AGA CCT T-3' R: 5'-GGC CAT ATC CCA TAG AGC ACC-3'

Table 7.10 Permeabilisation buffer		
Reagent:	Final concentration:	Quantity:
Triton X-100 (10%)	0.1%	500 µL
1x PBS+	-	49.5 mL
Can be stored at 4°C.		

Table 7.11 Blocking buffer		
Reagent:	Final concentration:	Quantity:
BSA (35%)	3.5%	500 µL
1x PBS+	-	49.5 mL
The blocking buffer must be prepared fresh.		

Table 7.12 Primary antibodies for HCI			
Reagent:	Species:	Dilution:	Supplier:
MAP2	Chicken	1:5000	Abcam (Ab5392)
SYP	Rabbit	1:200	Abcam (Ab14692)
PSD95	Mouse	1:300	Abcam (Ab13552)
The antibodies were added to the blocking buffer (Table 7.11).			

Table 7.13 Secondary antibodies for HCI		
Reagent:	Dilution:	Supplier:
Goat anti-chicken IgY H&L DyLight 488	1:500	Abcam (Ab96951)
Goat anti-mouse IgG H&L DyLight 550	1:500	Abcam (A96880)
Goat anti-rabbit IgG H&L DyLight 650	1:500	Abcam (Ab96902)
DAPI	1:1000	Thermo Fisher (62248)
The antibodies were added to the blocking buffer (Table 7.11).		

Table 7.14 Sample preparation for analysis with LC-MS-MS					
Sample name:	Tissue:	MQ water:	Standard:	Buffer:	Internal standard (IS):
0-sample	-	50 µL	-	100 µL	-
0+ sample	-	50 µL	-	50 µL	50 µL
Standard	-	50 µL	50 µL	-	50 µL
Control	-	50 µL	50 µL	-	50 µL
Control with tissue	50 µL of unexposed brain, lung, or yolk	-	50 µL	-	50 µL
Tissue sample	50 µL	-	-	50 µL	50 µL
All samples were added 500 µL ACN:MeOH (85:15)					

Table 7.15: Standards, controls, and internal standards for analysis with LC-MS-MS		
	Methadone hydrochloride (µM):	EDDP perchlorate (µM):
Standard 1	0.005	0.005
Standard 2	0.01	0.01
Standard 3	0.04	0.04
Standard 4	0.2	0.2
Standard 5	2	2
Standard 6	10	10
Standard 7	40	40
Standard 8	100	100
Standard 9	150	150
Control 1	0.006	0.006
Control 2	0.03	0.03
Control 3	2.4	2.4
Control 4	32	32
Control 5	80	80
Internal standard	0.5*	0.5**
* This is 13C6-methadone: 6 carbon atoms are substituted with the isotope carbon-13 ** This is EDDP-d3: 3 hydrogen atoms are substituted with the isotope deuterium		

8 Appendix B – protocols

8.1 Splitting of PC12 cells to a new passage

1. Use a microscope to determine the degree of confluence.
2. Remove old media by pouring it into a waste container.
3. Add 10 mL of fresh medium (approximately 37°C, Appendix A, Table 7.1) to the cell culture flask and tighten the cap completely.
4. Dislodge the cells from the bottom of the flask by hitting the sides.
5. Check under the microscope that the cells have been dislodged.
6. Triturate the cell culture by using a 10 mL pipette. Press the pipette opening against the bottom of the cell culture flask while triturating. This will reduce cell clumping and aggregates.
7. Check if the cell culture is free of aggregates and repeat step 6 if necessary. Use a Pasteur pipette with a smaller opening to reduce cell clumps even more.
8. Suck up all the cell suspension in a 10 mL pipette before adding 1-1.5 mL back to the flask (or a new flask). Discard the rest of the cell suspension in a waste container.
9. Add 20 mL of fresh medium to the cell culture flask.
10. Incubate the cells at 37°C and 5% CO_2. Split the cells every Monday and Thursday.

8.2 Splitting of PC12 cells to 96-well plates

1. Split the cells as described in points 1-7 in chapter 8.1.
2. Transfer some of the cell suspension to an Eppendorf tube.
3. Use a haemocytometer to count the cells. Add 10 µL of the cell suspension on both sides of the cover glass.
4. Count the cells in the 4x4 areas of the haemocytometer. Include cells on the left and top border of a 4x4 area. Count 3 of these areas on both sides of the haemocytometer. Calculate the density of the cell suspension.

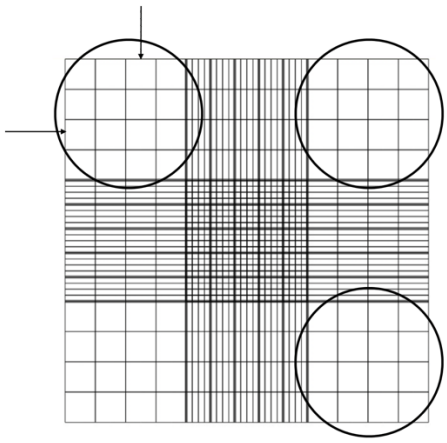

Figure 8.1: Illustration of a haemocytometer. The three 4x4 areas are marked with black circles. The black arrows point at the top and left border of the area. Cells on these borders were included in the count. The figure is modified and obtained from (172).

5. After counting, dilute the cell suspension in PC12 medium to the correct density for seeding, which in the case of PC12 cells was $7 \cdot 10^4$ cells/mL.
6. Seed 200 µL of the diluted cell suspension in each well. Use 60 wells, leaving the edge wells free of cells. Fill the edge wells with 200 µL PBS.

8.3 Preparation of chicken granule cell suspension

1. Eggs with chickens at development stage E17 are removed from the incubator.
2. The eggs are covered with ice for 7 minutes. This gives the chicks hypothermia, which acts as anaesthesia.
3. Sterilise the eggs in 70% ethanol before cracking them in a 14 cm petri dish.
4. Use a sterile scalpel to decapitate the chickens and transfer the heads to a different dish.
5. Transfer the petri dish with the heads to a vertical laminar flow hood. Use an aseptic technique for the rest of the procedure. The solutions (1-5) in this procedure are described in Appendix A, Table 7.5.
6. Cut open the scull with sterile scissors and isolate the cerebellum with sterile tweezers.
7. Transfer the cerebellum to a new sterile petri dish filled with solution 1.
8. After isolating, change gloves and clean them with 70% ethanol. Transfer one cerebellum to the back of your hand and roll it to remove the meninges.
9. Clean cerebellar tissue is transferred to a different petri dish with solution 1.

10. After gathering all the clean cerebellar tissue in the same dish, aspirate solution 1 and start cutting the tissue into smaller pieces with a sterile scalpel, cut in two different directions perpendicular to each other.
11. Add 10 mL of solution 1 to the dish and transfer the tissue to a sterile 50 mL Falcon tube.
12. Centrifuge at 1000 rpm for 1 minute.
13. Remove the supernatant.
14. Add 8 mL of solution 2 to the tube and pipette up and down to disperse the pellet. Continue using the tube or add the contents to a trypsinisation flask to increase the surface area of trypsin exposure.
15. Put the tube or trypsinising flask in a water bath at 37°C for 15 minutes. Shake the tube regularly. Keep the lid of the tube/the caps of the flask loose.
16. After trypsinising, fill the tube with solution 4.
17. Centrifuge at 1000 rpm for 2 minutes. If the supernatant is clear, continue with the next step. If the supernatant is cloudy, add a small amount of solution 3 before centrifuging at 1000 rpm for two more minutes.
18. Remove the supernatant.
19. Add 3 mL of solution 3 to the tube and disperse the pellet by carefully pipetting up and down approximately 15-20 times with a sterile 1 mL pipette.
20. Let the cell suspension sit for a few minutes to let lumps of tissue sink to the bottom.
21. Transfer the top lump-free part of the suspension to a new sterile 50 mL Falcon tube with 15 mL of solution 5.
22. Add 2 mL solution 3 to the tube with lumps of tissue and disperse the tissue. Repeat steps 20-21. Repeat step 22 until there are no more visible lumps of tissue left.
23. Centrifuge the now lump-free cell suspension at 900 rpm for 7 minutes.
24. Remove the supernatant.
25. Add 10 mL of CGN plating medium (Appendix A, Table 7.3) to the tube and disperse the pellet.
26. Transfer some cell suspension to an Eppendorf tube and dilute it 100x to make the counting easier. Use a haemocytometer for counting by adding 10 µL cell suspension to both sides of the cover glass. See point 4 in Chapter 8.2 and Figure 8.1 for more information.
27. After counting, dilute the cell suspension to a density of 1.5-1.7 x 10^6 cells/mL.

28. Seed the cells onto 96-well plates (0.2 mL), 10 cm dishes (10 mL) or 6-well plates (1.5-2 mL). The cells are exposed the next day.

8.4 Coating with PLL

1. Dilute the PLL stock (10 mg/mL) in autoclaved distilled water to 16 µg/mL for 96-well plates and 32 µg/mL for 6-well plates.
2. Add 1.5 mL PLL to each well for the 6-well plates and 100 µL for the 96-well plates.
3. Let the plates sit at room temperature for a minimum of 1 hour before aspirating as much as possible.
4. Let the plates sit at room temperature to dry.

8.5 *In ovo* injection

1. 13-day-old eggs are used for injections.
2. Candle the eggs to detect the embryo and determine a suitable injection site. Write an x with a marker for the injection point. Do not puncture the large and visible blood vessels.
3. Sterilise the injection point with an alcohol swab.
4. Puncture the shell with a 25G needle.
5. Inject 1 µL of the solution per gram of egg, approximately 2-3 mm inside the egg, using a single-use insulin syringe.
6. Cover the injection point with a piece of tape after injecting. Put the eggs back in the incubator.

8.6 Determination of viability with MTT

1. MTT assays were done in CGNs and PC12 cells. For CGNs, this is a continuation of chapter 8.3. For PC12 cells, split the cells as described in Chapter 8.2.
2. Remove the media from each well before exposing the cells to different solutions and drugs. Do not aspirate the cells; ensure that they do not dry out before adding solutions/media.
3. Add 100 µL of the exposure solutions or media in each well. The first column should only contain fresh media (blank).

4. Incubate the plate at 37°C and 5% CO_2 for 72 hours.
5. After 72 hours, remove the media/solutions from all wells except the blank.
6. Add 100 µL MTT medium (Appendix A, Table 7.6) in all wells except the blank.
7. Incubate the plate at 37°C and 5% CO_2 for 3 hours.
8. Remove the MTT medium and the medium in the blank column. Be careful when aspirating the media; the cells can be loose.
9. Add 200 µL PBS to each well.
10. Incubate the plate at 37°C for 30 minutes.
11. Use ClarioStar plate reader at 570 nm to measure the absorbance.

8.7 Lysis of cells for RT-qPCR

1. Remove the medium and wash the cells with 1 mL of ice-cold 1x PBS.
2. Aspirate the PBS and remove as much as possible.
3. Add 250 µL RLT lysis buffer (Appendix A, Table 7.7).
4. Scrape the cells off the surface using a plastic policeman. Aspirate the lysate and transfer it to Eppendorf tubes.
5. Freeze the lysate samples at -80°C.

8.8 RNA isolation

1. After thawing the samples, vortex the samples for 30 seconds to ensure homogenisation in the sample.
2. Transfer the samples to gDNA Eliminator Mini Spin Columns placed in 2 mL collection tubes.
3. Centrifuge at 10,000 rpm for 30 seconds and save the flow-through.
4. Add 350 µL of 70% ethanol in each sample and mix well by pipetting.
5. Transfer up to 700 µL of the sample to an RNeasy Mini Spin Column placed in a 2 mL collection tube.
6. Centrifuge at 10,000 rpm for 15 seconds and discard the flow-through.
7. Add 700 µL of Buffer RW1 wash buffer to the spin column.
8. Centrifuge at 10,000 rpm for 15 seconds and discard the flow-through.
9. Add 500 µL of Buffer RPE wash buffer to the spin column.
10. Centrifuge at 10,000 rpm for 15 seconds and discard the flow-through.

11. Add another 500 µL of Buffer RPE wash buffer to the spin column.
12. Centrifuge at 10,000 rpm for 2 minutes.
13. Put the spin column into a new collection tube. Centrifuge the spin column again at full speed (14,800 rpm) for 1 minute. This ensures the removal of possible residuals of Buffer RPE and previous flow-through remains on the outside of the spin column.
14. Place the spin column into new 1.5 mL collection tubes. Add 30 µL RNase-free water to the membrane.
15. To elute the RNA, centrifuge at 10,000 rpm for 1 minute.

8.9 Conversion of RNA to cDNA and RT-qPCR

1. Measure the RNA concentration using NanoDrop™ Lite Spectrophotometer at an absorbance of 260/280 nm. A blank of 1 µL RNase-free water was measured before measuring 1 µL of the samples. The instrument was wiped with tissue paper between every sample.
2. Calculate the amount of water needed to dilute the samples to 100 ng/9 µL. Dilute the samples with RNase-free water and add 9 µL to qPCR tubes (Multiply®-µStrip).
3. Add 11 µL of enzyme master mix (Appendix A, Table 7.8) to each sample.
4. By using the 2720 Thermal Cycler, incubate the samples at 37°C for 1 hour before stopping the reaction by heating the samples to 95°C for 5 minutes.
5. Add 180 µL RNase-free water to each sample. These are the finished cDNA samples.
6. Add 3 µL of the cDNA samples to a 96-well plate for qPCR.
7. Add 7 µL of SYBR® green master mix (Appendix A, Table 7.9).
8. Seal the plate with LightCycler® 480 Sealing Foil.
9. Centrifuge the plate.
10. Start the real-time qPCR using CFX96™ Touch Real-Time System. Temperatures, cycles, and melt curves:
    a. 95°C for 10 minutes.
    b. 95°C for 15 seconds.
    c. 60°C for 1 minute with plate read.
    d. Point b-c is cycled 40 times.
    e. Melt curve: 65.0 to 95.0°C (0.5°C increment) for 5 seconds with plate read.

8.10 Immunocytochemistry

The procedure must be done with manual pipetting to prevent the cells from falling off.

8.10.1 Fixation

1. Remove the media from each well.
2. Gently wash the cells once with 100 µL ice-cold PBS.
3. Add 4% formaldehyde to each well. Let the plate sit at room temperature for 10 minutes.
4. Aspirate the formaldehyde.
5. Gently wash the cells twice with 100 µL PBS (preferably PBS+, which contains magnesium and calcium).
6. The plate can be stored in the fridge for a few days before immunostaining.

8.10.2 Immunostaining

1. Remove the PBS.
2. Add 50 µL 0.1% Triton-X in 1x PBS+ (Appendix A, Table 7.10) in each well and let it sit at room temperature for 10 minutes.
3. Carefully aspirate the Triton-X.
4. Incubate the plate with 50 µL blocking buffer (Appendix A Table 7.11) at room temperature for 30 minutes.
5. Carefully aspirate the blocking buffer.
6. Add 50 µL of the primary antibodies (Appendix A Table 7.12) in each well, wrap the plate in aluminium foil and incubate the plate in the fridge at 4°C overnight.
7. Aspirate the primary antibodies.
8. Gently wash the cells twice with 100 µL 1x PBS+.
9. Add 50 µL of the secondary antibodies (Appendix A Table 7.13), protect the plate from light with aluminium foil and incubate the plate at room temperature for 1 hour.
10. Gently wash the cells twice with 100 µL 1x PBS+.
11. Add 200 µL 1x PBS+ in each well. Seal the lid of the plate with parafilm, wrap the plate in aluminium foil and store the plate in the fridge at 4°C until the analysis.

8.11 Homogenisation of lungs, brains, and yolk

1. Weigh the tissue in Eppendorf tubes.
2. Add 1:1 (tissue:water) for the brains and lungs, and 1:2 (tissue:water) for the yolks.
3. Homogenise the tissue by using an electric homogeniser and a plastic pistil. Clean the pistil with ethanol between every homogenisation.
4. Transfer 50 µL of the homogenised tissue into 2 mL kinetics tubes.
5. Snap-freeze the homogenised tissue in liquid nitrogen and store them at -80°C until the next step (8.12).

8.12 Determination of drug distribution in lungs, brains, and yolk

1. Add 50 µL MQ water to 5 mL kinetics tubes.
2. Add 50 µL of standards and controls to the tubes with MQ water. For the tissue controls, add 50 µL standard and 50 µL of unexposed tissue instead of MQ water. Mix lightly on a Whirl mixer.
3. Add 50 µL 5 mM ammonium formate buffer (pH 3.1) to the 0 samples and the harvested tissue samples and mix lightly on a Whirl mixer.
4. Add 50 µL of the internal standard to every tube except the 0 samples. Mix lightly on a Whirl mixer.
5. Add 500 µL of ice-cold ACN:MeOH (85:15) to every tube. See Appendix A, Table 7.14 for an overview of what was added to each sample category (0 samples, standards, controls, tissue controls, and tissue samples). See Appendix A Table 7.15 for information on the concentrations in the standards and controls.
6. Put the lids on and shake the tubes for 1 minute on a multi-tube vortexer.
7. Centrifuge the samples at 4°C at 4750 rpm for 2 minutes (in Allegra X-15R Centrifuge).
8. Filter 600 µL of the supernatant by using a Captiva EMR 96-well filter column with a 2 mL 96-well collection plate. Remove the column afterwards. Make sure that the right order of the samples is maintained.
9. Add 10 µL of 0.01% HNO_3 in MeOH to each well.
10. Evaporate the solvent on an SPE dry 96 solvent evaporator until dry.
11. Add 100 µL cold MeOH in water to each sample.

12. Seal the plate and shake it lightly on a Whirl mixer.
13. Analyse the samples with LC-MS-MS 31 (Aquity UPLC™ Xevo TQ-S), using BEH C18 5 cm column, 5 mM ammonium formate buffer pH 10.2 (mobile phase A), MeOH (mobile phase B), MeOH-wash between each sample, and injection volume 0.4 µL.
14. Oversaturated samples were diluted to 1000 µL and reanalysed.

9 Appendix C – supplementary figures

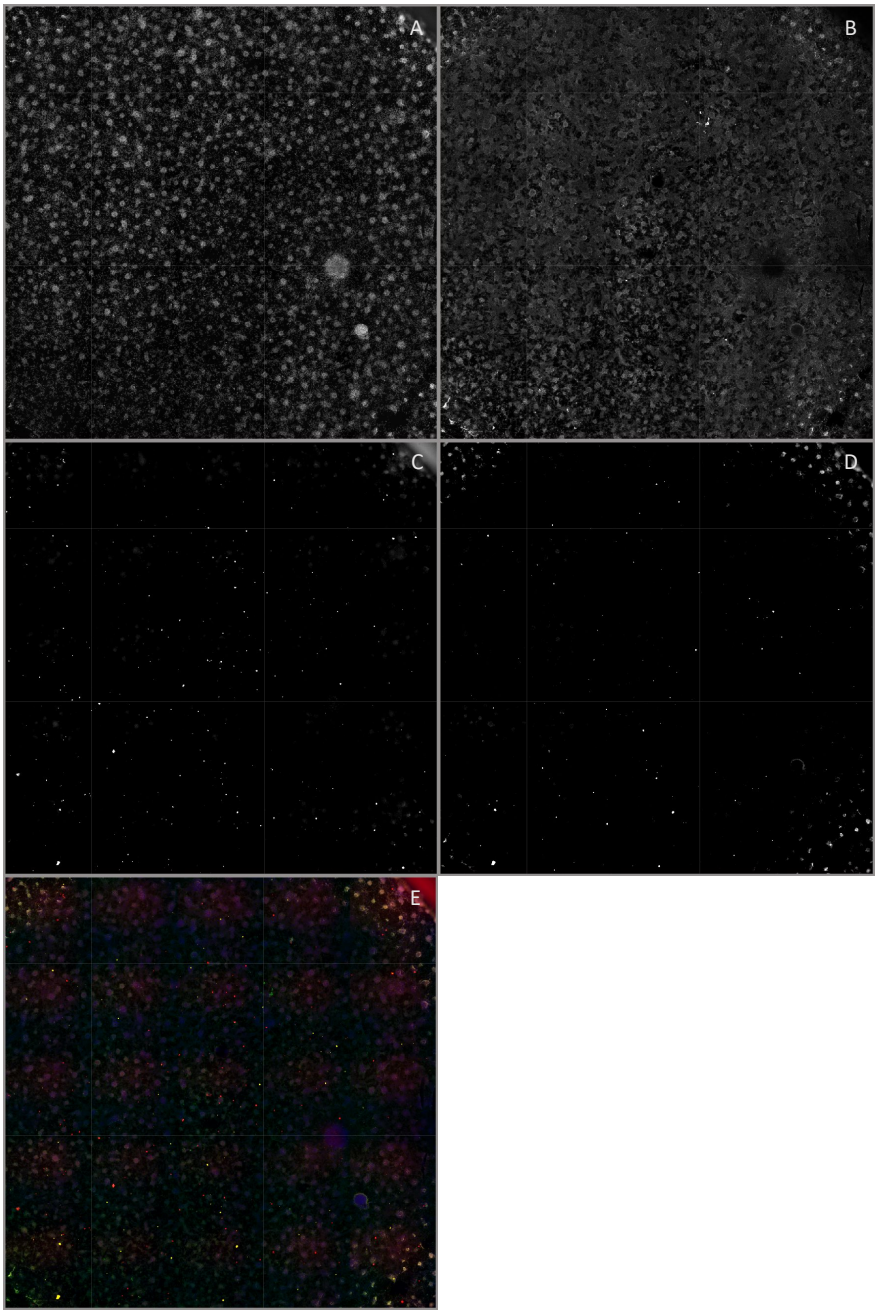

Figure 9.1: High-content images of CGNs exposed to the control. The different pictures show the expression of A) DAPI, B) MAP2, C) PSD95 and D) SYP. E) A composite picture of all stains in one picture. Blue=DAPI, green=MAP2, red=PSD95 and yellow=SYP.

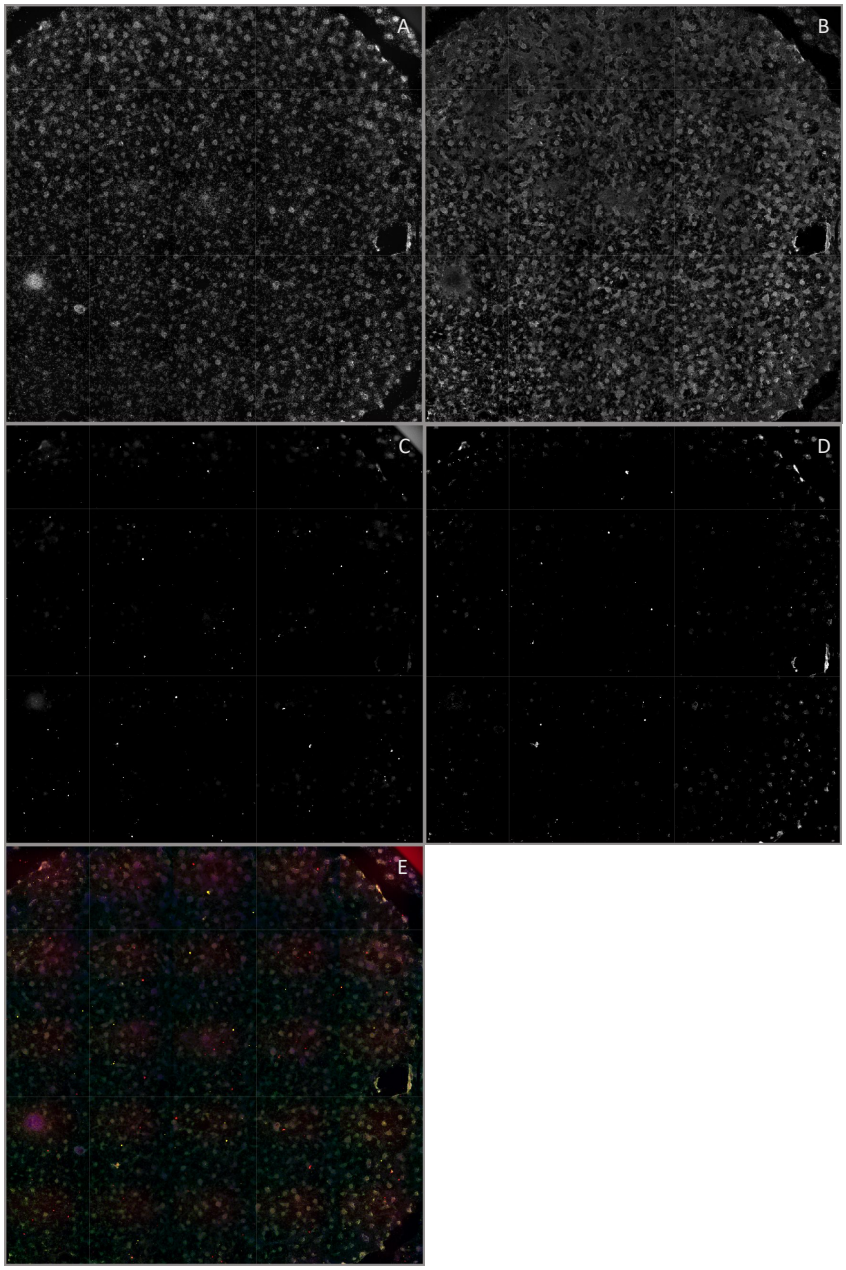

Figure 9.2: High-content images of CGNs exposed to 10 µM methadone. The different pictures show the expression of A) DAPI, B) MAP2, C) PSD95, and D) SYP. E) A composite picture of all stains in one picture. Blue=DAPI, green=MAP2, red=PSD95 and yellow=SYP.

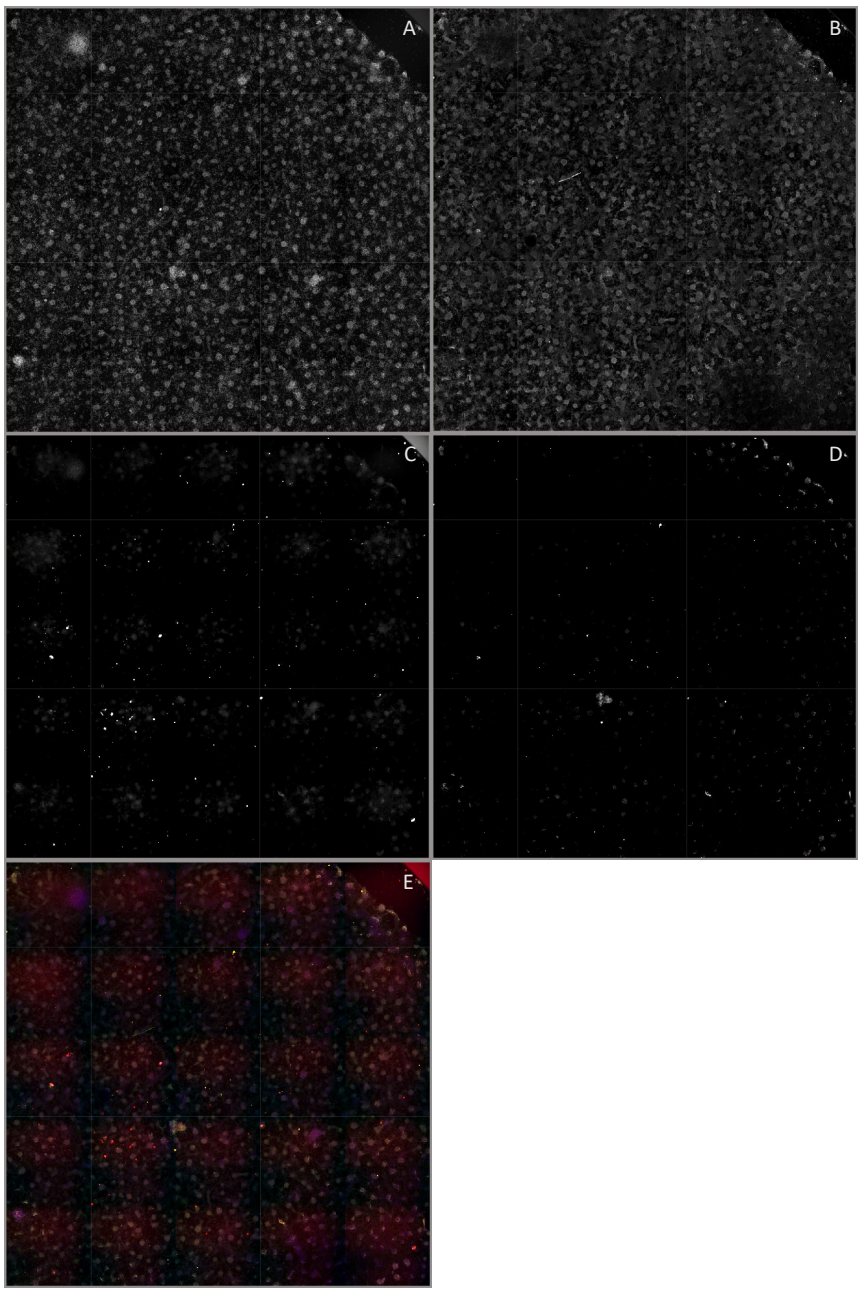

Figure 9.3: High-content images of CGNs exposed to 1 µM methadone. The different pictures show the expression of A) DAPI, B) MAP2, C) PSD95 and D) SYP. E) A composite picture of all stains in one picture. Blue=DAPI, green=MAP2, red=PSD95 and yellow=SYP.

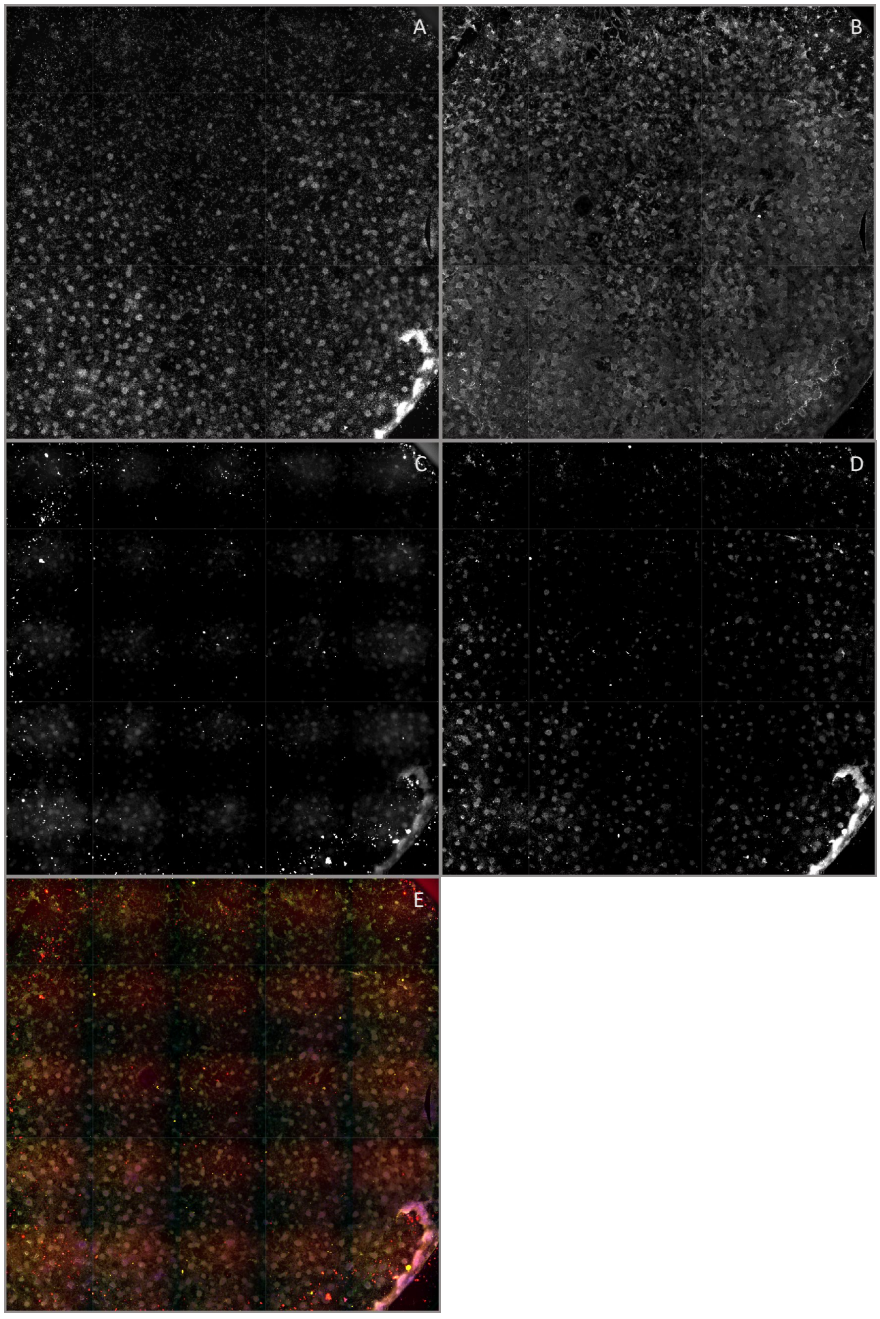

Figure 9.4: High-content images of CGNs exposed to 10 µM morphine. The different pictures show the expression of A) DAPI, B) MAP2, C) PSD95 and D) SYP. E) A composite picture of all stains in one picture. Blue=DAPI, green=MAP2, red=PSD95 and yellow=SYP.

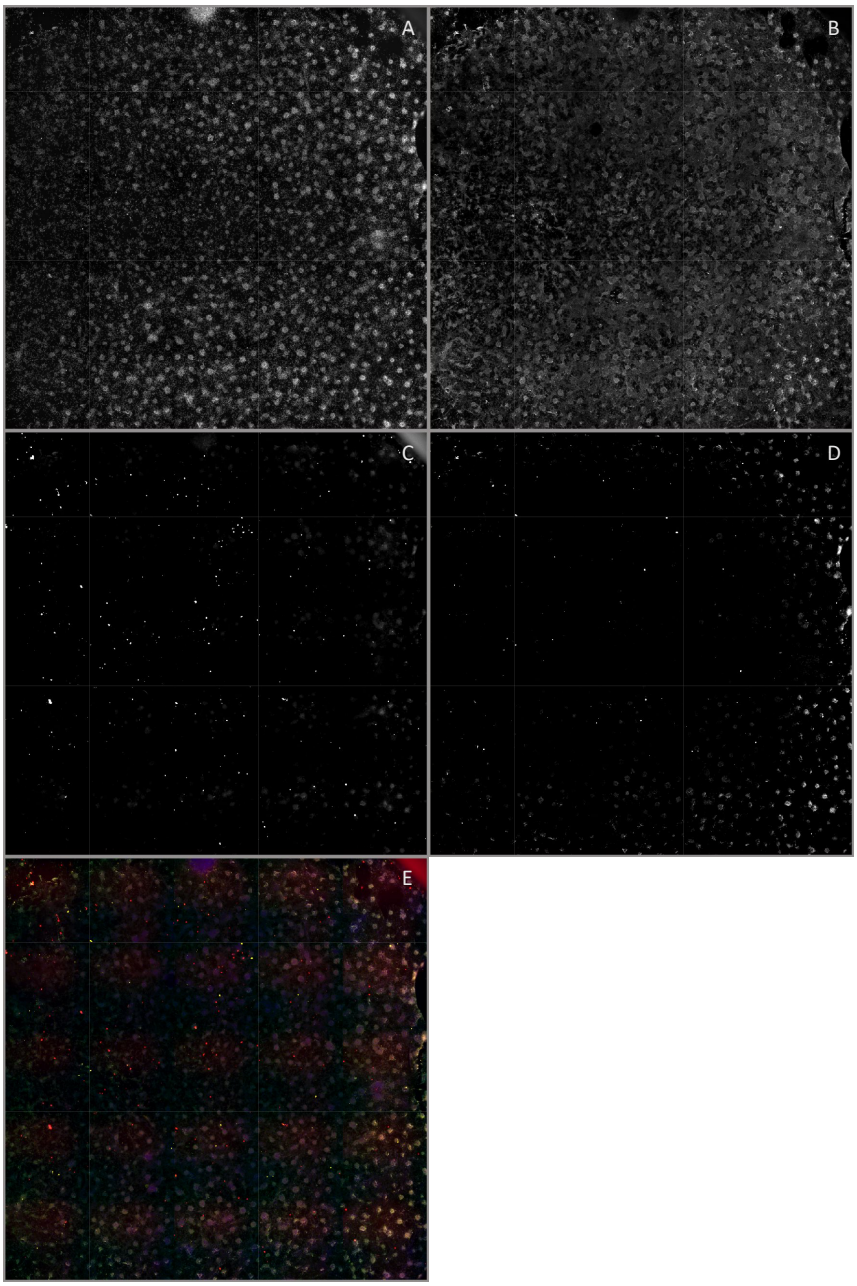

Figure 9.5: High-content images of CGNs exposed to 1 µM morphine. The different pictures show the expression of A) DAPI, B) MAP2, C) PSD95 and D) SYP. E) A composite picture of all stains in one picture. Blue=DAPI, green=MAP2, red=PSD95 and yellow=SYP.